Title

THERMOCHEMISTRY OF ACID-BASE STABILIZED TRANSITION METAL ALLOYS BY CARBIDE AND NITRIDE EQUILIBRIA AND KNUDSEN EFFUSION VAPOR PRESSURES

Author

Gibson, J.K.M.

Publication Date

1983-07-01

Lawrence Berkeley Laboratory

UNIVERSITY OF CALIFORNIA

Materials & Molecular Research Division

THERMOCHEMISTRY OF ACID-BASE STABILIZED TRANSITION METAL ALLOYS BY CARBIDE AND NITRIDE EQUILIBRIA AND KNUDSEN EFFUSION VAPOR PRESSURES

J.K.M. Gibson
(Ph.D. Thesis)

July 1983

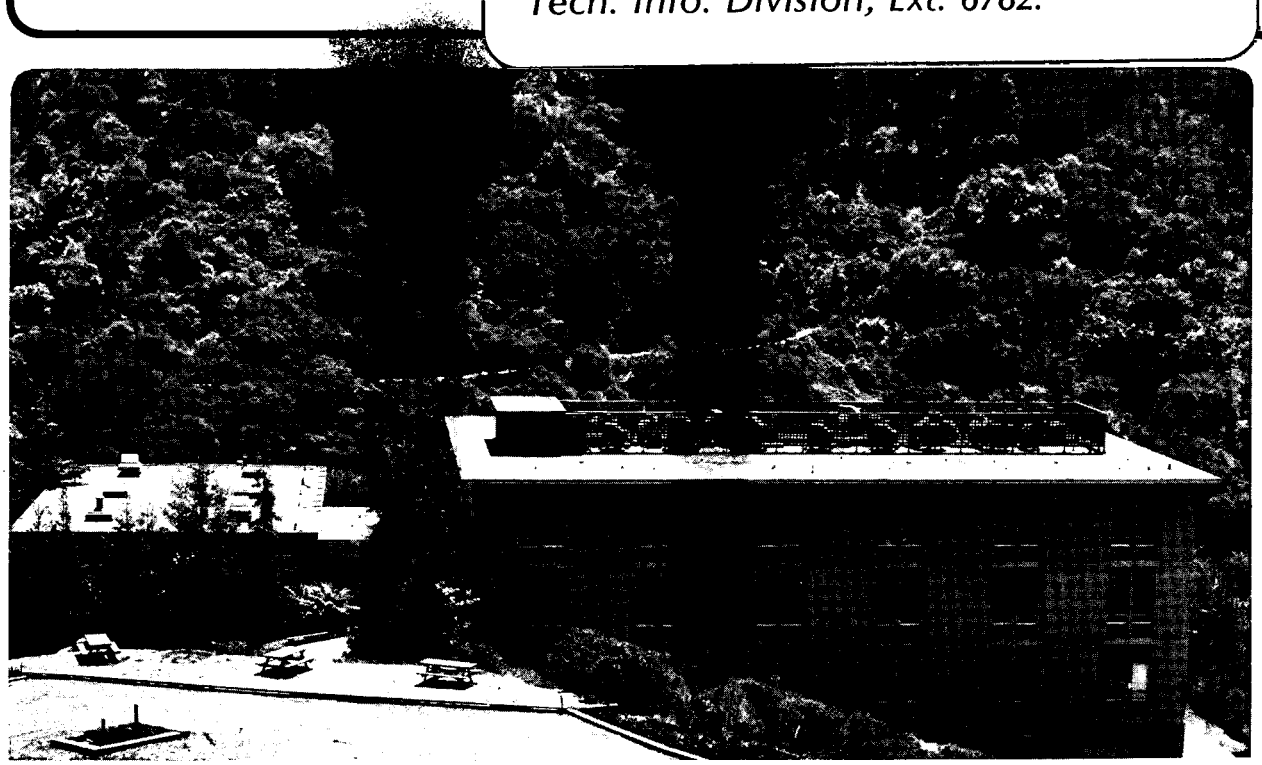

Prepared for the U.S. Department of Energy under Contract DE-AC03-76SF00098

DISCLAIMER

LBL-16233

THERMOCHEMISTRY OF ACID-BASE STABILIZED TRANSITION METAL ALLOYS BY CARBIDE AND NITRIDE EQUILIBRIA AND KNUDSEN EFFUSION VAPOR PRESSURES

John Knight Moulton Gibson

Materials and Molecular Research Division
Lawrence Berkeley Laboratory
and Department of Chemistry
University of California
Berkeley, CA 94720

This work was supported by the Director, Office of Energy Research, Office of Basic Energy Sciences, Materials Sciences Division of the U. S. Department of Energy under Contract Number DE-AC03-76SF00098.

TO MATER

THERMOCHEMISTRY OF ACID-BASE STABILIZED TRANSITION METAL ALLOYS BY CARBIDE AND NITRIDE EQUILIBRIA AND KNUDSEN EFFUSION VAPOR PRESSURES

John Knight Moulton Gibson

Materials and Molecular Research Division
Lawrence Berkeley Laboratory
and Department of Chemistry
University of California
Berkeley, CA 94720

ABSTRACT

The thermochemistry of several Lewis acid-base stabilized transition metal alloys has been investigated and the results interpreted within the context of the Engel-Brewer theory to further clarify and quantify the factors which determine the extent of this type of interaction. Binary alloys of a platinum group metal (Ru, Os, Ir, Pd, Pt, or Au) with a group IVB-VIB transition element (Ti, Zr, Hf, Nb, Ta, or W) were studied by equilibration of the alloy with the appropriate IVB-VIB carbide or nitride or by measuring the vapor pressure of one of the two components by thermogravimetric or mass spectrometric Knudsen effusion experiments. Twenty seven binary alloys were studied at temperatures ranging from 1425 K to 2750 K and the activities established ranged from $a_{Zr(ZrPt_3)} = 6 \times 10^{-6}$ to $a_{Pd(82\ at.\%\ Pd-Nb)} \simeq 1$, both at 1900 K. Among the implications of the results obtained are that reduced bonding ability due to crystal field effects can severely limit the extent of acid-base interaction and the effect of valence d orbital contraction is relatively minor for the 4d (e.g., Zr) compared with the 5d (e.g., Hf) elements but is significant for the 3d (e.g., Ti) elements.

THERMOCHEMISTRY OF ACID-BASE STABILIZED TRANSITION METAL ALLOYS BY CARBIDE AND NITRIDE EQUILIBRIA AND KNUDSEN EFFUSION VAPOR PRESSURES

CONTENTS

ACKNOWLEDGEMENTS

Professor Leo Brewer has managed to keep me entirely interested in this work from the day I met him while at the same time allowing a degree of freedom in choosing and carrying out this research which was clearly not the quickest route to results but has provided me with invaluable learning experiences. I shall always be grateful and indebted to him for his teaching, support, and guidance.

I would like to thank Professor Karl Gingerich of the Chemistry Department of Texas A&M University for making his high-temperature mass spectrometer available and for the assistance by him and his group in carrying out those experiments. Thanks also to Professor Sumner Davis of the Physics Department of U. C. Berkeley for the use of his laboratory facilities, to Professor Ian Carmichael of the Geology Department of U. C. Berkeley for providing the electron microprobe, and to Mark Rivers for his patient training and assistance on that instrument. Several of the arc-melted standard alloys were kindly prepared by Dr. Oscar Krikorian of Lawrence Livermore National Laboratory.

The technical support staff of the Materials and Molecular Research Division of Lawrence Berkeley Laboratory provided essential assistance throughout the course of this work and I am particularly grateful to John Holthuis who was always willing to help with any problem. I feel fortunate to have had many colleagues who have made life in the Lab a good bit more pleasant than it would otherwise have been; special thanks in that regard to Cil Davis, Bea-Jane Lin, Karl

Koshlap, Mike Cima, Ed Faizi, Soo-Han Choi, Dave Goodman, Karen Krushwitz, and Joe Bularzik.

Finally, I am very grateful to my wife Tomoko for her understanding and support over the past two years.

This work was supported by the Director, Office of Energy Research, Office of Basic Energy Sciences, Materials Sciences Division of the U. S. Department of Energy under Contract Number DE-AC03-76SF00098.

LIST OF FIGURES

LIST OF TABLES

INTRODUCTION

Many of the binary alloys of a group IVB or VB element (Ti, Zr, Hf, V, Nb, Ta) with a platinum-group metal (Rh, Ir, Pd, Pt) exhibit extraordinary stability. Quantifying the extent of bonding in these systems with thermochemical measurements is of value from two broad perspectives. Firstly, the thermodynamic stability of a given alloy provides a measure of the driving force for its formation when its constituents are brought together. In particular, the free energy of formation of certain of these alloys is negative enough that "chemically inert" platinum group metals may, in fact, react (sometimes violently) with other transition metals with which they are brought into contact. For example, a platinum thermocouple can react with its zirconia sheath under a reducing atmosphere to form a very stable Zr-Pt intermetallic.[1]

The second motivation for establishing the strength of atomic interaction in this class of alloys is to gain a better understanding of the nature of the bonding involved. That these systems would exhibit an unusual stability was predicted by Brewer[2] based upon his development of a correlation between electronic configuration and crystal structure which was first proposed by Engel.[3-5] The Engel-Brewer correlation assigns electronic configurations to the stable crystal structures of the transition metals; these assignments provide for less than five valence d electrons for those elements at the left of the periodic table and more than five for those at the right. The strong bonding between a d-electron-excess element and a

d-electron-deficient element is taken to be due to a generalized Lewis acid-base effect whereby the hyperelectronic element donates one or more electron pairs to form chemical bonds using vacant orbitals of the hypoelectronic element. It is to further refine and develop this model of bonding in these very stable transition metal alloys that a study of their thermochemical properties has been undertaken. Among the possible applications of these alloys is to tailor the catalytic properties of platinum group metals by adjusting their electronic character with the addition of electron acceptor metals.

The Engel-Brewer correlation in its simplest form results in the integral valence electronic configuration assignments for the high-temperature structures of the transition metals shown in Figure 1. (A detailed and exact development of the theory can be found in Refs. 6-9.) For each element, the high-temperature crystal structure (bcc = body centered cubic; hcp = hexagonal close packed; fcc = face centered cubic) and the corresponding valence electronic configuration are shown. The valence configuration shows the electronic distribution outside of the non-bonding closed core electrons and does not include the outermost f electrons since they are quite localized and do not participate appreciably in bonding. The valence d orbitals belong to a principal quantum shell one below that of the valence s and p orbitals and are significantly more localized and less effective in bonding overlap, but must nonetheless participate in bonding as evidenced by the properties of the transition elements. Tungsten, for example, has but a single valence s electron (like the alkali metals)

Sc	Ti	V	Cr	Mn	Fe	Co	Ni	Cu
$3d^2$ $4s^1$ bcc	$3d^3$ $4s^1$ bcc	$3d^4$ $4s^1$ bcc	$3d^5$ $4s^1$ bcc	$3d^6$ $4s^1$ bcc	$3d^7$ $4s^1$ bcc	$3d^6$ $4s^1 4p^2$ fcc	$3d^7$ $4s^1 4p^2$ fcc	$3d^8$ $4s^1 4p^2$ fcc
Y	**Zr**	**Nb**	**Mo**	**Tc**	**Ru**	**Rh**	**Pd**	**Ag**
$4d^2$ $5s^1$ bcc	$4d^3$ $5s^1$ bcc	$4d^4$ $5s^1$ bcc	$4d^5$ $5s^1$ bcc	$4d^5$ $5s^1 5p^1$ hcp	$4d^6$ $5s^1 5p^1$ hcp	$4d^6$ $5s^1 5p^2$ fcc	$4d^7$ $5s^1 5p^2$ fcc	$4d^8$ $5s^1 5p^2$ fcc
La	**Hf**	**Ta**	**W**	**Re**	**Os**	**Ir**	**Pt**	**Au**
$5d^2$ $6s^1$ bcc	$5d^3$ $6s^1$ bcc	$5d^4$ $6s^1$ bcc	$5d^5$ $6s^1$ bcc	$5d^5$ $6s^1 6p^1$ hcp	$5d^6$ $6s^1 6p^1$ hcp	$5d^6$ $6s^1 6p^2$ fcc	$5d^7$ $6s^1 6p^2$ fcc	$5d^8$ $6s^1 6p^2$ fcc

XBL 836-10315

Figure 1

yet is the most tightly bound of all of the solid elements, as measured by its internal pressure; this stability must be largely due to the bonding contribution of its five valence 5d electrons. Very stable alloys may result when non-bonding valence d electrons are made available to participate in interatomic bonding, as by a generalized acid-base effect.

Each of the transition elements has available five valence d orbitals which can accommodate up to two (spin-paired) electrons each. The most stable electronic distribution for a hypoelectronic element, such as Ta, has before bonding each valence d electron unpaired in one of the five available orbitals with one or more valence d orbital remaining vacant and all of these unpaired electrons can participate in interatomic bonding. A hyperelectronic element, such as Ir, must have one or more sets of internally paired electrons in its five valence d orbitals. The valence electronic configurations for pure Ta and Ir metals are shown at the top of Figure 2 where each box represents an available orbital and each arrowhead a valence electron; opposing arrowheads signify spin-paired electrons as required by the Pauli exclusion principle. The internally paired 5d electrons on Ir are localized and are forbidden from participating in bonding unless a symmetrically and energetically appropriate orbital on a neighboring atom is vacant and thus available for bonding, in which case an electron pair bond may be formed with both electrons being donated by the Ir. Such a generalized acid-base reaction may proceed between Ir and Ta utilizing the vacant 5d orbital of Ta and the fully occupied 5d

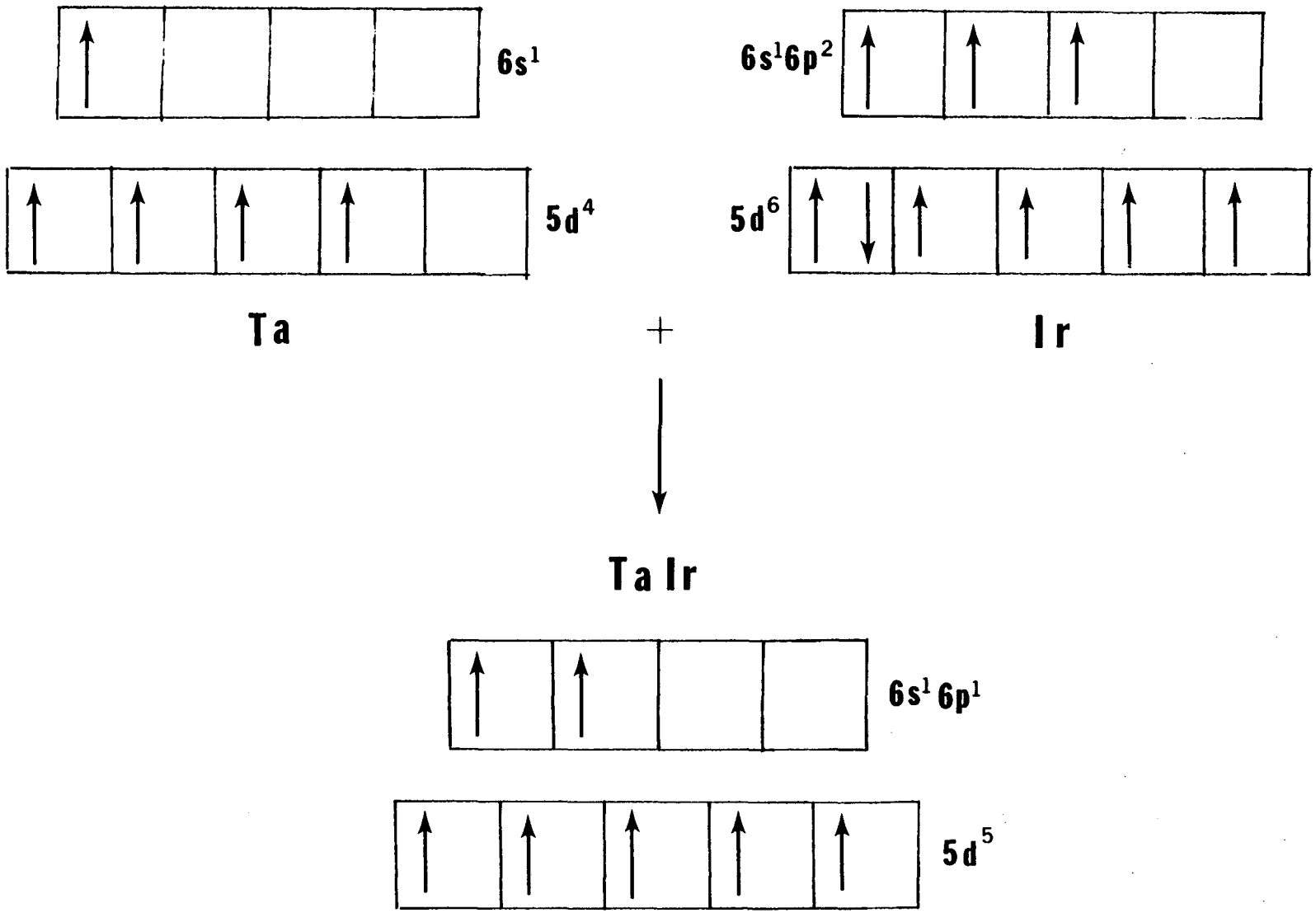

XBL 836-10316

Figure 2

orbital of Ir in which case Ta would be acting as an acid and Ir as a base. For electron counting purposes the average valence electronic configuration given by this scheme for a stoichiometric TaIr alloy is shown at the bottom of Figure 2. The number of bonding electrons per atom is five for pure Ta metal (one 6s and four 5d), seven for pure Ir metal (three 6s and 6p and four 5d), and seven for TaIr (two 6s and 6p and five 5d) so that the average number of bonding electrons has been increased from six per atom in the elemental metals to seven per atom in the alloy. It is this net increase in bonding which stabilizes this class of acid-base alloys relative to the pure metals.

This scheme is undoubtedly greatly oversimplified and does not consider such probable effects as significant polarization of the bonding electrons towards the more electronegative base metal (e.g., Ir) and backbonding through higher energy orbitals to reduce or effectively negate any net charge transfer to the more electropositive acid metal. Generalized acid-base bonding involving donation of a non-bonding electron pair from a relatively electronegative to a more electropositive but hypoelectronic element is well known, as in the case of tetrahedrally coordinated Al (acid) and P (base) in the solid compound AlP[10] and similar behavior should be expected in alloys of hyperelectronic with hypoelectronic transition metals.

A picture similar to that presented above for TaIr can be derived for all alloys of a hyperelectroic transition metal (greater than five valence d electrons) with a hypoelectronic transition metal (less than five valence d electrons) but the actual extent of the acid-base

interaction is expected to depend on several factors. The heat of formation of the acid-base alloy $HfPt_3$ is about -24 kcal/g.atom[11] but if the corresponding first transition series elements are substituted the analogous $TiNi_3$ alloy is found to have a heat of formation of about -8 kcal/g.atom,[12] so it is clear that the acid-base interaction is more effective in stabilizing the Hf-Pt system. Quantitatively predicting the extent of acid-base stabilization for a particular alloy is almost impossible at this stage in the development of solid-state theory but consideration of factors which ought to be significant allows some rather straightforward qualitative predictions to be made.

In order for interatomic bonding to occur it is necessary for the atomic orbitals involved to overlap in real space to form molecular orbitals. The extent of stabilization of the alloys of interest here is expected to be sensitive to the degree of valence d orbital overlap. The approximate degree of extension beyond the closed electron core of the two types of valence orbitals is shown schematically for the group IVB elements in Figure 3, where the large circles represent the closed cores and the lobes represent the valence orbitals without consideration for shape or symmetry. Ionic radii of the +4 ions were used to arrive at core sizes while the metallic radii were taken to roughly reflect the valence s orbital radii; d-state-radii from Harrison[13] were used for the valence d orbital radii. The readily apparent trends going down this group are typical of all of the transition metal groups: upon going from the first to third

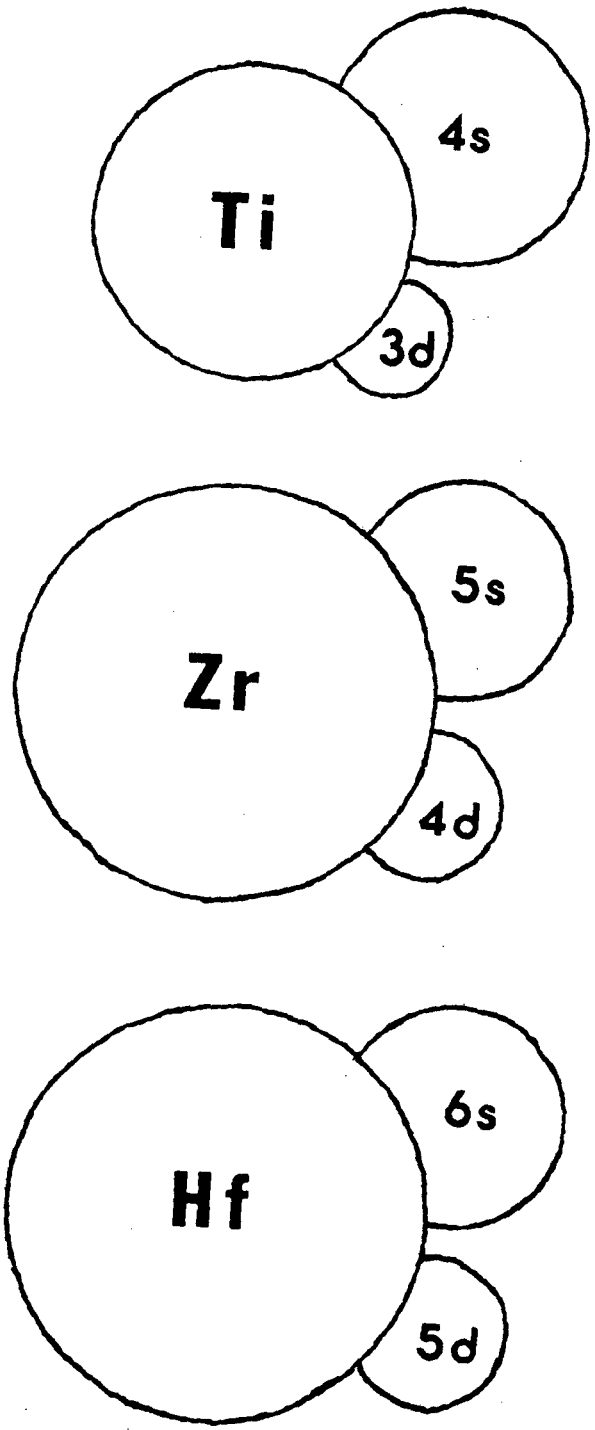

XBL 836-10317

Figure 3

transition series the valence s and p electrons become less effective in bonding while the valence d electrons become more effective due to increasing delocalization. Since d orbital overlap increases upon going down the periodic table it is to be expected that the extent of acid-base stabilization involving d orbitals will also increase and a 5d acid-base alloy should be more strongly bound than the analogous 3d alloy in accord with the $HfPt_3$ - $TiNi_3$ comparison discussed above. It would be of value to establish the importance of this effect for other systems and particularly for alloys of elements from different transition series.

The second general trend which is of interest can be approached by comparing the various elements in the same transition series. In Figure 4 are shown the elements of the third transition series from La to Au, and for each the effective nuclear charge outside of the closed core (Z'), the total number of valence d electrons (# d e^-), and the corresponding number of vacant valence d orbitals for the acidic elements (# vacant) or number of pairs of non-bonding valence d electrons for the basic elements (# pairs), all of these quantities for the stable high-temperature form. Since the intermediate elements W and Re, with neither vacant valence d orbitals nor non-bonding valence electron pairs, may act as acids or bases through p orbital effects they have been labelled with a "?". Taking Z' as a measure of electronegativity it might be expected that the more electronegative Ta will be a better electron acceptor than Hf. On the other hand, the two available vacant valence d orbitals of Hf may make it a more effective

	La	Hf	Ta	W	Re	Os	Ir	Pt	Au
Z′	3	4	5	6	7	8	9	10	11
# $d e^-$	2	3	4	5	5	6	6	7	8
# vacant	3	2	1	0	0	0	0	0	0
# pairs	0	0	0	0	0	1	1	2	3
	ACIDS			?		BASES			

XBL 836-10314

Figure 4

effective acid than Ta with its single such orbital, this particularly since the sole vacant valence d orbital of Ta may be much less favorable than the others for bonding due to a crystal field splitting.[97] This latter consideration may well be composition dependent in that the greater number of acceptor orbitals of Hf may be a much more significant factor in systems rich in an electron-excess element than in those with relatively few non-bonding electron pairs to be accommodated. Considering the two hyperelectronic elements Ir and Pt, the analogous considerations predict that Ir should be a better electron donor based upon its lower Z' but Pt should be the more effective base if the number of pairs of non-bonding valence d electrons is most important. Extensive characterization of acid-base stabilization as a function of binary (and possibly higher-order) alloy combinations and compositions is necessary to fully understand and quantify the importance of these, and possibly other, competing effects.

Since the introduction of the Engel-Brewer correlation and its predictions of extraordinary stability of a particular class of alloys several investigators have thermochemically studied several of these alloys with a variety of experimental methods. No attempt will be made here to provide a comprehensive review of all of the relevant work but rather an overview of some of the more directly pertinent results will be provided. It should be noted that the interpretations here and throughout of the thermochemical stabilities of these systems are based upon electronic considerations and ignore contributions (usually destabilizing) from size and internal pressure differences

between the alloyed elements, this because these effects are expected to be of relatively small significance in these very strongly bound alloys of the group IVB and VB elements with the platinum group elements.

Meschter and Worrell[14-15] studied Pt-rich alloys of the IVB elements in the 1100-1400 K range with solid state galvanic cells and found, at 1300 K: $\Delta G^o_f(TiPt_3) = -17.8$ kcal/g.at. ($\Delta H^o_f = -20.4$ kcal/g.at), $\Delta G^o_f(ZrPt_3) = -22.9$ kcal/g.at. ($\Delta H^o_f = -27.1$ kcal/g.at), and $\Delta G^o_f(HfPt_3) = -24.3$ kcal/g.at. Srikrishnan and Ficalora[11] determine enthalpies of formation for the $ZrPt_3$ and $HfPt_3$ intermetallics by fluorine bomb calorimetry with results: $\Delta H^o_{f,298}(ZrPt_3) = -30.5$ kcal/g.at. and $\Delta H^o_{f,298}(HfPt_3) = -33.0$ kcal/g.at. metal. These results suggest extraordinary stability for these systems and reflect the expected trend of increasing bonding effectiveness upon moving down the IVB group from Ti(3d) to Zr(4d) to Hf(5d). Carbonara and Blue[16] measured P_{Zr} and P_{Pt} above $ZrPt_3$ by high-temperature mass spectrometry and found that $\Delta G^o_{f,2200\ K}(ZrPt_3) = -20.5$ kcal/g.at. in rather good accord with the Meschter and Worrel results which extrapolate to $\Delta G^o_{f,2200\ K}(ZrPt_3) = -20.1$ kcal/g.at. Schaller[1] determined zirconium activities in Pt and Pd alloys by reducing ZrO_2 at 1300 K and obtained: $\gamma^{\infty}_{Zr(Pt)} = -87.0$ kcal/g.at. and $\gamma^{\infty}_{Zr(Pd)} = -84.1$ kcal/g.at., this also in at least qualitative accord with expectations based upon reduced d orbital delocalization of Pd(4d) compared with Pt(5d).

The Pt-rich IVB-Pt alloys and particularly $ZrPt_3$ are probably the most comprehensively studied of the Engel-Brewer alloys to date and only rather scattered and sometimes incomplete data exist on a few other systems. Gingerich, et al.[18,19] studied several compositions of the Ti-Ir system with high-temperature mass spectrometric vapor pressure measurements and found a maximum stability at the composition TiIr where $\Delta\bar{G}_{1623K} = -30\pm3$ kcal/g.at. for both components; this result suggests that only one of the two vacant valence d orbitals of Ti may be significantly involved in acid-base bonding since otherwise the stability peak might be expected to be skewed somewhat towards Ir-rich compositions. The same method was used to study TiPd and Pd-rich Ti-Pd alloys[20] with the result: $\Delta G^{o}_{f,1873K}(TiPd) = -16$ kcal/g.at.; that this alloy is apparently significantly less stable than the TiIr system may be attributable to greatly reduced valence d orbital overlap. Kleykamp[21] carried out solid state galvanic cell measurements on a Rh-rich Nb-Rh alloy and found $\Delta\bar{G}^{xs,}_{Nb(Rh),1200\ K} = -48$ kcal/g.at. Brewer and Wengert[22] equilibrated Ru, Rh, Pd, Ag, Re, Os, Ir, Pt, and Au with ZrC and graphite and determined the composition of the binary alloys with the Zr activity fixed by the carbide. Their results suggest a maximum in stabilization between Rh and Pd for the second series donor metals alloyed with Zr and between Ir and Pt for the corresponding third series elements. The only unexpected result of their studies is that the 4d element Ru binds Zr more strongly than the 5d element Os does but this apparent discrepancy has been cleared up with this work.

These and the few other data available on this class of alloys clearly confirm the prediction of extraordinary stability and agree, at least qualitatively, with the expectations outlined above as to what factors might be significant in determining the extent of acid-base interaction: 1) delocalization of valence d orbitals which occurs upon moving down a group in the periodic table clearly leads to greater bonding effectiveness, and 2) there does appear to be a competition between the effects of increasing nuclear charge and number of fully occupied valence d orbitals which results in a maximum donor effectiveness in the region of Pt and Ir. Nonetheless, so few systems have been well characterized that quantitative predictions about the behavior of as yet unstudied systems remains impossible. The research reported here involved the use of three experimental methods to obtain thermochemical information on several Engel-Brewer alloys so as to better understand the nature of the interactions involved and be able to predict the extent of generalized acid-base interactions in other systems.

EXPERIMENTAL

Each of the three sets of experiments which have been carried out to establish the thermodynamic activity of one of the components of several binary acid-base transition metal alloys will be described in turn; the results of all of the experiments will be presented subsequently.

I. CARBIDE EQUILIBRATION

This method has been used by Brewer and Wengert[22] to thermodynamically characterize the extent of binding of Zr with the platinum-group metals. With the work reported here, certain of their results are confirmed, one is clarified, and the approach is extended to alloys of other of the group IVB and VB metals and W. The theory and experimental procedures used here are substantially the same as used for the earlier work[22] but they will be reviewed here.

Theory:

In Figure 5 are presented the basic thermodynamics for the study of the Ta-Ir acid-base pair by this method; this general approach is applicable to all of the alloys of one of the group IIIB - VIB transition metals or a lanthanide or actinide element with one of the platinum-group metals (Ru, Os, Rh, Ir, Pd, Pt, Ag, Au). An incomplete

Carbide Equilibration

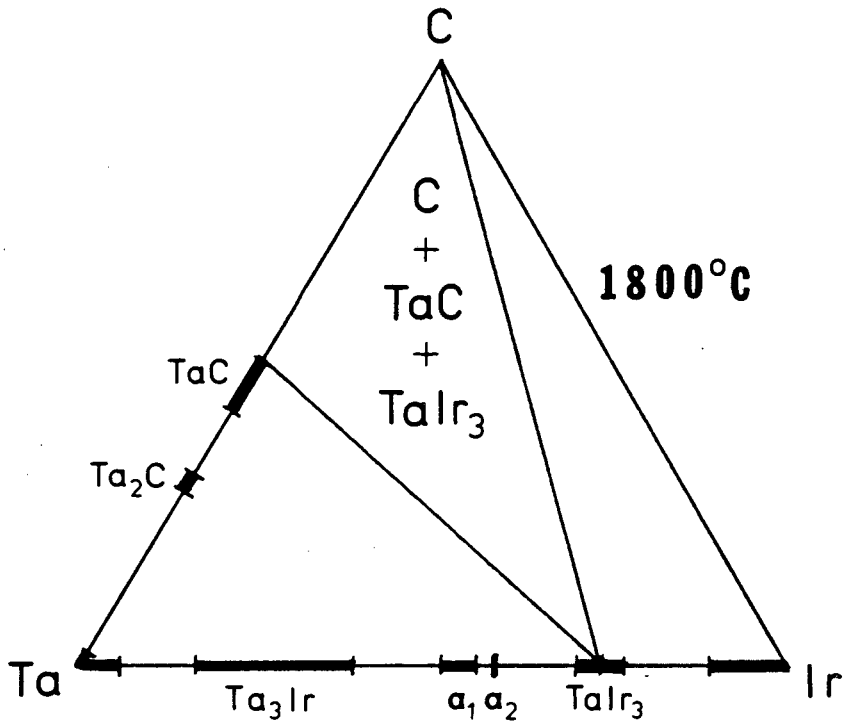

$$a_{Ta}^{C} = a_{Ta}^{TaIr_3} = a_{Ta}^{TaC}$$

$$Ta + C = TaC$$

$$\Delta G_f^{\circ}(TaC) = RT \ln a_{Ta} \cdot a_C \cdot a_{TaC}^{-1}$$

$$\begin{matrix} & \approx & \approx \\ & 1 & 1 \end{matrix}$$

XBL 831-7636

Figure 5

version of the 1800°C secton of the Ta-Ir-C ternary phase diagram is shown with the Gibbs triangle; all known binary phases are indicated along the edges but only the ternary tie lines related to these experiments are included. At fixed temperature and pressure, by the Phase Rule, three phases of fixed composition may be in equilibrium for this system. The net composition of the system is chosen such that two of these will be TaC and C and the third will be some Ta-Ir alloy, shown here as $TaIr_3$ in accord with an experimental result to be presented later. As shown at the bottom of the figure, when these three phases are in equilibrium the activity of Ta in each of them must be equal since the chemical potentials of Ta, μ_{Ta}, must be equal by definition of thermodynamic equilibrium; the relationship between activity and chemical potential is:

$$RT\ln a_i = \mu_i - \mu_i^o \text{ (Raoult)}$$

The Raoult's Law standard state is used throughout.

As shown in the figure, the free energy of formation of the carbide can be used to establish the activity of Ta in the equilibrium phases if it is assumed that the activities of both graphite and the carbide are approximately unity. This assumption amounts to stating that both the equilibrium graphite and carbide phases are present with little contamination, and particularly that they have not dissolved

appreciable amounts of the platinum-group metal, here Ir. This latter fact can, and has been confirmed with electron probe microanalysis (EPMA) of the carbide and graphite phases at the same time that the alloy composition was determined. The composition of the alloy with the Ta activity fixed by the carbide and graphite phases is established by X-ray diffraction and/or EPMA, neither of which technique is particularly sensitive to interstitial carbon contamination. Significant interstitial carbon in the equilibrium alloy could appreciably affect its thermodynamic properties and is unacceptable when the stability of the pure binary alloy is of interest, so it is important to establish that this is not a problem and it is unfortunate that the analytical methods available for this work are not adequately sensitive to the detection of such contamination. Of course, the X-ray diffraction method is sensitive to the existence of a micro-crystalline carbide phase with structure different from that of the alloy and no such ternary carbide compounds were ever identified which makes a carbon content of greater that perhaps 10 at.% very unlikely. In fact, even that high a carbon content seems improbable in view of the high platinum-group content of the equilibrium alloys given the known properties of the platinum-group metals with respect to carbon dissolution.

All of the equilibrated alloys studied were of composition MPl_3 (M = carbide metal, Pl = platinum-group metal) or richer in the platinum-group metal. Although several investigators have reported the existence of carbides of Os, Ru, and Re, as indicated in Shunk's

review,[23] it seems likely that no carbides of second or third transition series elements to the right of group VIB exist[24-28] with the possible exception of TcC,[29] and the solid platinum-group metals dissolve very little carbon[25,28] (though the liquid metals often do dissolve appreciable amounts). The $HfIr_3$ intermetallic had the lowest average valence electron concentration of any of the systems studied so that it might be expected to be the most susceptible to high interstitial carbon concentrations through no nonisostructural carbide was detected by X-ray diffraction. The average total valence electron concentration for this alloy is 7.75 per atom ([1Hf · $4e^-$/Hf + 3Ir · $9e^-$/Ir] ÷ 4at.), close to that of Os (8 per atom). It is the s and p valence electrons of the transition metals which interact most strongly with interstitial elements and their concentration may be estimated using the Engel-Brewer correlation: [1Hf · ~1(s+p)/bccHf + 3Ir · ~3(s+p)/fccIr] ÷ 4at. ≃ 2.5 valence (s+p) electrons per atom. This valence s+p concentration is between that of Os and Ir and it might be expected that the $HfIr_3$ alloy has an even smaller affinity for carbon than does pure Os, which dissolves only very small amounts of graphite and forms no carbide phase,[24] and there is not expected to be any significant carbon dissolution in this or any of the other (more platinum-like) alloys studied. In accord with this, Raub and Falkenburg[32] determined portions of the phase diagrams for the Ti-Ru-C and Ti-Pt-C systems and did not find any ternary carbides and report minimal solubility of carbon in the intermetallics, this despite the high affinity of Ti for C.

Several reviews[33-39] and critical compilations of the thermochemical data[40,41] were surveyed to obtain the best available thermodynamic quantities for the carbides used in these experiments. The selected values of $\Delta H^{o}_{f,298}$ and $\Delta S^{o}_{f,298}$ along with estimated uncertainties and references are given in Table 1. Since all equilibrations were carried out in the presence of graphite, the stoichiometric or near-stoichiometric carbide thermal quantities are used. The uncertainities in the room temperature quantities combined with those in the values necessary to obtain free energies of formation at the equilibration temperatures (e.g., in ΔC_p) are used to obtain an approximate uncertainty in $\Delta G^{o}_{f,2000\ K\sim\ equil.\ T}$ and the resulting uncertainty in the value of $a_{M(MC)}$, δa_M, through:

$$\delta a_M = \frac{\partial a_M}{\partial \Delta G^{o}_{f}(MC)} \cdot \delta \Delta G^{o}_{f}(MC) = \frac{a_M}{RT} \cdot \delta \Delta G^{o}_{f}(MC)$$

Because of the generally small temperature dependence of the phase equilibria, as discussed below and illustrated with results presented later, the total uncertainties are dominated by those in the thermodynamic quantities and the values of δa_M given in Table 1 are taken to reflect the total uncertainties for these experiments.

TABLE 1

Carbide	$\Delta H^o_{f,298}$ (kcal)	$\Delta S^o_{f,298}$ (cal/K)	$\Delta G^o_{f,2000\ K}$ (kcal)	$\delta a_{M,2000\ K}$	Ref.
TaC	-34.2±1	-1.17±.02	±2	±.5a_M	37
NbC	-33.0±1	-1.7±.5	±3	±.7a_M	36
ZrC	-48.0±1	-2.69±.04	±2	±.5a_M	38
HfC	-54.0±1.5	-2.64±.01	±2	±.5a_M	39
WC	-8.4±2	+0.3±.5(est.) (H.T. ΔC_p also est.)	±2	±.5a_M	33

Equilibration Procedures:

A list of the starting materials for these and the nitride experiments are given in Table 2 with their purities and suppliers; the graphite powder was 99.999%, the carbides all at least 99%, and the metals all at least 99.7%. In those cases where an alloy (e.g., ZrPt, NbPd) was used as one of the reactants, it was prepared by arc-melting the pure foils or rods on a water-cooled copper hearth with a tungsten electrode, the entire procedure performed under a Ti-gettered argon atmosphere. For some of the earlier runs, the arc-melted buttons were homogenized for about 20 hr. at 100-200^{o}C below the melting point but this procedure was found to be unnecessary if the buttons were flipped several times during the arc-melting procedure to insure good mixing. The brittle intermetallics were pulverized very easily in a hard steel mortar and pestle and an alloy powder of uncharacterized particle size was used as the starting material.

The weighed reactant powders (graphite, carbide, and pure platinum-group metal or alloy) were thoroughly mixed in glass jars with glass mixing beads for about 20 hr. on a V-mixer. A sample of approximately 3 gm. was transferred into a hot-press die and the die into the hot-press as shown schematically in Figure 6. The die is of 99.5% ATJ grade graphite and is 3.81 cm o.d., 1.27 cm i.d., and 3.81 cm tall. Variable uniaxial pressures can be applied to the powders by a hydraulic pump and all runs were carried out at 490 bar; this pressure is adequate to insure good solid-solid contact for equilibration but should not appreciably affect these solid transformations for which ΔV

TABLE 2

Material	Purity	Supplier
TiC, -325 mesh pwdr.	99.5%	Cerac
ZrC, -325 mesh pwdr.	99%	Cerac
HfC, -325 mesh pwdr.	99%	Cerac
VC, -325 mesh pwdr.	99%	Cerac
NbC, -325 mesh pwdr.	99.8%	Cerac
WC, -325 mesh pwdr.	99%	Cerac
TiN, -325 mesh pwdr.	99.5%	Cerac
ZrN, -325 mesh pdwr.	99%	Cerac
VN, -325 mesh pwdr.	99%	Cerac
NbN, -325 mesh pwdr.	99.5%	Cerac
TaN, -325 mesh pwdr.	99%	Cerac
HfN, -200 mesh pwdr.	99.8%	Noah
TaC, pwdr. (? mesh)	99.95%	Atomergic
C(graphite), -200 mesh powder	99.999%	Cerac
N_2(g)	99.996% (by vol.)	Liquid Carbonic
Ru, -60 mesh sponge	99.8%	Apache
Ru, -80 mesh pwdr.	99.9% (metal purity)	Alfa
Os, -60 mesh pwdr.	99.9% (metal purity)	Alfa
Ir, pwdr (? mesh)	99.7%	LBL Stock

TABLE 2, continued

Material	Purity	Supplier
Pd, -325 mesh pwdr.	99.8%	LBL Stock
Pd, .010" sheet	99.95%	LBL Stock
Pd, 1/8" rod	99.99%	M.R.C.
Pd, -60 mesh pwdr.	99.9% (metal purity)	Alfa
Pt, +100 mesh pwdr.	99.9%	Apache
Pt, .010" sheet	99.95%	LBL Stock
Zr, 1/8" rod	99.94%	Johnson-Matthey
Zr, -325 mesh pwdr.	99.6+%	Atomergic
Nb, 1/8" rod	99.97%	M.R.C.
Nb, -150 mesh pwdr.	99.8%	Cerac
graphite die material	99.5%	National Carbon
tungsten liner foil, .001"	99.95%	LBL Stock

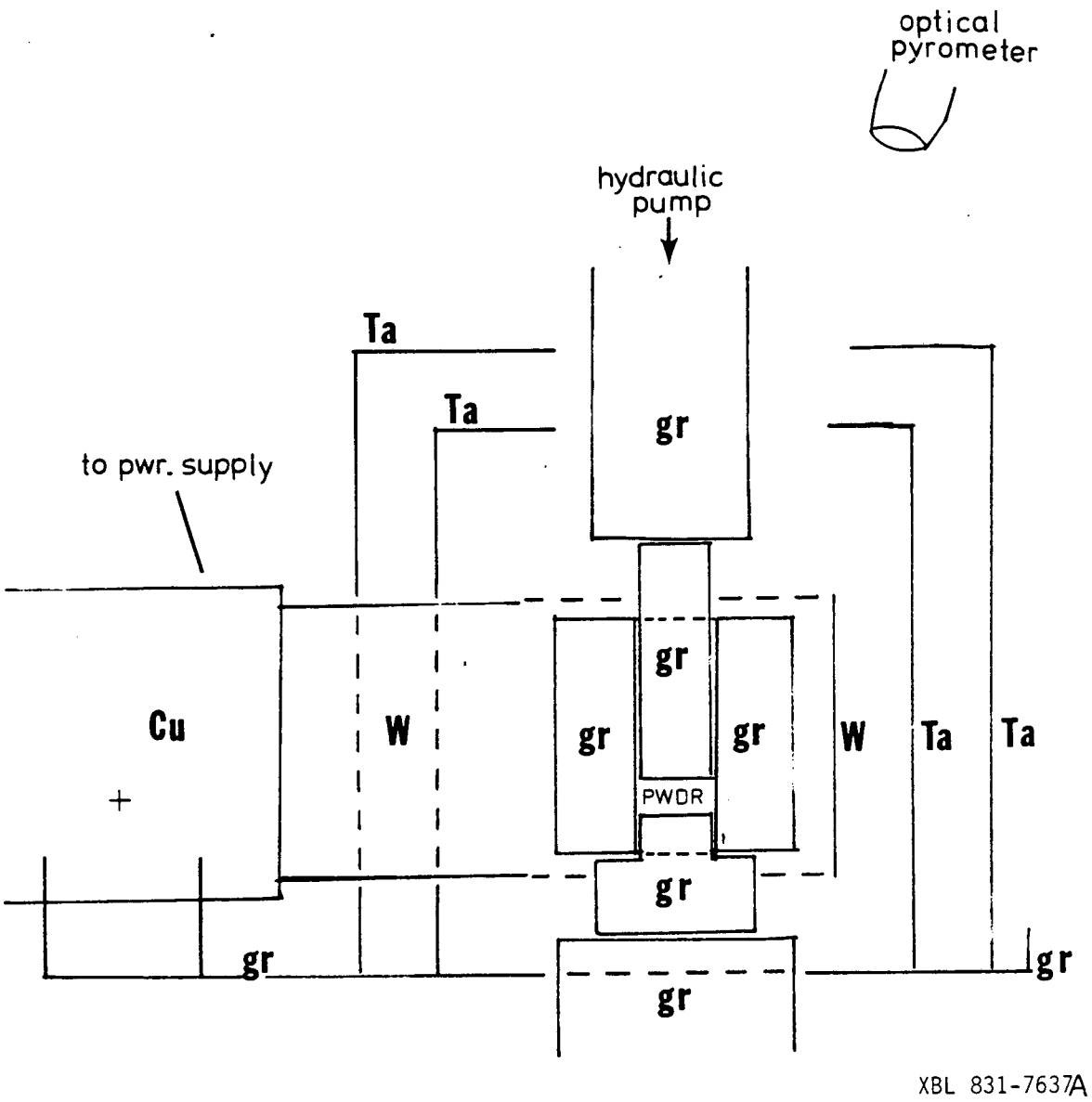
optical
pyrometer
hydraulic
pump
Ta
Ta
gr
to pwr. supply
Cu
W
gr
gr
gr
W
Ta
Ta
PWDR
gr
gr
gr
gr
XBL 831-7637A

Figure 6

are small. In Figure 6 the various components are labelled with what they are made of: a 30mm high, 0.25mm thick W heating element surrounds the sample and Ta heat shields supported on a graphite base are concentric with the heating element. The heating element is clamped to water-cooled Cu electrodes which are connected to a variable power supply that can provide up to about 580A at 12.2V (7.1kW) for a maximum sample temperature of about 2100°C. A diffusion pump provides a vacuum of better than 10^{-4} torr in the hot press chamber as monitored throughout with an ionization vacuum gauge. In a few cases the dense hot-pressed pellets were reequilibrated at higher temperature in the graphite tube resistance ("King") furnace used for the nitride equilibration experiments described below.

Temperature measurements were by 653nm Leeds and Northrup optical pyrometers sighting onto the top of the die through a quartz window in the chamber wall with corrections made for window attenuation determined empirically as less than 3° below 1300°C up to 25° at 2100°C. The optical pyrometers used were periodically checked against a pyrometer calibrated at the National Bureau of Standards using the 1968 International Practical Temperature Scale and small corrections were applied where necessary. Since the sightings were not into a blackbody cavity, emissivity corrections were made by the method of Battuelo and Ricolfi[30] using an emissivity of rough graphite of .79 at 653nm in the temperature range of these experiments.[31] These corrections ranged from +29° at 1500°C up to +48° at 2000°C but the uncertain character of the surface and

possible partial blackbody character of the chamber formed by the inner heat shield raises the question as to whether these corrections are called for. Large temperature gradients along the die, which is in a relatively small hot zone and is in good thermal contact with heat sinks in the form of the ram and base, are likely and introduce an additional uncertainty in the sample temperature. It is thus fortunate that the results of several temperature-dependence experiments indicate that the composition of the equilibrium alloy changes undetectably (by the analyses used here) when the equilibration temperature is varied by several hundred degrees. These results are consistent with the expectation that $\Delta\bar{H}_{M(MC)} \simeq \Delta\bar{H}_{M(M_xPl_{1-x})}$ at equilibrium, this since $\Delta\bar{S}_M$ should be small for each and $\Delta\bar{G}_M$ is, of course, the same for both at equilibrium. A net uncertainty in equilibration temperature of 100^o for the carbide-alloy systems is assigned but this apparently large value is acceptable in light of the small temperature-dependence of the equilibria being studied.

At the conclusion of the high-temperature, high-pressure equilibration of duration 1-5 hr. the power supply to the heating element was discontinued and rapid cooling of the sample ensued, a typical case being from 1900^oC to 1500^oC within 30 sec. and to 1000^oC within 150 sec. In light of the relatively sluggish solid-state diffusion involved and the small temperature dependence, as discussed above, this cooling rate is taken to be adequate to preclude any problems with significant reequilibration at lower temperature. As

detailed in the results section below, a few key runs were made beginning with M_xPl_{1-x} alloys richer in M than the equilibrium alloy to insure that equilibrium was being attained under the equilibrium conditions beginning with pure Pl. After removal from the die, the dense carbide-graphite-alloy pellet was polished down into the bulk with coarse SiC paper and then fine-polished with a 1 micron alumina-water paste on a felt polishing wheel. The phases were examined metallographically and their composition determined by X-ray diffraction and/or EPMA.

Analyses:

In Figure 7 is shown an optical micrograph of the polished surface of a typical carbide-alloy-graphite equilibrated pellet, here WC, graphite, and Os(.4at.%W) equilibrated at 1940°C. The presence of the carbide and graphite are easily verified by obtaining the X-ray diffraction patterns of their known crystal structures[42-46] but the composition of the equilibrium alloy can be obtained with reasonable accuracy by this approach only when it is an intermetallic compound of narrow composition range and known crystal structure. Such is the case for $HfIr_3$,[48] $ZrIr_3$,[49] $TaPd_3$,[90] $ZrPt_3$,[50] $ZrPd_3$,[48] and $TaIr_3$[48] which are all hexagonal $TiNi_3$-type ($ZrPd_3$, $ZrPt_3$), tetragonal ($TaPd_3$)

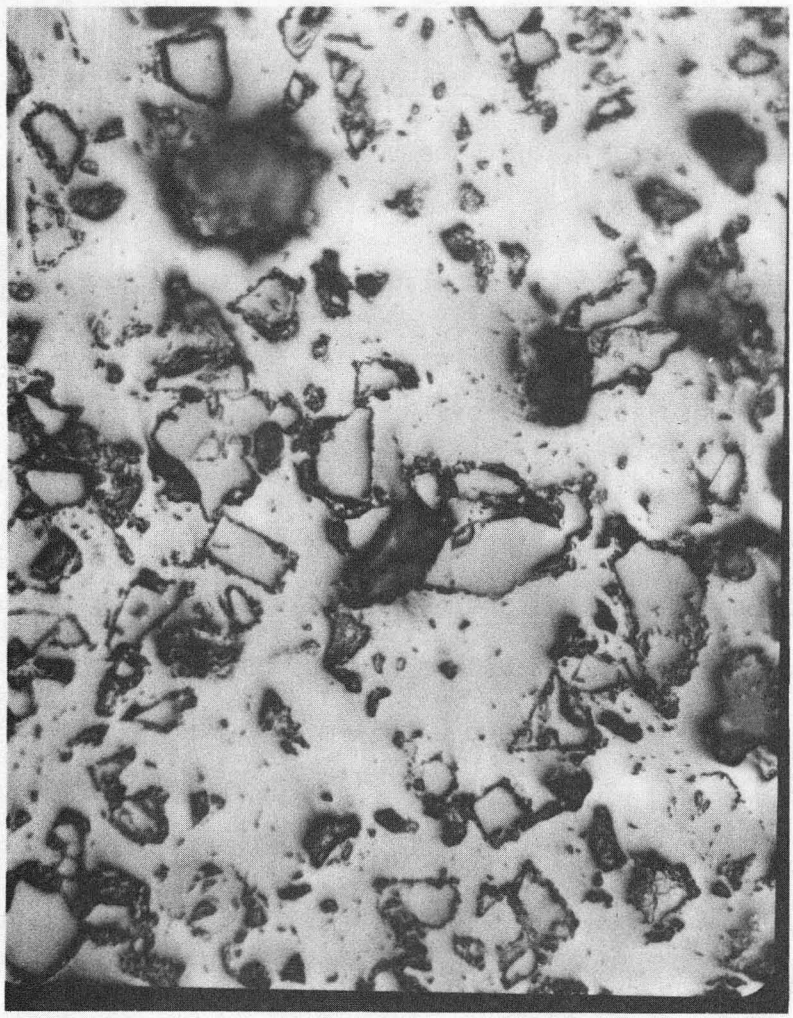

XBB 836-5394

100μ

WC — C — Os

Figure 7

or cubic intermetallics of compositional width ranging from about 6 at.% in the case of $TaIr_3$ at 1800°C[37] (see Fig. 5) to significantly less for $ZrPt_3$ in the same temperature range.[38] All of the X-ray diffraction patterns were obtained with a Picker X-ray diffractometer which records diffracted intensity vs. 2θ; FeK_α or CuK_α radiation was used.

The other equilibrium alloys were all terminal solid solutions in the platinum-group metal and were not readily amenable to quantitative analysis by X-ray diffraction though the lattice parameters should vary smoothly with composition. These systems were therefore analyzed by electron probe microanalysis (EPMA) using an eight channel A.R.L. instrument which is interfaced with a microcomputer and uses the MAGIC V program[51] to iteratively correct raw X-ray emission counts for absorption and fluorescence excitation of each line and average atomic number effects on electron energy loss and backscattering.[52] A LiF, ADP, or TAP crystal monochrometer was tuned to the L_α (K_α for Ti; the α_1 and α_2 lines could not be distinguished) emission energy of the element to be analyzed with the channel and a 20kV electron beam of a few microns diameter focused onto the region of the sample to be analyzed. As can be seen in Figure 7, a typical carbide pellet included grains of each of the equilibrium phases - dark graphite, metallic alloy, and bright carbide matrix - of adequate size for analysis without interference from adjoining phases. Background

counts for each element were obtained by the average atomic number method, whereby counts for the analyzed elements are measured from several elements of widely varying atomic number and the background from the unknown sample for each of the component elements is taken as an interpolation to the average atomic number of the unknown.

In all cases, 100% standards were used for each element analyzed. To check the accuracy of the analyses, and particularly the appropriateness of using pure standards for very dilute (e.g., <1 at.%) unknowns, several standard alloys were prepared and analyzed. Attempts were made to prepare dilute standards by hot-pressing but the pellets were found by metallography and EPMA to be inhomogenous. Even arc-melting failed to produce a homogenous 4 at.% Zr in Os alloy but other dilute alloys were prepared by this method. The results of the preparation and analyses of the standard alloys are presented in Table 3. Since the analyses of the dilute Zr(Ru) standards gave low values of X_{Zr}, the results for the unknowns containing dilute Zr in Ru were multiplied by a factor of 1.5 and an uncertainty of several tenths is assigned to the at.% of Zr. The EPMA results for the Nb(Os) and Zr(Ru) standards suggest that analyses of dilute alloys with 100% standards are not unreasonable but that an uncertainty of up to perhaps 50% of the analyzed concentration for the dilute element(s)

TABLE 3

Standard Composition	Preparation	EPMA Analysis
1 at.% Zr - Ru	hot-pressed, 1900°C — inhomogeneous	~100 at.% Zr + ~100 at.% Ru
2.9 at.% Nb - Os	hot-pressed, 2050°C — inhomogeneous	none
3.6 at.% Zr - Os	arc - melted	inhomogeneous
2.9 at.% NbH - Os	arc - melted	2.4 at.% Nb
3.3 at.% Nb - Os	arc - melted	3.4 at.% Nb
1.4 at.% Zr - Ru	arc - melted	1.1 at.% Zr
1.0 at.% Zr - Ru	arc - melted	0.5 at.% Zr
75 at.% Pd - Nb	arc - melted	78 at.% Pd
50 at.% Pd - Nb	arc - melted	52 at.% Pd
75 at.% Au - Zr	arc - melted	77 at.% Au
75 at.% Pd - Zr	arc - melted	78 at.% Pd
75 at.% Pt - Zr	arc - melted	73 at.% Pt
70 at.% Pt - Zr	arc - melted	72 at.% Pt
50 at.% Pt - Zr	arc - melted	48 at.% Pt
49 at.% Pt - Zr	arc - melted	50 at.% Pt

should be assigned. For the more concentrated alloys the standard analyzes results suggest an uncertainty assignment of perhaps up to ±3 at.% when 100% standards are used for elements in the concentration range of 25 to 75 at.%. Small corrections based upon the standard analyses can be applied in certain cases and there an uncertainty of ±2 at.% seems reasonable.

II. NITRIDE EQUILIBRATION

Goodman[53] carried out nitride equilibration experiments to establish the zirconium activity in a platinum-rich Zr-Pt alloy and obtained a result in conflict with the carbide experiments performed on this system by Brewer and Wengert.[22] The ZrN-Pt experiments have been repeated using a different method for alloy composition analysis with results in disagreement with the previous nitride work and in accord with the carbide studies. The nitride approach was also extended to several other acid-base transition metal alloys and to higher nitrogen pressures.

Theory:

The relevant aspects of the ternary phase diagram for the Zr-N-Pt case are shown in Figure 8. The analogy to the carbide equilibration approach is readily apparent, the key difference being that the main group element - nitrogen rather than graphite - is present as a gas whose pressure may be varied rather than as a solid of approximately unit activity. When the three phase equilibrium between nitrogen gas, the nitride MN, and the acid-base alloy M_xPl_{1-x} has been established, the acid metal activity (e.g., a_{Zr}) must be identical in each phase and is related to the standard free energy of formation of its nitride (e.g., ZrN) as shown at the bottom of Figure 8. The nitride is present as a relatively pure solid phase at equilibrium as established by EPMA analysis for contaminants (particularly the platinum-group metal) so that its activity is close to unity. Under the

Nitride Equilibration

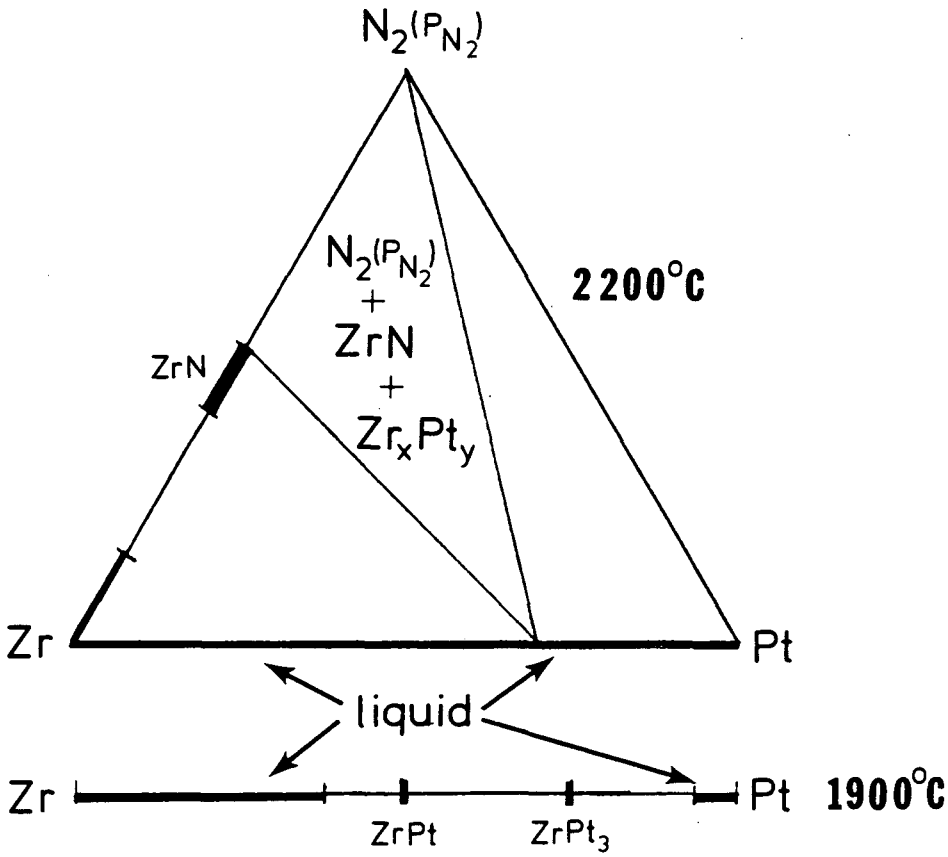

$$a_{Zr}^{gas} = a_{Zr}^{Zr_xPt_y} = a_{Zr}^{ZrN}$$

$$\Delta G_f^{\circ}(ZrN) = RT \ln a_{Zr} \cdot f_{N_2}^{1/2} \cdot a_{ZrN}^{-1}$$

$$\approx P_{N_2}^{1/2} \quad \approx 1$$

XBL 831-7639

Figure 8

experimental conditions of high temperature (>2000 K) and moderate pressure (<12 bar) the nitrogen fugacity, f_{N_2}, is very well represented by its pressure, P_{N_2}, as may be confirmed by use of the Berthelot equation of state[54] to estimate the ratio f/P:

$$\ln(f/P) = \frac{9}{128} \cdot \frac{T_c}{P_c} \cdot \frac{P}{T} \cdot \left(1 - 6 \frac{T_c^2}{T^2}\right).$$

With T_c = 126.20 K and P_c = 33.331 bar for N_2, this relation gives f/P = 1.0015 or f = 12.17 bar when P = 12.16 bar and T = 2000 K. Most equilibrations were carried out under conditions of higher temperature and/or lower pressure with f/P even closer to unity and any corrections to the measured pressures would be entirely negligible relative to other sources of uncertainty.

The primary advantage of this method over carbide equilibration is that the activity of M in its nitride, MN, may be controlled to some extent by adjusting P_{N_2}; the range of a_M available is actually rather limited due to experimental constraints on equilibrium nitrogen pressures coupled with the low order (square root) dependence of a_M on P_{N_2} and the results will make evident that variable composition studies of very stable alloys are not particularly amenable to this approach. High-temperature equilibration of a solid nitride with nitrogen gas introduces the possibility of appreciable but uncertain substoichiometry of the nitride and the resulting uncertainty in the relevant thermodynamic quantities. Under conditions of gas-phase equilibration it is impractical to continuously compact the reactants

as was done for the carbide experiments so these experiments were generally carried out at a high enough temperature that the equilibrium alloy was liquid so that it wetted and equilibrated with the solid nitride phase; these conditions increase the probability of significant nitrogen dissolution in the equilibrium alloy and perhaps of re-equilibration during cooling and further complicate analysis of the alloy composition which has been fixed by the acid metal activity.

In Table 4 are presented the selected thermodynamic quantities for the near stoichiometric nitrides along with the approximate uncertainty in a_M, δa_M, at 2300 K which does not consider possible additional error due to nitride substoichiometry. Low pressure (~0.1 bar N_2) equilibrations with TiN and ZrN resulted in homogeneously grey (rather than the usual yellow) pellets which is attributed to significant nitrogen substoichiometry of the nitrides since a similar color effect has been reported for certain of the corresponding substoichiometric carbides[55] and the oxygen pressure should have been very low (<<0.1%) due to the gettering effect of the hot graphite tube in which the equilibrations were carried out. Although the variation of x in MN_{1-x} with P_{N_2} and T has not been established for any of the nitrides used, their decomposition pressures have been determined and are compiled by Fromm and Gebhardt.[57] At a typical equilibration temperature of 2300°C the approximate decomposition pressures of the substoichiometric group IVB nitrides are as follows: 10^{-1} torr for $\delta TiN_{\sim.54}$, 10^{-2} torr for $ZrN_{\sim.94}$, and 10^{-3} torr for $HfN_{\sim.78}$.
As might be expected from its significantly reduced stability

TABLE 4

Nitride	$\Delta H^o_{f,298}$ (kcal)	$\Delta S^o_{f,298}$ (cal/K)	$\delta G^o_{f,2300\ K}$ (kcal)	δa_M, 2300 K	Ref.
NbN	-55.9±0.4	-21.4±1(est.)	±3	±.75a	33(ΔH^o_f (Nb_2O_5) from Ref. 36)
ZrN	-88.0±0.6	-23.1±0.3	±2	±.5a	38
HfN	-89.3±0.6	-22.1±1.5(est.)	±4	±1a	39
TiN	-80.8±1	-22.98±0.06	±2	±.5a	41

relative to the IVB nitrides, $\varepsilon NbN_{\sim 1.0}$ decomposes under 7600 torr N_2 at approximately 1400°C, $\gamma NbN_{\sim .82}$ decomposes under 10 torr N_2 at approximately 1500°C, and $\beta NbN_{\sim .52}$ decomposes to αNb(~14at.%N) under 10 torr N_2 at approximately 2200°C. Under the conditions of certain of these experiments the problem will clearly be most acute for NbN, possibly to the extent of decomposition to lower nitrides and even to αNb(N). Based upon the phase diagrams given by Fromm and Gebhardt[57] it seems certain that the 11 bar N_2, 2100°C equilibrations carried out on the group IVB nitrides with platinum involved only minimal substoichiometry and are reliable. On the other hand, even the 11 bar N_2, 2150°C run with NbN is suspect.

Some idea of the possible magnitude of the effect of substoichiometry on the thermodynamic quantities for equilibrations carried out under conditions of low nitrogen pressure and high temperature may be obtained by considering ZrN_{1-x} for which the enthalpy of formation has been determined as a function of stoichiometry[56]:

$$\Delta H^{o}_{298}(ZrN_x) = -48.3 - 40.5x \text{ kcal/mol} \qquad .78<x<1.$$

Ignoring the effects of a more favorable (less negative) $\Delta S^{o}_{298}(ZrN_x)$ as x decreases and the $a_{Zr(ZrN_x)} \propto P_{N_2}^{-x/2}$ dependence, both of which partially counteract the enthalpy increase, the above expression would imply a $\Delta G^{o}_{f,298}(ZrN_{.78})$ which is 8.9 kcal less negative than for the stoichiometric nitride. In the case of such a large increase in the free energy as this, the zirconium activity would be increased by approximately a factor of seven at typical equilibration

temperatures (ignoring also an unknown $\Delta[\Delta C_p]$). It proved impractical to analyze the equilibrated nitrides for small deviations from stoichiometry but, as mentioned above, the highpressure IVB nitride experiments should have involved minimal substoichiometry and are considered to be reliable to the extent indicated for the thermodynamic quantities given in Table 4.

The problem of nitrogen dissolution in the liquid equilibrium alloys is also expected to be minimal for the group IVB - Pt experiments but possibly more significant for those involving Nb. As with the carbide equilibrated alloys, it proved impractical to analyze for nitrogen contamination in the alloys but consideration of available data on the solubility of nitrogen in the pure metals and a couple of related alloys gives some indication of the probable extent of the effect for the systems studied. The solubility of nitrogen in liquid Hf at 2300°C is 4at.%N[58] and has been estimated at the same value for liquid Ti and Zr at the same temperature[59] but is about 20at.%N in liquid Nb at 2500°C.[60] Hansen, et al.[61] report that nitrogen is insoluble in Pd at 1400°C but no further information is available for the pure platinum group metals. No nitrides of the platinum group metals are known to exist and it is expected that the addition of Pt or Pd to the group IVB elements or Nb inhibits the solubility of nitrogen. The only pertinent alloy data available indicate that the activity coefficient of nitrogen in a 20at.% Re-Nb alloy is 6.3 times greater at 2500 K than in pure Nb[56] and, from Taylor and Doyle,[62] that:

$$\Delta\bar{H}_N(10\text{at.\% W-Nb}) = -40\pm2 \text{ kcal/g.at.N}$$

compared with

$$\Delta\bar{H}_N(\text{pure Nb}) = -46.2\pm2 \text{ kcal/g.at.N.}$$

It is clear that the addition of even small amounts of a group VIB or VIIB element to Nb significantly reduces nitrogen solubility and this effect is expected to be more pronounced upon moving further over in the periodic table to the platinum group metals. In fact, all of the equilibrium alloys studied by this method contained at least 67at.% of Pt or Pd and the extent of nitrogen dissolution in the liquids at the equilibration temperatures is expected to be minimal for the group IVB - Pt systems and small for the Nb-Pd alloys - certainly much less than the 20 at.%N reported for pure Nb at 2500^{o}C.

As reported below, the results of several experiments indicate that the temperature dependence of the alloy composition in equilibrium with the nitride and nitrogen is small relative to the uncertainty involved in the alloy composition analyses so that the relatively large temperature uncertainty is not manifested in the results. The uncertainty in the measured pressures is entirely negligible relative to the thermodynamic uncertainties reported in Table 4. Since the stoichiometric theymodynamic quantities were used an additional error to that given in Table 4 must be applied when significant substoichiometry is possible: i.e., for the low pressure (esp. <1 bar N_2) group IVB nitride runs and for all of the NbN runs.

Equilibration Procedures:

The starting materials and their purities are given in Table 2. The nitrogen gas was admitted to the furnace through a purification filter[63] which reduced its oxygen content to <0.1ppm and its water content to <0.5ppm. The platinum group metal before equilibration was in the form of 0.25mm or 0.51mm thick sheet of either the pure metal or a binary alloy richer in the nitride metal than the equilibrium alloy, this to confirm that equilibrium was being attained. To prepare the alloy discs an arc-melted button produced by the procedure described above was cut into ~0.5mm thick slices with a diamond wafering blade run at low r.p.m. through a lubricant reservoir.

The disc of pure platinum group metal cut from sheet or the slice of alloy button was rinsed in acetone and cold-pressed into the center of approximately 3gm of nitride power using 2wt.% naphthalene as a binder. An appropriate amount of naphthalene was added to a weighed quantity of the nitride powder and dissolved by the addition of an excess of anhydrous diethyl ether which was then vaporized while stirring to leave a thin coating of binder on the powder. About 2 gm of this powder was lightly packed into a 11.1mm diameter hard steel die and the pure metal or alloy slice followed by the rest of the nitride powder was placed on top. Uniaxially pressing at 6900 bar for 3 min. resulted in a pellet about 6mm thick, the surface of which was cleaned by gently grinding on SiC polishing paper. Finally, the nitride - metal pellet was placed in a vacuum oven at 180^{o}C for at least 1 hr. to vaporize the naphthalene.

A King-type furnace similar to that described by Brewer, et al.[64] and shown schematically in Figure 9 was used for all equilibrations. The graphite resistor tube is 1.27cm i.d. and is tapered in wall thickness to compensate for large heat losses through the ends and provides a 15cm long relatively uniform hot zone. At the maximum power input available of about 21kW (1.1kA; 19V) a temperature of approximately 2500°C was attained. For all runs, the graphite resistance tube was lined with 0.25mm thick tungsten sheet onto which the nitride pellet was placed; slight adhesion of the pellet to the liner sometimes occurred but the effect was superficial and tungsten contamination of the internal nitride or alloy was never detected by EPMA. Sublimation and/or vapor transport from the hot graphite tube and degassing (of H_2O, O_2, N_2, etc.) from the large mass of porous graphite heat shields necessitated that the furnace be operated under some backfill and for the low-pressure (~0.1 bar N_2) runs the furnace pressure was observed to drift up by several percent over the course of a few hour equilibration at >2000°C but it was not clear how much of this effect was due to heating of the shields and surrounding gas and how much to degassing.

At the start of each run the furnace was pumped down to less than 20μm of Hg as measured with a thermocouple vacuum gauge and the temperature increased to 1000 - 1100°C while maintaining this vacuum. Before increasing the temperature further, nitrogen gas was admitted to the system. Due to the effect of degassing it was not practical to operate at high temperature below about .1 bar of N_2. The lower

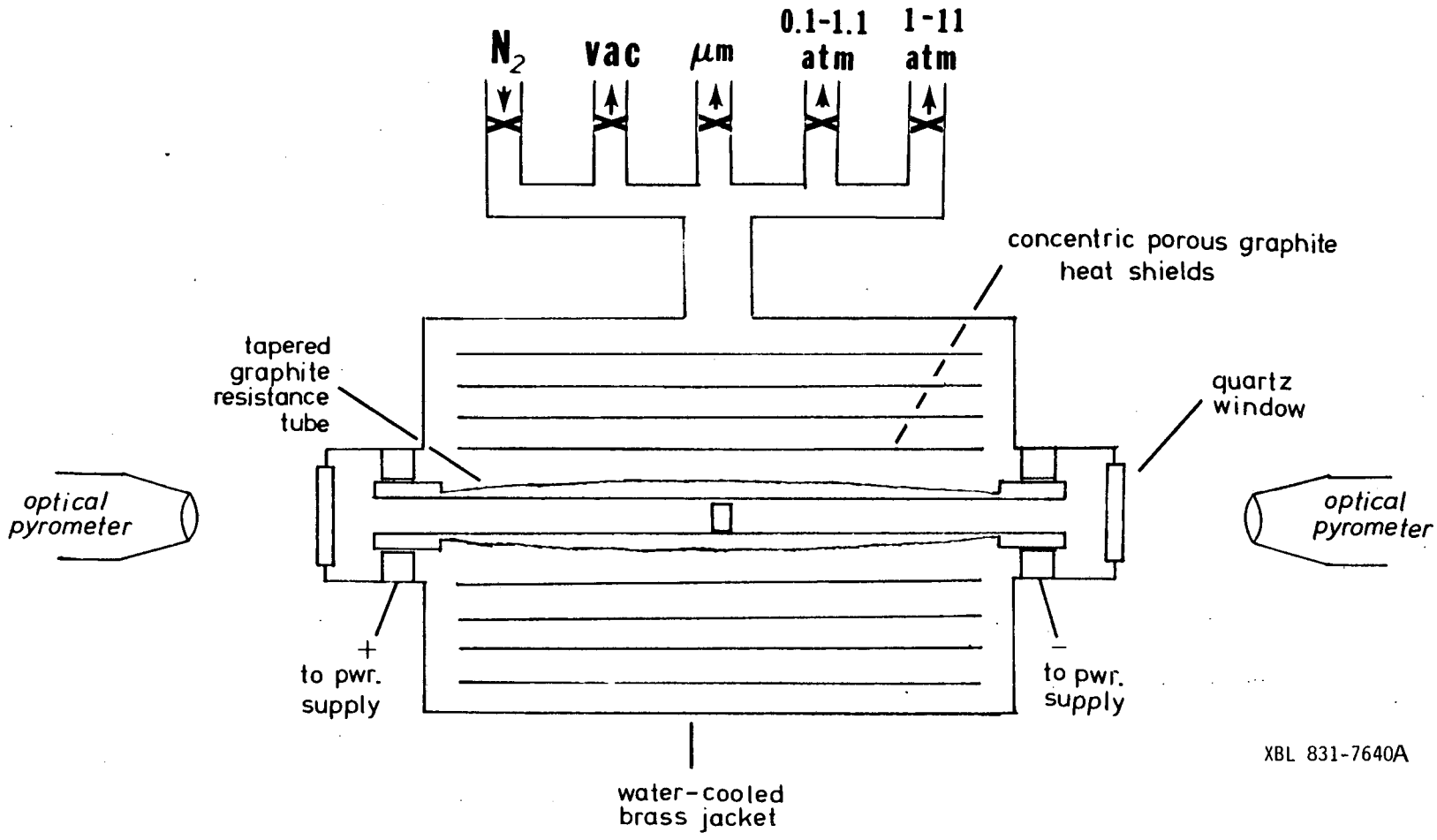
N_2
vac
μm
0.1-1.1 atm
1-11 atm
concentric porous graphite heat shields
tapered graphite resistance tube
quartz window
optical pyrometer
optical pyrometer
+ to pwr. supply
− to pwr. supply
water-cooled brass jacket
XBL 831-7640A

Figure 9

pressures (0.1 - 1.1 bar) were measured to ±2 torr with a mercury manometer which was protected by a dry ice in acetone cooled trap between it and the furnace and all measured heights were corrected to the density of mercury at $0^{o}C$. Pressures of greater than 1.1 bar (generally ~11 bar) were measured with a mechanical Bourdon-type gauge to ±0.03 bar. Since slight pressure drifts could occur, the pressure measured at the end of the equilibration period was taken as the equilibrium nitrogen pressure. For the 1.1 bar N_2 and lower pressure runs the furnace was isolated from the gas supply tank after bringing up to pressure but continual pressure decrease (i.e., leakage out of the furnace and/or manifold) for the ~11 bar runs necessitated maintaining a continual supply throughout through a 0 to 14 bar reducing valve in the gas line between the high-pressure tank and the furnace. As will be shown with results, the alloy composition is relatively insensitive to pressure variations in the range available so that the uncertainties involved in maintaining and measuring the nitrogen pressure have a negligible effect on the results. Its standard free energy of formation[40] predicts that 0.33 torr of CN(g) will be in equilibrium with 11.1 bar N_2(g) and graphite at 2500 K and small amounts of H_2 could result in significant quantities of HCN(g) but none was ever detected around the furnace or at the exhaust outlet by a methyl orange - mercuric chloride indicator.

Temperature measurements were with Leeds and Northrup 653nm optical pyrometers which were periodically checked against a standard pyrometer which was calibrated at the National Bureau of Standards using

the 1968 International Practical Temperature Scale. Sightings onto the surface of the pellet were made from both ends of the furnace through quartz windows for which attenuation corrections ranging from $+5^{o}$ at $1500^{o}C$ to $+25^{o}$ at $2500^{o}C$ were made. The temperatues measured on the two pellet surfaces separated by approximately 10mm differed by up to 100^{o} and by even more in a few extreme instances. The average of the two readings was taken as the equilibrium temperature and the difference between this value and the actual readings taken as a minimum uncertainty in the reported temperature. Although the character of the pellet surfaces were uncertain and variable, emissivity corrections were applied using the method of Battuelo and Ricolfi[30] and the emissivity values given for the nitrides by Touloukian and DeWitt.[31] These corrections ranged from $+31^{o}$ for ZrN at $1855^{o}C$ to $+77^{o}$ for TiN at $2370^{o}C$. In light of the large temperature gradients typically observed across the nitride pellets and the large emissivity corrections - which may not be called for given the generally rough pellet surfaces and the partial blackbody character of the hot containing tube - a temperature uncertainty of perhaps up to $\pm 100^{o}$ is typical. It is therefore fortunate that the results of several temperature dependence experiments discussed below show undetectable (by the analytical methods used here) variation in alloy composition with a several hundred degree variation in equilibration

temperature. This is taken to reflect a small $\Delta\bar{H}$ for the transfer of the acid metal from its nitride to the alloy which is in accord with the equilibrium condition ($\Delta\bar{G} = 0$) and the small $\Delta\bar{S}$ involved in such a solid-solid transfer.

Following an equilibraton period of 2 to 8 hours the power supply to the furnace was shut off and cooling of the sample ensued at a rate limited by heat transfer to the cold furnace walls. A typical pellet would cool from an equilibration temperature of 2000°C to 1400°C within 30 sec. and to below 1000°C within 150 sec. The equilibrium alloy composition of the alloys studied did not usually exist as a stable phase in the solid system so that segregation of the liquid to two solid intermetallics generally occurred. Although the nitrogen pressure dropped during the cooling period, transmission of the effect of this on the acid metal activity through the solid nitride to the alloy is not anticipated with these relatively rapid cooling rates. The relative temperature insensitivity of the equilibria studied suggests that the problem of reequilibration in the cooling liquid alloys should have been minimal and reequilibration in the solids should certainly have been severely diffusion limited.

After cooling, the equilibrated pellet was removed from the furnace, cut in half, and the cut surfaces polished on SiC paper followed by 1μ alumina-water paste on a felt polishing wheel. Optical metallographic examination and EPMA analyses were performed on the nitride and equilibrium alloy phases.

Analyses:

In Figure 10 is shown an optical micrograph of the surface of a typical equilibrated nitride-alloy pellet. In this case the bulk matrix is ZrN and the small metallic grains are the Zr-Pt alloy whose composition must be determined. The situation indicated with the phase diagrams in Figure 8 for the Zr-Pt system is typical of the systems studied in that the liquid metals are competely miscible but solidify into a two-phase mixture of intermetallics (e.g., ZrPt - $ZrPt_3$). An X-ray diffracton pattern of the solid alloy grains would show the existence of the two intermetallics but quantitative determinations of the amounts of each of the two phases would be necessary to establish the net composition of the equilibrium single-phase liquid. Such quantitative X-ray diffraction studies proved impractical with the equipment available so that all analyses of alloy compositions were done by the EPMA method described above (pp. 30-33).

The cooling rates for these experiments were rapid enough that each of the alloy regions visible in Figure 10 includes very small grains of both of the solid intermetallic phases. In fact, these individual intermetallic grains were generally smaller than the cross section of the EPMA electron beam (i.e., $<\sim 1\mu$) so that analysis of various locations showed variations about the average composition but not to the extreme of the compositions of the component intermetallic phases. The net composition of the equilibrium liquid alloy was taken as the average of several analyses taken at different points around the two-phase alloy particles.

XBB 836-5393

100 μ

ZrN – Pt

Figure 10

A more intractable problem involved interference in the analyses from the nitride phase. In the course of the equilibration the sheet of metal melted and crept into the surrounding matrix of nitride particles less than 78μ in diameter. As a result, the solid alloy particles generally had inclusions of the nitride phase which gave very high counts for the nitride metal when the electron beam impinged upon that region of the particle. To obtain accurate analyses of the isolated alloy the electron beam was focused to the best available resolution (~1μ) and the nitride metal counts (e.g., the Zr counts for the ZrN-Pt equilibrations) were minimized by scanning across the alloy particle. Only the lowest nitride metal composition analyses were used but the problem nonetheless necessitated the assignment of relatively large uncertainties to the net alloy compositions reported: up to ±4at.% in the worst cases.

III. KNUDSEN EFFUSION VAPOR PRESSURE

The vapor pressure of one or both components of several binary acid-base transition metal alloys has been determined by Knudsen effusion experiments using high-temperature mass spectrometry or thermogravimetry. Comparison of the partial pressures over the alloy with those over the pure elements provides a measure of the relative extent of bonding in the alloy. Both of these experimental methods have been used extensively by others, but for only a few of the very stable alloys of interest here.[65-67]

Background:

When a condensed and gaseous phase are in equilibrium the chemical potential of a species M must be identical in both phases and is related to its fugacity by:

$$\mu_{M(condensed)} = \mu_{M(gas)} = RT\ln f_M \approx RT\ln P_M$$

As indicated, the fugacity is very well represented by the partial pressure under the molecular flow conditions of Knudsen effusion experiments. The thermodynamic activity of the component M in the condensed phase is obtained by comparison with its pressure over the standard state phase:

$$RT\ln a_M = \mu_{M(alloy)} - \mu_M^o = RT\ln(f_{M(alloy)}/f_M^o) \approx RT\ln(P_{M(alloy)}/P_M^o)$$

$$\text{or, } a_M \approx P_{M(alloy)}/P_M^o$$

The Raoult's Law standard state is used here so that P_M^o represents the equilibrium pressure of M over the pure condensed element.

In a Knudsen effusion experiment the partial pressure of a component in a cell is related to its flux into a vacuum through a well-defined orifice in the cell wall. The Kinetic Theory of gases gives the mass flux of a component M of an ideal mixture across an area A in terms of its partial pressure P_M, molecular weight M_M, and the temperature T as:[68]

$$dw/dt_{(gm/s)} = 44.32\ P_{M_{(atm)}} \cdot A_{(cm^2)} \cdot (M_{M_{(gm/mol)}} \div T_K)^{1/2}$$

Knudsen[69] established that this molecular effusion formula accurately represents the flux through a thin-edged orifice under conditions of low pressure so that the gas is behaving ideally and the species have relatively long mean free paths and are thus effusing essentially independently. Carlson, et al.[70] established that the molecular flow description was entirely valid for saturated Hg vapor effusing through a 0.04cm diameter orifice up to a pressure of 0.07 torr at 345 K. Using the metallic diameter[71] to approximate the gas phase collision diameter and the standard collisional cross section ($\sigma = \pi d^2$) and mean free path ($\lambda = kT/\sigma\sqrt{2}P$) expressions[72] this result implies molecular flow behaviour if $\lambda/D > 3$ for Hg at 345 K where D is the orifice diameter. In the fully hydrodynamical flow regime (>7 torr Hg) it was found that the apparent pressure was greater than the actual equilibrium vapor pressure by a nearly constant factor of

1.65 implying greater loss due to cooperative flow of the the non-independent effusing species. The valid experiment closest to hydrodynamical behaviour performed here involved Pd vapor at 0.08 torr and 2000 K effusing through a 0.24cm diameter orifice. In this case the value of λ/D was approximately 3.4 and the much higher temperature relative to the Hg experiments should certainly have reduced the effect of collisions since a large kT will diminish the influence of the interatomic potential. Although this treatment is somewhat qualitative it seems highly probable that the molecular flow equations describe the conditions of these experiments.

Application of the Kinetic Theory equations to effusion through an orifice to obtain the equilibrium vapor pressure(s) above a condensed phase assumes that there is no resistance to flow from the cell into a perfect vacuum and that the cell is saturated with the equilibrium vapor species. Information concerning resistance to gaseous flow from a Knudsen cell is commonly contained in Clausing factors[73] and any resistance is usually dominated by the finite width of the orifice edge. Except for the mass spectrometric experiments which included internal calibration for this and other effects the orifice edge width was generally on the order of 10% and always less than 20% of the orifice diameter (see Fig. 12) and a Clausing factor of close to unity was assumed. The vacuum outside of the cell was always maintained at 10^{-4} torr or less during experiments implying a mean free path of at least 1m and negligible chance of reflection back into the cell - i.e., effectively a perfect vacuum.

The assumption of a saturated vapor space is valid as long as the sample surface area is at least as large as the orifice area and the vaporization coefficient, α_v, is close to unity. The first condition was observed to hold for all experiments and the second is taken to be valid for the substances studied. For species which require a large activation energy to form on the condensed phase surface before entering the gas phase - such as P_4 vaporizing from red phosphorous[85] - α_v can be very small, but the vaporization coefficient for atomic metal species vaporizing from metal surfaces, as studied here, is generally close to unity.[73,86] Dreger and Margrave,[74] for example, performed Langmuir sublimation studies on solid Pd and obtained vapor pressures for Pd(g) very close to those from equilibrium studies[75] which implies a value for α_v close to unity.

When working with incongruently vaporizing multicomponent systems the possibility of depletion of the more volatile species from the solid surface must be considered. This was checked for several alloys by obtaining an EPMA composition profile of a partially vaporized solid and by checking for continuity in partial pressure upon passing through the alloy liquidus; no significant surface depletion effects were detected, implying that diffusion of Pd from the bulk solid alloy to the surface was rapid relative to vaporization of Pd. One more complication is the possibility of molecular species (such as Pd_2 or NbPd from a Nb-Pd alloy) making a significant contribution to the

total-weight-loss experiments. That such species were making a negligible contribution is rather certain for the homoatomic molecular species[87-89] and was confirmed for the heteroatomic (and homoatomic) species over the Nb-Pd system using the mass spectrometer. For the other systems it was assumed that molecular species were making a negligible contribution to the total weight loss.

After assuming a vaporization coefficient and Clausing factor close to unity, a relatively small molecular species pressure (e.g., less than 1% of the total pressure), and molecular flow behaviour, the total effusion rate from a cell may be related to the pressures of the atomic species. In particular, if one component (e.g., Pd) is much more volatile than the other component (e.g., Nb) of a binary alloy the mass flux may be related to the partial pressure of the volatile monomer by the Kinetic Theory expression given above (p. 52). All of the acid-base alloys studied by the thermogravimetric method were of a volatile component (Pd, Au, or Ti) with a relatively nonvolatile component (Nb, Zr, Ta, Hf, or Ir) and the total mass loss was taken to be due to monomeric species of the volatile component so that its pressure and activity in the alloy were obtained. The pure condensed phase vapor pressures of the two elements were always separated by at least four orders of magnitude and the alloys were approximately 75at.% in the more volatile component (keeping its activity relatively high) so that the rate of mass loss should have been entirely dominated by the volatile species.

Knudsen effusion methods depend upon a measurable material loss and the thermogravimetric method in particular depends upon a weighable loss so that appreciable composition changes may occur during an experiment. Since all alloys studied were rich in the primary effusing species composition changes were generally small (a few at.%) but are reported with the results. To obtain the relatively large losses required for this method, rather large orifices (e.g., 0.24cm diam.) were utilized; the high α_v and adequate sample surface area permitted this convenience. Except for the single successful Ti effusion experiment the effusing species was relatively inert Pd or Au so that gas - cell wall chemical interactions which can cause deviations from cosine law effusate distribution and a reduction in total effusion[76] should have been minimal.

Mass Spectrometric Experimental Background:

The mass spectrometric method is based upon monitoring only that portion of the effusing gas which is ionized by an electron beam intersecting its path. The various ionized species are mass selected with the mass spectrometer and their relative intensities measured with an ion detector/electron multiplier system. A calibration constant, k_M, is necessary to obtain the pressure of M in terms of its measured ion current, I_M^+:[77]

$$P_M = k_M I_M^+ T$$

The calibration constant is different for each species and depends upon geometric and material features of the Knudsen cell (i.e., the Clausing factor), alignment of the cell with the mass spectrometer ion source, and variable instrument sensitivity so that a calibration constant was determined at the start of each run after alignment but before taking data on the alloy. The calibration method used here involved monitoring the vaporization of pure Ag(s,1) which completely vaporized before the vapor pressures of the alloy components became appreciable. The ion current intensities for both Ag(g) and $Ag_2(g)$ were monitored at several temperatures. Insertion of I^+_{Ag}, the measured temperature, T, and the known vapor pressure of Ag(g) over Ag(s,1), P^o_{Ag},[75] into the above expression yields k_{Ag}. This assumes unit Ag(s,1) activity which is valid provided that the calibration is carried out at a low enough temperature that reaction with the cell or sample has not occurred.

When both the monomer and dimer intensities were measured at the same temperature their ratio could be used in conjunction with available thermodynamic data on the Ag/Ag_2 equilibrium to obtain the calibration constant through:[78]

$$k_{Ag} = \frac{\sigma_{Ag}\gamma_{Ag}I^+_{Ag_2}E^2_{Ag}n^2_{Ag}}{\sigma_{Ag_2}\gamma_{Ag_2}(I^+_{Ag})^2E_{Ag_2}n_{Ag_2}T} \cdot \exp[(-D^o_0 - T\Delta\,[G^o_T - H^o_0]/T\,)/2.303RT].$$

where σ_i is the ionization cross section, γ_i is the detector multiplier gain, n_i is the isotopic abundance (see Table 5), and E_i

TABLE 5

Species	Isotopic Abundance[83]
Ag^{107}	51.817%
Ag^{109}	48.183%
Ag_2^{214}	26.850%
Ag_2^{216}	49.934%
Ag_2^{218}	23.216%
Pd^{102}	0.96%
Pd^{104}	10.97%
Pd^{105}	22.23%
Pd^{106}	27.33%
Pd^{108}	26.70%
Pd^{110}	11.81%
Nb^{93}	100.00%

is the ionization efficiency at the operating ionizing electron energy relative to the maximum efficiency. The calculated σ_i from Mann[79] were used and it was assumed that $\sigma_{Ag} = 1.5\sigma_{Ag}$ [80] (this approximate value is based on experimental results for other diatomics). It was not possible to measure γ_{Ag} due to rapid Ag(g) vaporization at the high pressures/temperatures necessary to make this measurement so it was assumed that:[81]

$$\gamma_{Ag_2}^{218} = \gamma_{Ag}^{107} \cdot [107/218]^{0.4}$$

All measurements were made with an ionizing electron energy of 20eV which was found to be very close to the ionization efficiency maximum for all species monitored so the E_i were taken as unity. The dissociation energy, D_0^o, and free energy functions for Ag_2 are from Hilpert and Gingerich[82] while the free energy functions for Ag are from Hultgren, et al.[75]

There are clearly rather large uncertainties in several of the parameters (σ_i, γ_i, and the thermodynamic quantities) necessary to use the Ag/Ag_2 method to obtain a calibration constant and the value of k_{Ag} so obtained may be uncertain by up to a factor of two. The primary motivation for including the dimer measurements was to check the generally more reliable vapor pressure calibration and in particular the assumption of unit silver activity. The reasonable agreement between the calibration constants obtained by the two methods is encouraging and the k_{Ag} values are considered to be accurate to within significantly better than a factor of two.

The pressure calibration constant for another species, Pd for example, was obtained from that for Ag by:[77]

$$k_{Pd} = k_{Ag} \cdot \left[\frac{\sigma_{Ag}}{\sigma_{Pd}} \cdot \frac{\gamma_{Ag}}{\gamma_{Pd}} \cdot \frac{E_{Ag}}{E_{Pd}} \cdot \frac{n_{Ag}}{n_{Pd}} \right]$$

where the symbols have the same meaning as above. The γ_i were measured, the E_i were again close to unity, and the n_i are accurately known isotopic abundances given in Table 5. The σ_i were taken from Mann[79] and though their absolute uncertainties are rather large (perhaps a factor of two) the ratio uncertainty is small - particularly for such similar elements as Pd and Ag. Thus the net uncertainty in the Pd pressure calibration constant (also that for Nb although no useful results were obtained for Nb(g)) is only slightly greater than that associated with k_{Ag}, and k_{Pd} is taken to be valid to within better than a factor of two. All of the calibration constants obtained are presented below with the results.

Among the advantages of the mass spectrometric method is that no assumptions regarding the nature of the effusate need be made since its composition may be established; that the Pd^+ intensity was seen to be several orders of magnitude greater than that of Nb^+ or any diatomic species for even the Nb-rich Nb-Pd alloy partially motivated the weight loss experiments which were to follow. Other advantages are the extreme sensitivity of the mass spectrometric technique, the internal calibration for non-unity Clausing factors and/or deviations from a cosine distribution of effusate, and the ability to obtain pressures over a wide temperature range in a relatively short period

of time. It also proved beneficial to follow I^{+}_{Pd} through the alloy liquidus to ensure, through continuity, that solid-state diffusion was not limiting.

The particular aspects of the temperature measurements used for these experiments are described below, but for purposes of establishing an approximate overall uncertainty in the results a typical temperature error of $\pm 25^{o}$ at 1800 K is considered. For pure Pd with $\Delta H^{o}_{v,1800} = 87.5$ kcal[75] such an error translates into a $\pm 1.4X$ variation in the measured pressure. The actual uncetainty in the mass spectrometric temperature measurements in particular is probably somewhat less than 25^{o} at even the highest temperatures attained; the uncertainty in the thermogravimetric temperature may be somewhat greater than 25^{o} in general. Since the calibration constant, k_{Ag}, was obtained under experimental conditions it partially compensated for any systematic temperture measurement errors and random errors (i.e., pyrometer reading errors) were largely removed by many pressure-temperature values being taken. An uncertainty in the reported pressures of approximately $\pm 2X$ is assigned for all of the Knudsen effusion experiments but this quantity is dominated by temperature uncertainties (of typically $\pm 30^{o}$ as discussed below) for the thermogravimetric runs and by calibration constant uncertainties (which partially compensate for inherent temperature uncertainties) for the mass spectrometric runs.

Obtaining an activity from a measured vapor pressure requires knowledge of the vapor pressure over the standard state - here the pure element - and the values given by Hultgren, et al.[75] were used. Most of the results give a Pd activity and several attempts were made to measure P^{o}_{Pd} by the thermogravimetric method but the uncertainties involved rendered the values obtained significantly less reliable than those available from work performed by others. The uncertainty in the P^{o}_{M} reported in the literature for the elements monitored here is perhaps 10 - 30% so that the net possible error in the reported activities is only slightly greater than the ±2X value assigned to the measured pressures.

Procedures:

A. Mass Spectrometric

The three Nb-Pd alloys studied were prepared by arc-melting 99.99% Pd rod and 99.97% Nb rod (both M.R.C. MARZ grade) by the procedure described above. The arc-melted button was cut with a SiC blade into pieces small enough to fit into the Knudsen cell. EPMA was used to confirm the pre-run alloy compositions as well as to establish the composition at the end of each run; the procedure described above (pp. 30-33) was used. For each run, 300-500 mg of alloy was used.

Depending upon the alloy composition the Knudsen cell was machined from >99.7% graphite (Union Carbide CS grade) or from 99.8% NbC (Cerac -325 mesh powder) which had been hot-pressed into slugs at 1600°C

and 490 bar for 2 hr. using the hot-press described above. Graphite cells were used for the 18at.% and 50at.% Nb-Pd systems since the a_{Nb} were expected to be lower than $a_{Nb(NbC)}$ and a NbC cell was used for the 80at.% Nb-Pd sytem. The first (18at.% Nb-Pd) experiment was performed with a 0.102 cm diam. orifice but the later runs were with 0.254 cm. diam. orifices in hope of attaining greater sensitivity to the more refractory Nb component. Since the ~0.005 cm. thick orifice edge used for the first run showed slight indications of attack and orifice enlargement the subsequent runs were carried out with sturdier ~0.05 cm. thick orifice edges; any resistance to flow resulting from this thickness was accounted for with the silver calibraton. Although the particular cell diagrammed in Figure 12 was for a thermogravimetric experiment, the shapes of all Knudsen cells used were identical to this. For the mass spectrometric experiments the cell was placed into a tantalum holder which included a 0.051 cm. diam. X 0.152 cm. deep blackbody hole in the center of its bottom and three support holes; the design of the Ta cell-sheath was such that it did not interfere with the vapor effusion.

The high-temperature mass spectrometer used was a Nuclide 12-90HT and is shown schematically in Figure 11 and described by Gingerich.[84] Temperature measurements were with a calibrated Leeds and Northrup optical pyrometer sighting through a quartz prism and shutter-protected window into the blackbody hole in the bottom of the Ta cell-sheath. The inductively wound tungsten (thoriated) heating element extended

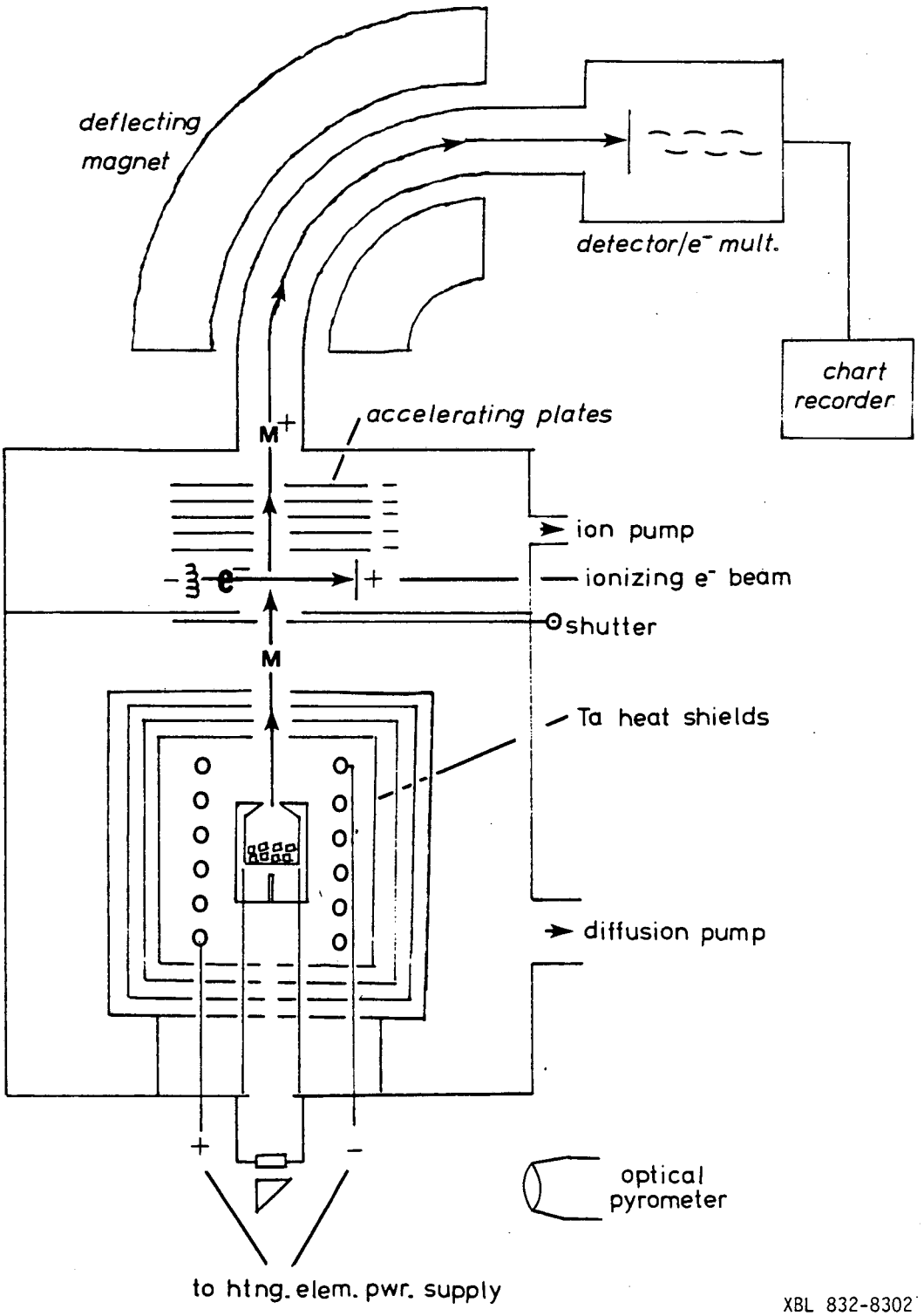
deflecting magnet
detector/e⁻ mult.
chart recorder
accelerating plates
M+
ion pump
ionizing e⁻ beam
shutter
M
Ta heat shields
diffusion pump
optical pyrometer
to htng. elem. pwr. supply
XBL 832-8302

Figure 11

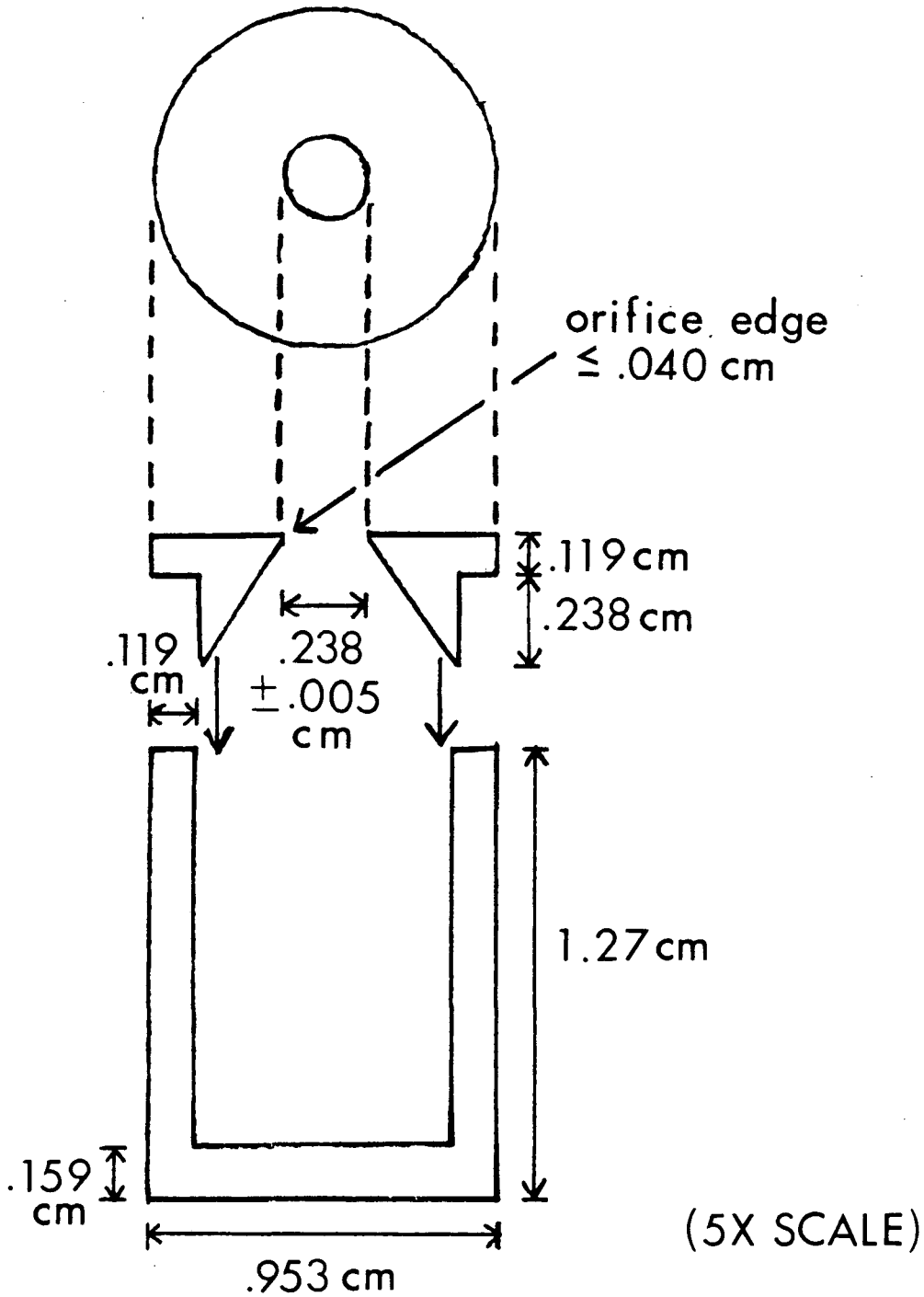

XBL 836-10319

Figure 12

well beyond the ends of the cell to reduce the possibility of large temperature gradients along the cell. The extent of the gradient problem had previously been checked for this configuration by sighting simultaneously onto the top and bottom of the cell with the optical pyrometer and the difference in the two measured temperatures was less than 10^{o} up to 2350 K.[84] The inherent uncertainty in the pyrometric measurements combined with the window and prism corrections leads to a measurement uncertainty of $\pm 10^{o}$ up to 2000^{o}C. Since the blackbody hole was situated close to the sample its temperature is considered to be relatively representative and a gradient uncertainty of $\pm 10^{o}$ is assigned yielding a net temperature uncertainty of $\pm 20^{o}$ up to 2000^{o}C though, as mentioned above, this uncertainty is at least partially compensated for by the internal calibration procedure. The power supply provided a maximum sample temperature of 2300^{o}C (at ~19V and ~200A) but the results above 2000^{o}C were not particularly useful.

The system was differentially pumped such that pressures of $<10^{-6}$ torr in the Knudsen cell region, $<10^{-7}$ torr in the ion source region, and $<10^{-8}$ torr in the analyzer region (all measured with ionization gauges) were maintained throughout. At the start of each run, before calibration, the horizontal position of the cell was externally adjusted to maximize I^{+}_{Ag}. All measurements were made with an ionizing electron energy of 20eV and ionization efficiency curves showed this value to be very close to the efficiency maximum

for all of the primary species monitored. The ion accelerating voltage was held constant at 3kV and the various mass to charge species selected by adjusting the magnetic field. When the ion intensity was adequate the electron multiplier gain was measured directly by simultaneously monitoring the outputs from the 50% transmission grid and the 20 stage Cu-Be dynode multiplier.

All ion intensities were taken as the difference between the recorded electrometer output with the shutter fully open to that with it fully closed. At any given temperature the intensity was allowed to come to a constant value before assuming that the equilibrium pressure had been attained - this generally took a few minutes from the time of heater power input increase/decrease. Mass scans and ionizaton efficiency determinations were frequently performed to confirm the identity of all species monitored. Different isotopes were monitored depending upon the ion intensity: Pd^{106} (27 isotopic %) at low Pd(g) pressures or Pd^{102} (1 isotopic %) at high Pd(g) pressures, for example.

The calibration consisted of vaporizing approximately 10 mg of pure Ag wire and monitoring I^{+}_{Ag} and $I^{+}_{Ag_2}$ at several temperatures in the temperature range 1050 - 1400 K (Ag m.p. = 1234 K). Before increasing the temperature further all of the Ag was vaporized out of the cell as established by its vanishing signal. The pressure of Pd(g) could be monitored down to 1410 K for the 82at.% Pd-Nb alloy ($P_{Pd} = 7 \times 10^{-9}$ atm.) and up to 2150 K for the 20at.% Pd-Nb alloy

(P_{Pd} = 4 X 10^{-6} atm.) The maximum pressure measured was 2 X 10^{-2} atm. Pd(g) over the 82at.% Pd-Nb alloy. The refractory nature of Nb made it impossible to obtain an I^{+}_{Nb} below 2144 K (P_{Nb} = 2 X 10^{-9} atm.) for even the 80at.% Nb-Pd alloy and the Nb results were not particularly valuable since severe Pd depletion was occurring at such high temperatures from the already Pd-dilute alloy. The alloy liquidus for the 82at.% Pd-Nb system was reproducibly established by a halt in the I^{+}_{Pd} vs. time plot which reflected the latent heat of melting. All of the results are presented and discussed below.

It generally proved impossible to cleanly separate the cell assembly frm the tungsten support rods at the end of a run due to partial fusion. This precluded accurate reweighing and calibration by integration of the I^{+}_{Pd} vs. time plot. In the case where the alloy remained solid (50at.% Nb-Pd) the pieces were removed from the cell and polished on SiC paper followed by 1μ alumina-water paste. Where the alloy had melted the cell was cut longitudinally in half with a diamond wafering blade and the exposed alloy/cell surfaces polished as above. The residual alloys were compositionally analyzed alongside pieces of the unused starting alloys by the EPMA procedure described above. The results showed severe depletion in two cases (80at.% Nb-Pd; 18at.% Nb-Pt, in the latter case due to prolonged operation at elevated temperature after taking the data reported here) and negligible depletion or compositional gradients in the third case (50at.% Nb-Pd).

B. Thermogravimetric

The alloys were prepared as above but pulverized to a very coarse powder/gravel in a hard steel die rather than cut into pieces since smashing proved easier and quicker than sawing for these adequately brittle alloys. The starting materials for the alloys were as follows: 99.99% Pd rod and 99.97% Nb rod supplied by M.R.C.; 99.97% Ti rod and 99.97% Hf rod supplied by Noah; 99.94% Zr rod supplied by Johnson-Matthey; 99.9% Ta foil supplied by Alfa; >99.9% Ir wire supplied by Engelhard; and 99.99% Au wire from LBL stock. Most of the cells were of >99.7% C CS grade graphite supplied by Union Carbide although several were of >99.99% C ECV grade graphite also supplied by Union Carbide; the extreme porosity of the very high purity material made it unsuitable for certain liquid alloy runs. A few runs were with graphite cells which had been internally vapor coated with a 1-10μ layer of Nb or Ti and fired empty at ~1900^{o}C for at least 1 hr. before using. Cups of 99.9% W or 99.8% Al_2O_3 were used inside of graphite Knudsen cells for a few runs. Other effusion experiments were with cells made of 99.8% Al_2O_3, 97% ZrO_2 (CaO stabilized), or 99.5% ThO_2. The motivation for this variety of cell materials was to minimize interaction of the alloy, especially when a liquid, with the container material and/or to avoid creep of a liquid alloy up the cell walls and possibly out through the orifice. The EPMA method described above was used in several cases to investigate for both of these complicating effects by analyzing the inside of the cell at the alloy-container interface and analyzing the outer surface

of the cell lid for signs of bulk creep. The particular material used for each run and the results of these analyses are presented below with the experimental results.

The basic design of all of the cells was as shown in Figure 12 though the exact dimensions varied from cell to cell and the taper of the lid to the orifice was somewhat less for the oxide cells. For a few runs a liner cup of W or Al_2O_3 was inserted into the cell and extended about two-thirds of the way up the cell interior. Most experiments were with orifices in the range 0.229-0.305 cm. diameter but a few were with 0.508 cm. diameter orifices; all diameters were measured to ±0.005 cm. As discussed above, the orifice edges were thin enough that negligible resistance to effusion was assumed - i.e., a unity Clausing factor. The only successful experiment on a Ti alloy was carried out in a ThO_2 crucible for which no lid was available so that its inside diameter of 1.080 cm. was taken as the "orifice diameter." The validity of this run in particular and possibly other of these effusion experiments with large orifices depends upon an adequate alloy surface area (which was observed to be the case) coupled with a high vaporization coefficient for the monatomic metal species of interest (which was assumed, as discussed above).

All of the thermogravimetric experiments were carried out using the hot-press furnace shown in Figure 6 but with the Knudsen cell(s) in place of the graphite die and the hydraulic ram raised. Four 0.952 cm. o.d. or two 1.27 cm. o.d. graphite Knudsen cells were slip-fitted into a graphite cell holder which was then placed inside of the

tungsten heating element. The 25 cm. tall holders were only slightly shorter than the 30 cm. high heating element and the cell tops were slightly recessed below the top of the cell holder. This design was intended to allow running a cell containing pure Pd or Au alongside alloy containing cell(s) but the vaporization of liquid Pd or Au from a graphite container gave results which suggested a vapor pressure up to an order of magnitude lower than the known equilibrium value; the possible causes of this low vaporization coefficient effect are discussed below. The pure metal containment problem as well as temperature gradient difficulties necessitated using the literature values for P^o_{Pd}, P^o_{Au}, and P^o_{Ti} rather than internally established values but running two or more alloys simultaneously provided somewhat more reliable relative activities for systems studied together. Since the oxide cells were significantly larger, only one was placed in the center of the hot zone for a run; several shielding configurations were utilized for some of these runs to reduce temperature gradients and provide reliable P^o_{Pd} values. Although the agreement was reasonable (confirming that the low P^o's from graphite were due to a container problem and not to an inherent flaw in the experimental technique) the literature values were eventually taken to be more accurate. The amount of heat-shielding used above the cells was limited to provide a free effusion path and a line of sight into the cells for optical pyrometric temperature measurements. This lack of top shielding coupled with a relatively short hot zone caused severe radiative losses from the lid such that its temperature was often up to

100^{o} lower than that of the cell interior and in a few cases as much as 200^{o} lower. These severe temperature gradients frequently caused condensation of the volatile alloy component onto the inside of the lid but given the adequate vaporizing surface areas and the large vaporization coefficients the amount of flow through the orifice should not have been appreciably affected by partial internal condensation onto a cold region. The temperature for which the pressure was determined was thus taken as that of a cell interior and the condensation problem was ignored provided that it was not so severe as to partially block the orifice and/or significantly alter the bulk vaporizing alloy composition.

All Knudsen cells were weighed before and after each experiment to ±0.05 mg. although such accuracy proved excessive given other experimental uncertainties. Blank runs showed a weight loss from empty cells in the range 0.5–2 mg. and a small correction of ~1 mg. was accordingly made to weight loss results from alloy-containing cells. Details are presented with the results, but typical runs began with 1 - 2 gm. of alloy or pure metal and involved a loss of 10–100 mg. Smaller losses provided inadequate accuracy given the blank cell loss values and larger losses resulted in significant compositional variation and probably partially hydrodynamical flow conditions at the high pressures necessary to complete a run in a reasonable amount of time. Runs were from 1 to 25 hours in duration and the temperature was increased and reduced rapidly enough that virtually all vaporization occurred at the reported plateau temperatures. An ionization gauge in

the furnace indicated a vacuum of at least 10^{-4} torr during all runs and that the system was operating at less than 10^{-3} torr was confirmed with a mercury McLeod gauge.

Temperature measurements were with calibrated Leeds and Northrup optical pyrometers sighting into the Knudsen cell (which was taken to be close to a blackbody cavity) through an attenuation-calibrated quartz window in the furnace wall. The pyrometer manufacturer reports an uncertainty of up to $\pm 8^{o}$ in the temperature range of these experiments and the pyrometers used were calibrated to better than this accuracy against a pyrometer which had been calibrated at the National Bureau of Standards using the 1968 International Practical Temperature Scale but a net measurement error of $\pm 15^{o}$ is considered reasonable in light of the window corrections which ranged from negligible below $1300^{o}C$ to $+15^{o}$ above $1700^{o}C$. The possibility of vertical and/or horizontal temperature gradients within an individual cell leads to a net temperature uncertainty assignment of $\pm 30^{o}$ for most experiments which proved to be the dominant experimental uncertainty factor. To obtain some indicaton as to the possible extent of vertical temperature gradients a blank run was performed without cell lids; although the cell top to cell bottom gradients were up to 35^{o} with the top always colder, this effect undoubtedly reflected the large radiative heat losses from the top of the lidless cells and the bottom to middle differences of only up to about 15^{o} are taken to better reflect the situation under experimental conditions. Horizontal gradients from cell to cell across the cell holder were often up to 50^{o} but the

effect within a given cell should have been much smaller. The above discussion and the net temperature uncertainty of up to $\pm 30^{o}$ applies only to the graphite cells in a holder - the Al_2O_3-cell-with-lid experiments are assigned a temperature uncertainty of $\pm 40^{o}$ and the ThO_2- or ZrO_2-cell-without-lid experiments an uncertainty of $\pm 50^{o}$, this due to more significant temperature gradients within these larger cells and radiative losses/nonblackbody conditions for the lidless cells. Agreement between a W-Re thermocouple placed into a hole drilled in the top center of a cell holder and the pyrometric readings into the Knudsen cells to within 15^{o} during a trial run is considered good given the large temperature gradients typically observed across the cell holder. To protect the quartz window from being coated with effusate it was protected with an externally controllable shield between the brief pyrometer reading periods.

Since running two different alloys in adjacent Knudsen cells simultaneously removed at least some of the temperature measurement uncertainty on a relative basis - this was part of the motivation for the unsuccessful attempts at including internal calibration cells which contained the pure metal - the relative temperature uncertainty is taken as $\pm 20^{o}$ for alloys run together. The various temperature uncertainties assigned result in the following variations in pressure (given for the pure elements using the values of Hultgren, et al.[75] but approximately applicable to the partial pressure over the alloys studied) at typical experimental temperatures:

$\pm 30^{o} \longrightarrow P_{Pd}$ ±1.5X at 1800 K (absolute uncertainty)

$\pm 20^{o} \longrightarrow P_{Pd}$ ±1.3X at 1800 K (relative uncertainty)

$\pm 30^{o} \longrightarrow P_{Au}$ ±1.55X at 1600 K

$\pm 50^{o} \longrightarrow P_{Ti}$ ±2.0X at 2000 K

The actual net uncertainties in the reported activities will be perhaps ±2X for Pd and Au and ±2.6X for Ti due to the uncertainties in the P^{o} values used[75] of approximately ±1.3X in the temperature range of interest. The relative activity comparisons between alloys are unaffected by the P^{o} uncertainties and should be about ±1.3X for alloys run simultaneously or about ±1.5X for alloys run independently.

RESULTS

The results of the experiments carried out by the above-described procedures are presented in this section. A discussion of their interconsistency, significance, and relation to relevant work of others will subsequently be offered in the final section of this report.

I. CARBIDE EQUILIBRATION

Table 6 comprises a summary of the results of all carbide equilibration experiments performed; the significant aspects of each of the twenty runs are presented in chronological order. In most cases the reactant powders were weighed out in proportions given by the indicated stoichiometry but sometimes a small unweighed quantity of graphite powder was included as indicated by a " ?C." Except where noted, all equilibrations were carried out under a uniaxial pressure of 490 bar. To obtain the higher temperatures indicated for runs 5 and 6, previously hot-pressed pellets were transferred to a graphite container in the graphite tube "King" furnace for reequilibration under a pressure of ~1 bar Ar(g). Runs 18-20 were carried out in graphite dies in the hot-press but with no applied pressure since the highest temperature liquidus in >50at.% Pd-Nb systems occurs at about 1900 K (and ~75at.% Pd) and the lowest at about 1830 K (pure Pd)[95] and it is likely that these values are further depressed by the presence of graphite.[27] Before releasing the hydraulic ram and ramping up to the equilibration temperature for these runs the powder mixtures were hot-pressed for ~1/2 hr. at 1600-1700 K.

TABLE 6

Reactant Powder Mixture	T(K) (±100°)	time (hr.)	Equilib. Alloy (w/ MC + graph.)	$a_{M(MC)}$ (±~2X)†	$\gamma_{M(M_xPt_{1-x})}$
1. 3.0 Ir + 1.0 HfC	2133	1	$HfIr_3$ (no HfC)	$<1.4X10^{-5}$	$<5.6X10^{-5}$±2X
2. 2.0 Pt + 1.0 ZrC	1905	3	$ZrPt_3$	$5.6X10^{-6}$	$2.2X10^{-5}$±2X
3. 1.9 Ir + 1.0 ZrC	1915	3	$ZrIr_3$	$6.2X10^{-6}$	$2.5X10^{-5}$±2X
4. 2.0 Pt + 1.0 ZrC	1926	3	$ZrPt_3$	$6.8X10^{-6}$	$2.7X10^{-5}$±2X
5. From Run 3 (no pressure)	2321	2	$ZrIr_3$	$1.2X10^{-4}$	$4.8X10^{-4}$±2X
6. From Run 4 (no pressure)	2300	2	$ZrPt_3$	$1.0X10^{-4}$	$4.0X10^{-4}$±2X
7. 2.0 Ir + 1.0 TaC	2154	3	$TaIr_3$	$3.4X10^{-4}$	$1.4X10^{-3}$±2X
8. 2.0 Pd + 1.0 TaC	1786	4.5	$TaPd_3$	$7.3X10^{-5}$	$2.9X10^{-4}$±2X
9. 1.0 ZrPt + 2.7C	2061	4	$ZrPt_3$	$2.0X10^{-5}$	$8.0X10^{-5}$±2X
10. 1.0 $Zr_{1.2}Pt_{1.0}$ ($ZrPt^{92}$ + $Zr_5Pt_3^{93}$ by XRD) + 3.1 C	2019	3	$ZrPt_3$	$1.5X10^{-5}$	$6.0X10^{-5}$±2X
11. 1.9 Os + 1.0 TaC	2170	4	1.0±0.4at.%Ta-Os	$3.6X10^{-4}$	$3.6X10^{-2}$±3X
12. 1.7 Ir + 1.0 WC + ?C	2237	4	9.5±2at.%W-Ir	$3.0X10^{-2}$	$3.2X10^{-1}$±2.5X
13. 2.3 Os + 1.0 ZrC + ?C	2216	4	<0.1±~0.05at.%Zr-Os*	$6.0X10^{-5}$	$>6.0X10^{-2}$±3X
14. 2.0 OS + 1.0 HfC + ?C	2211	4	0.3±0.2at.%Hf-Os	$2.2X10^{-5}$	$7.3X10^{-3}$±4X
15. 2.0 Os + 1.0 NbC + ?C	2196	4	0.8±0.3at.%Nb-Os	$7.6X10^{-4}$	$9.5X10^{-2}$±3X
16. 2.0 Os + 1.0 WC + ?C	2216	4	0.4±0.2at.%W-Os	$2.9X10^{-2}$	7.3±3X
17. 1.9 Ru + 1.0 ZrC + 1.0 C	2061	2	0.1±2Xat.%Zr-Ru	$2.0X10^{-5}$	$2.0X10^{-2}$±3X
18. 2.0 Pd + 1.0 NbC + 0.6 C (no pressure)	2321	1.5	15±2at.%Nb-Pd	$1.2X10^{-3}$	$8.0X10^{-3}$±2X

TABLE 6 (continued)

Reactant Powder Mixture	T(K) ($\pm 100^{o}$)	time (hr.)	Equilib. Alloy (w/ MC + graph.)	$a_{M(MC)}$ ($\pm$~2X)†	$\gamma_{M(M_xPl_{1-x})}$
19. 4.0 NbPd + 1.1 NbC + 0.6 C	2268	2	15±2at.% Nb-Pd	$9.7X10^{-4}$	$6.5X10^{-3}\pm 2X$
20. 2.0 Pd + 1.0 NbC + 0.6 C (no pressure)	2331	2	16±2at.% Nb-Pd	$1.2X10^{-3}$	$7.5X10^{-3}\pm 2X$

*Zr(Os) concentration below EPMA detection limit - approx. detection limit estimted.[91,94]
†"±2X" is used to signify an uncertainty range corresponding to one half of the given value up to twice the given value.

In the fourth column of Table 6 is presented the composition of the alloy in equilibrium with the corresponding carbide and graphite, the presence of the latter two phases having been established by identification of their X-ray diffraction (XRD) patterns (C[42], TaC[44], ZrC[44], HfC[45], NbC[43], WC[46]) in the composite pattern taken for the the equilibrated pellet. As noted, the reactant stoichimetry for run 1 resulted in complete consumption of the HfC so that none remained after equilibration and only an upper limit to a_{Hf} was established. For runs 1-10 the compositional analyses consisted of identifying the narrow (generally a few at.% wide) AB_3 phases through their X-ray diffraction patterns ($HfIr_3$[48], $ZrPt_3$[50], $TaPd_3$[90], $ZrIr_3$[49], $TaIr_3$[48]). The X-ray diffraction patterns for equilibrated pellets 11-20 showed the equilibrium alloy to be a terminal solid solution of the acid (carbide) metal in the platinum group metal so that EPMA was used to establish the compositions of these systems. The uncertainties assigned to these analyses are based upon both the systematic errors revealed by the analyses of standard alloys (see Table 3) and the fluctuations observed between the several analyses performed for each unknown alloy. For run 13 the Zr(Os) concentration was found to be below the EPMA detection limit. Several relations of the same basic form provided estimates of this detection limit based upon a statistical treatment of background and standard X-ray count levels[91,94] and application of these various formulas to the Zr(Os) analysis resulted in detection limits ranging from 0.7at.% Zr-Os at an 80 confidence level to 1.5at.% Zr-Os at a 99.7% confidence level; a

detection limit of 0.1±0.05at.% Zr-Os was chosen here. Where EPMA analyses were performed, no significant concentration of the platinum group metal was detected in the carbide so that the assumption of the applicability of the binary carbide thermodynamics is valid.

One motivation for the highest temperature equilibrations was to obtain some indication as to the magnitude of the temperature dependence of the equilibria being studied. That the ~1900 K (runs 2-4) and ~2300 K (runs 5,6) equilibrations with ZrC and graphite all resulted in either $ZrPt_3$ or $ZrIr_3$ confirms that the temperature-dependent compositional variations are in fact small here and the $\pm 100^{o}$ temperature uncertainty is therefore acceptable. The activities were obtained from the thermodynamic data presented in Table 1 using the ΔC_p values given in the corresponding references to extrapolate to the equilibration temperatures. Although the actual uncertainties may be as small as indicated in Table 1, a more conservative uncertainty of $\pm\sim 2X$ is applied to all of the reported activities. When the compositional uncertainty is large relative to the acid solute metal concentration (e.g., $>\sim\pm 20\%$ of the solute concentration) the resulting activity coefficient for the solute reflects this with a greater net uncertainty assignment than applied to the activity.

That the $ZrPt_3$ or $ZrIr_3$ phases resulted upon equilibration with ZrC and graphite at both ~1900 K and ~2300 K for approximately the same length of time supports the inherent assumption that the alloys formed are not diffusion-controlled and equilibrium has been

attained. An even more conclusive confirmation of this was established by equilibrating both the pure platinum group metal (Pt with ZrC and graphite in runs 2,4,6 or Pd with NbC and graphite in runs 18,20) and an alloy richer in the acid metal than the equilibrium alloy (ZrPt or $Zr_{1.2}Pt$ with ZrC and graphite in runs 9,10 or NbPd with NbC and graphite in run 19) in separate experiments and obtaining the same equilibrium alloy. Since the acid metal (Zr or Nb) had to diffuse from its carbide into the platinum group metal in the former case and vice versa in the latter case these results decisively confirm that $ZrPt_3$ and 15±2at.% Nb-Pd are the equilibrium alloys. These results are also taken to firmly support the assumption of equilibration for the other, similar, systems which were equilibrated under similar conditions.

These results will be summarized with those obtained by the nitride equilibration and vapor pressure methods later and interpretations and implications will be offered there.

II. NITRIDE EQUILIBRATION

In Table 7 is presented a chronologically ordered summary of all of the successful nitride equilibration experiments though the results of several additional runs with TaN, VN, NbN, and ZrN are not reported since very small alloy grain size resulted in unacceptably inaccurate EPMA analyses in those cases. Although the reactant stoichimetries were not accurately established, optical microscopy and EPMA analysis always showed the requisite two phases to exist after equilibration.

TABLE 7

Reactants	P_{N_2} (atm.)	T(K)*	time (hr.)	Equilib. Alloy	$a^{**}_{M(MN)}$	$\gamma^{**}_{M(M_xPt_{1-x})}$
1. Pt + NbN	0.99	2594±91	2	50±4at.%Nb-Pt	$1.9X10^{-1}$±3X	$3.8X10^{-1}$±3X
2. Pt + ZrN	1.11	2392±54	4	28±3at.%Zr-Pt	$7.2X10^{-4}$±2X	$2.6X10^{-3}$±2X
3. Pt + ZrN	0.98	2371±93	8	27±3at.%Zr-Pt	$6.5X10^{-4}$±2X	$2.4X10^{-3}$±2X
4. Zr_3Pt_2 + ZrN	0.96	2314±41	8	27±3at.%Zr-Pt	$4.0X10^{-4}$±2X	$1.5X10^{-3}$±2X
5. Pt + ZrN	11.2	2350±42	8	29±3at.%Zr-Pt	$1.6X10^{-4}$±2X	$5.6X10^{-4}$±2X
6. Pt + ZrN	11.2	2536±78	4	28±3at.%Zr-Pt	$6.7X10^{-4}$±2X	$2.4X10^{-3}$±2X
7. Pt + ZrN	1.00	2159±46	8	30±3at.%Zr-Pt	$9.6X10^{-5}$±2X	$3.2X10^{-4}$±2X
8. Pt + ZrN	0.114	2361±53	8	28±3at.%Zr-Pt	$1.7X10^{-3}$±2X†	$6.2X10^{-3}$±2X
9. Pt + TiN	1.00	2440±82	8	28±3at.%Ti-Pt	$3.5X10^{-3}$±2X	$1.3X10^{-2}$±2X
10. Pt + TiN	11.1	2414±81	9.5	29±3at.%Ti-Pt	$8.9X10^{-4}$±2X	$3.1X10^{-3}$±2X
11. Pt + TiN	0.157	2461±68	8	32±3at.%Ti-Pt	$1.0X10^{-2}$±2X†	$3.2X10^{-2}$±2X
12. Pt + TiN	11.0	2683±105	6.5	31±3at.%Ti-Pt	$4.6X10^{-3}$±2X	$1.5X10^{-2}$±2X
13. Pt + TiN	1.00	2720±97	6	30±3at.%Ti-Pt	$1.9X10^{-2}$±2X	$6.3X10^{-2}$±2X
14. Pt + HfN	11.1	2432±79	9.5	25±4at.%Hf-Pt	$1.2X10^{-4}$±3X	$4.9X10^{-4}$±3X
15. Pt + HfN	0.99	2427±69	8	24±4at.%Hf-Pt	$4.0X10^{-4}$±3X	$1.7X10^{-3}$±3X
16. Pt + HfN	11.1	2783±85	4	33±4at.%Hf-Pt	$1.4X10^{-3}$±3X	$4.3X10^{-3}$±3X

TABLE 7 (continued)

Reactants	P_{N_2} (atm.)	T(K)*	time (hr.)	Equilib. Alloy	$a^{**}_{M(MN)}$	$\gamma^{**}_{M(M_xPt_{1-x})}$
17. Pt + HfN	0.99	2756±88	4	26±3at.%Hf-Pt	$3.9X10^{-3}$±3X	$1.5X10^{-2}$±3X
18. NbPd + NbN	0.98	2406±83	4	34±3at.%Nb-Pd	$1.0X10^{-1}$±3X	$2.9X10^{-1}$±3X
19. Pd + NbN	0.99	2406±63	4	34±3at.%Nb-Pd	$1.0X10^{-1}$±3X	$2.9X10^{-1}$±3X
20. NbPd + NbN	10.8	2422±99	4	27±3at.%Nb-Pd	$3.3X10^{-2}$±3X	$1.2X10^{-1}$±3X

*The given uncertainties correspond to the sum of the emissivity correction and half of the temperature gradient measured for that run.

**The given approximate uncertainties are based upon the near-stoichiometric nitride thermodynamic quantities and do not include effects of possible substoichiometry.

†The nitrides equilibrated under ~0.1 atm. N_2 had a greyish (rather than the usual yellowish) appearance which is attributed to appreciable substoichiometry; this effect is expected to result in a somewhat greater uncertainty than that given.

The reported nitrogen pressures are taken as accurate to the last significant figure reported except for the lowest pressure runs for which the uncertainty is ±0.004 atm., this due to both measurement error and pressure drift. As discussed above, the temperature gradient across each pellet was established by sighting with an optical pyrometer onto opposite sides and the average of the two readings was used as the equilibrium temperature with the observed gradient establishing a minimum uncertainty. Since the applied emissivity corrections are of questionable applicability under the conditions of these experiments the reported uncertainties consist of the full value of that correction plus one half of the observed temperature gradient for that particular run; the emissivity correction results in higher reported temperatures so that the actual temperature is more likely to be somewhat lower than the value given.

All of the alloy analyses were by EPMA due to difficulties with and the inappropriateness of using X-ray diffracion for these sytems. The assigned uncertainties are again based upon the standard analyses and the observed scatter and are generally larger than for the carbide equilibration analyses due to the severe interferences from the surrounding nitride matrices. None of the platinum group metal was ever detected in the nitride phase by EPMA thus eliminating the possibility of ternary nitride phase formation but assigning the known nitride peaks to the very complex X-ray diffraction patterns for these nitride-alloy composites proved impossible. These difficulties in identifying the known structures may have been related to substoichiometry

and/or reequilibration with a falling nitrogen pressure during cooling but is more likely due to the relatively high temperatures and slow quench rates for these experiments relative to most crystallographic studies - some, but possibly incomplete, structural reequilibration during the cooling period likely occurred.

Although the starting platinum group metal or alloy always melted at a temperature lower than the equilibration temperature, a consideration of the phase diagram for the Zr-Pt system[38] reveals that the $ZrPt_3$ melting point occurs at 2400 K so that the equilibrium alloy for all of the ZrN-Pt runs except #6 may have consisted of a small amount of liquid in equilibrium with $ZrPt_3$. Inspection of the equilibrated pellets revealed that the Pt or Zr_3Pt_2 had always melted and crept into the nitride matrix (see Fig. 10) so that good contact and equilibration seem assured; agreement of the 2536 K run (#6) with the lower temperature runs and the consistent Zr_3Pt_2 run (#4) result support this assumption. The highest temperature solidus in the Ti-Pt system occurs at ~2200 K at $TiPt_3$[60] and all Nb-Pd alloys consisting of >45at.% Pd are completely liquid above ~1900 K[95] so that all runs with these systems should have involved only liquid alloy phases and post-run inspection revealed the typical nitride wetting behavior in all cases. Although the phase boundaries of the Hf-Pt system are not accurately known, it seems certain that the >2700 K HfN-Pt equilibrations involved a liquid alloy and the wetting of the nitride matrix by the alloy was also observed for all of the HfN-Pt runs as it was for the sole NbN-Pt run. The nitrides always remained

solid, contained all of the liquid alloy, and exhibited only minor surface reaction with the W liner up to the highest equilibration temperatures.

Though in certain cases their application is somewhat inappropriate, the thermodynamic values given in Table 4 for the near-stoichiometric nitrides have been used with the corresponding ΔC_p's from the references to obtain the activities and associated maximum uncertainties given for each run in Table 7. The uncertainties in the resulting activity coefficients are taken to be essentially identical to the activity uncertainties since the alloy composition uncertainties were always relatively small (i.e., $<\pm 20\%$ of the acid metal concentration). Most equilibrated pellets had a yellowish appearance similar to that of the near-stoichiometric nitrides although some appeared somewhat more metallic which is likely attributable to substoichiometry. The two low-pressure runs (#'s 8,11) with ZrN and TiN each resulted in greyish nitrides which is taken to reflect significant substoichiometry and the given activities for these runs may be somewhat inappropriate so that perhaps a slightly larger uncertainty than that shown should be assumed although the variation of $a_{M(MN_{1-x})}$ with x may be minimal since $\Delta G_f^o(MN_{1-x})$ shouldn't change much.

As alluded to above, that the equilibration of a Zr-rich Zr-Pt alloy in run 4 resulted in essentially the same final composition as the runs beginning with pure Pt assures that equilibrium was being attained (run 4, in fact, resulted in a slightly less Zr-rich alloy if

there was any detectable difference which is the opposite of what non-equilibration would have produced). Similarly, the consistency of run 18, beginning with NbPd, and run 19, beginning with pure Pd, assures that 34±3 at.% Nb-Pd is the equilibrium alloy under those conditions. Equilibration was assumed for the TiN-Pt, NbN-Pt, and HfN-Pt runs, most of which were carried out at a higher temperature than runs 4 or 18.

Several runs were carried out under essentially the same nitrogen pressure with the same reactants but at temperatures differing by 200-400^{o} (e.g., compare runs 3 and 7, 9 and 13, 10 and 12, 14 and 16, 15 and 17) to check for the dependence of these equilibria on temperature. The results reveal that the equilibrium alloy composition is constant within the accuracy of the analyses used here over a range of hundreds of degrees; this is fortunate from the viewpoint of the relatively large temperature uncertainties involved but eliminates the possibility of obtaining any indication of the sign of $\Delta\bar{H}_M$(MN - alloy) although a relatively small absolute value for this quantity is implied.

Equilibrations for the ZrN-Pt and TiN-Pt systems were carried out over a range of two orders of magnitude in nitrogen pressure (one order in $a_{M(MN)}$) and a one order of magnitude (one half order in $a_{M(MN)}$) variation was investigated for the HfN-Pt and NbN-Pd systems. In all cases except one the resulting alloy compositions were basically indistinguishable given the large uncertainty assignments; comparing runs 16 and 17, for example, the equilibrium alloy compositional

ranges just barely overlap but the apparent trend is in the wrong direction (greater a_{Hf} associated with lower Hf concentration) so that no meaningful conclusions may be drawn from the pressure dependences of these equilibria. The sole case where the resulting alloys may be distinguishable is in the comparison of runs 18 and 19 with run 20 (for the Nb-Pd system) for which the trend is as would be expected but the effect is relatively small and inexact so that no quantitative conclusions are available from this result. This relative pressure independence implies a rapid variation of $a_{M(alloy)}$ with $X_{M(alloy)}$ for these very stable acid-base systems such that, for example, a variation in a_{Zr} by an order of magnitude at constant temperature (compare runs 5 and 8) results in no more than a few at.% variation in the equilibrium Zr-Pt alloy composition. Since the Nb-Pd system was the least strongly bound combination studied, it is not surprising that the variation of X_{Nb} with a_{Nb} was detectable; the change from 0.1 to 0.03 in a_{Nb} has greater impact than the change from 0.0002 to 0.002 in zirconium activity in the Zr-Pt system (the latter change in activity was not detectable). It should perhaps be noted that although the absolute activities are rather uncertain, the relative activities for the same nitride under different nitrogen pressures are not affected by the absolute uncertainties and comparisons such as these are valid.

The lack of success in obtaining quantitatively significant information from the pressure variation studies may be taken to suggest that the effect of nitride substoichiometry was not significant for

these experiments. Since reduced pressure would increase nitrogen substoichiometry and both lower pressure and substoichiometry serve to increase the nitride metal activity ($a_{M(MN)}$), a significant problem with substoichiometry would have been manifested as extra large increases in acid metal concentration with falling nitrogen pressure; that no such effect was detected with pressure variations of up to two orders of magnitude suggests that substoichimetry was not a significant problem within the accuracy of these experiments.

Due to the rather large uncertainties in the available thermodynamic quantities at this time, this method is most useful for relatively strongly bound systems (e.g., TiN, ZrN, HfN) and less so for weakly bound systems (e.g., NbN) where the uncertainties are particularly significant. The results of these nitride equilibrations will later be compared with those from other experiments.

III. THERMOGRAVIMETRIC

In Table 8 are chronologically listed the results of all of the weight loss experiments; two or more runs identified by the same number (e.g., 1a, 1b) were performed simultaneously with the Knudsen cells in the same cell holder so that the relative uncertainties in those cases are smaller than the given absolute uncertainties. The average composition and associted uncertainty given for each alloy sample corresponds to the compositional range inferred from the mass loss (of the volatile component) and does not consider the possible effect of carbide formation which is discussed below. The orifice

TABLE 8

	Material Studied	Cell Material	Orifice Diam. (cm.)	Cell Tare (g.)	Cell Gross (g.)	Mass* Loss (g.)	T(K)±30°† (solid or liquid)	Time (hr.)	p^{o}_{75}(atm.) Pd, Au, or Ti	Ideal Std. St. Loss (g.)	Activity Pd, Au, or Ti ±2X**
1a.	70.7±3.9 at.%Pd-Nb	99.7% graph.	0.238	0.9516	2.6039	0.4008	1974 (1.)	3.5	2.35×10^{-4}	1.358	0.30
1b.	pure Pd	99.7% graph	0.238	0.9313	2.3219	0.0375	(1974) (1.)	3.5	2.35×10^{-4}	1.358	0.028
2a.	71.3±3.3 at.%Pd-Nb	99.7% graph.	0.238	0.9112	2.4920	0.3393	1954 (1.)	2.5	1.89×10^{-4}	0.785	0.43
2b.	pure Pd	99.7% graph.	0.238	0.9313	2.2384	0.0954	1951 (1.)	2.5	1.83×10^{-4}	0.760	0.13
2c.	pure Pd	99.7% graph.	0.238	0.8987	3.2374	0.2444	1941 (1.)	2.5	1.64×10^{-4}	0.682	0.36
3a.	71.6±3.0 at.%Pd-Nb	99.7% graph.	0.238	0.8682	1.9271	0.2124	1877 (1.)	4.5	7.85×10^{-5}	0.597	0.36
3b.	pure Pd	99.7% graph.	0.238	0.8829	2.9449	0.1582	1880 (1.)	4.5	8.14×10^{-5}	0.619	0.26

*1mg. subtracted from measured losses due to blank losses; no correction to blank runs or to oxide cell runs; 1mg. uncertainty for graphite cell runs.

†±40° for Al_2O_3 cells; ±50° for ZrO_2 and ThO_2 cells; "()" denotes possibility of greater uncertainty (e.g., ±40°).

**±2.6X for $a_{Ti(Ti\ Ir)}$.

TABLE 8 (cont'd.)

	Material	Cell	Diam.	Tare	Gross	Loss	T(K)	Time	p^o	S.S. Loss	Activity
3c.	pure Pd	99.7% graph.	0.238	0.9375	2.9982	0.2154	(1880) (1.)	4.5	$8.14X10^{-5}$	0.619	0.35
4a.	75.1±0.1 at.%Pd-Nb	99.7% graph.	0.238	0.9211	3.0741	0.0064	1693 (s.)	16.0	$6.33X10^{-6}$	0.180	0.036
4b.	pure Pd	99.7% graph.	0.238	0.9067	3.2593	0.2319	(1705) (s.)	16.0	$7.60X10^{-6}$	0.216	1.07
4c.	pure Pd	99.7% graph.	0.238	0.8781	2.4305	0.2561	1720 (s.)	16.0	$9.52X10^{-6}$	0.269	0.95
5a.	75.1±0.1 at.%Pd-Zr	99.7% graph.	0.238	0.9211	3.0667	0.0006	1640 (s.)	21.0	$2.73X10^{-6}$	0.104	0.0058
5b.	74.7±0.2 at.%Pd-Nb	99.7% graph.	0.238	0.9209	2.4383	0.0174	1659 (s.)	21.0	$3.71X10^{-6}$	0.140	0.12
5c.	pure Pd	99.7% graph.	0.238	0.9067	3.0264	0.1635	1687 (s.)	21.0	$5.77X10^{-6}$	0.216	0.76
5d.	pure Pd	99.7% graph.	0.238	0.8781	2.1734	0.1972	1715 (s.)	21.0	$8.84X10^{-6}$	0.328	0.60

TABLE 8 (continued)

	Material	Cell	Diam.	Tare	Gross	Loss	T(K)	Time	P^o	S.S. Loss	Activity
6a.	75.0±0.1 at.%Pd-Zr	99.7% graph.	0.238	0.9211	3.0651	0.0144	1865 (s.)	4.5	$6.8X10^{-5}$	0.519	0.028
6b.	~75 at.% Pd-Nb	99.7% graph.	0.238	0.9209	2.4199	Severe Creep	2003 (1.)	4.5	-------	-----	-----
6c.	pure Pd	99.7% graph.	0.238	0.9067	2.8619	0.5330	(1930) (1.)	4.5	$1.45X10^{-4}$	1.088	0.49
6d.	pure Pd	99.7% graph.	0.238	0.8781	1.9752	0.6152	1915 (1.)	4.5	$1.22X10^{-4}$	0.920	0.67
7a.	74.8±0.1 at.%Pd-Zr	99.7% graph.	0.238	0.9211	3.0497	0.0156	1981 (s.)	1.25	$2.54X10^{-4}$	0.522	0.030
7b.	pure Pd	99.7% graph.	0.238	0.9067	2.3279	0.1212	2063 (1.)	1.25	$5.88X10^{-4}$	1.186	0.10
7c.	pure Pd	99.7% graph.	0.238	0.8781	2.5019	0.1925	2008 (1.)	1.25	$3.37X10^{-4}$	0.688	0.28
8a.	72.5±2.5 at.%Au-Zr	99.99% graph.	0.284	1.0147	3.7291	0.5246	(1668) (1.)	19.5	$1.07X10^{-5}$	0.722	0.73
8b.	pure Au	99.99% graph.	0.284	1.0271	3.2649	0.3715	1668 (1.)	19.5	$1.07X10^{-5}$	0.722	0.51
9a.	75.0±0.1 at.%Au-Zr	99.99% graph.	0.292	1.0640	2.4801	0.0080	1487 (s.)	22.0	$5.13X10^{-7}$	0.0439	0.18
9b.	pure Au	99.99% graph.	0.292	1.0467	3.3372	0.0198	1487 (1.)	22.0	$5.13X10^{-7}$	0.0439	0.45

TABLE 8 (cont'd)

Material	Cell	Diam.	Tare	Gross	Loss	T(K)	Time	P^o	S.S. Loss	Activity
9c. pure Au	99.99% graph.	0.284	1.0314	2.8855	0.0289	1503 (l.)	22.0	$6.9X10^{-7}$	0.0556	0.52
10a. 74.8±0.2 at.%Pd-Hf	99.99%	0.269	1.0679	3.0457	0.0202	2010 (s.)	2.0	$3.44X10^{-4}$	1.436	0.014
10b. pure Pd	99.99% graph.	0.269	1.0472	2.4831	0.1177	1998 (l.)	2.0	$3.03X10^{-4}$	1.270	0.093
11a. 74.9±0.3 at.%Pd-Zr	99.99% graph.	0.244	1.0326	2.5323	0.0345	1955 (s.)	3.5	$1.92X10^{-4}$	1.167	0.030
11b. 74.7±0.3 at.%Pd-Hf	99.99% graph.	0.244	1.0695	3.0517	0.0319	1955 (s.)	3.5	$1.92X10^{-4}$	1.167	0.027
11c. pure Pd	99.99% graph.	0.269	1.0590	2.4891	0.3126	2058 (l.)	3.5	$5.60X10^{-4}$	4.041	0.077
11d. blank	99.99% graph.	0.285	1.0034	-----	0.0017	1997	3.5	--------	-----	-----
12a. 56±19 at.%Pd-Nb	99.99% graph.*	0.234	1.9622	3.0307	0.6622	2050 (l.)	2.5	$5.17X10^{-4}$	2.021	0.33

*Double cell - cup within cell of same material.

TABLE 8 (cont'd.)

Material	Cell	Diam.	Tare	Gross	Loss	T(K)	Time	p^o	S.S. Loss	Activity
12b. pure Pd	99.99% graph.*	0.234	1.9737	3.3437	0.1705	2050 (l.)	2.5	$5.17X10^{-4}$	2.021	0.084
13a. blank	99.99% graph.**	0.251	2.1224	-----	0.0018	2233	~1	-------	-----	-----
13b. blank	99.99% graph.**	0.251	2.1059	-----	0.0015	2233	~1	-------	-----	-----
14a. 66.1±8.8 at.%Pd-Nb	from run 13a	0.251	2.1206	3.4572	0.5677	2058 (l.)	2.0	$5.60X10^{-4}$	2.011	0.28
14b. pure Pd	from run 13b	0.251	2.1044	3.3458	0.1718	2058 (l.)	2.0	$5.60X10^{-4}$	2.011	0.085
15a. ~75at. Pd-Ta	99.99% graph.	0.238	0.8949	2.5253	Severe Creep	2068 (l.)	<1.5	-------	-----	-----
15b. 74.8±0.1 at.%Pd-Hf	99.99% graph.	0.238	0.8729	2.9215	0.0222	2053 (s.)	<1.5	$5.33X10^{-4}$	<1.292	>0.017
15c. 75.0±0.2 at.%Pd-Zr	99.99% graph.	0.238	0.8745	2.5981	0.0242	2053 (s.)	<1.5	$5.33X10^{-4}$	<1.292	>0.019
15d. blank	99.99% graph.	0.238	0.8403	-----	0.0007	2053	<1.5	-------	-----	-----

*Double cell - cup within cell of same material.

**Double cell internally coated with a 1 micron layer of Nb.

TABLE 8 (cont'd.)

	Material	Cell	Diam.	Tare	Gross	Loss	T(K)	Time	p_O	S.S. Loss	Activity
16a.	74.5±0.6 at.%Pd-Ta	99.99% graph.	0.238	0.8739	2.0964	0.0461	1808 (s.)	21.5	$3.31X10^{-5}$	1.226	0.038
16b.	74.5±0.4 at.%Pd-Nb	99.99% graph.	0.238	0.8691	2.2170	0.670	1761 (s.)	21.5	$1.73X10^{-5}$	0.649	0.10
16c.	pure Pd	99.99% graph.	0.238	0.8698	1.9232	0.8246	1811 (1.)	21.5	$3.45X10^{-5}$	1.275	0.65
17a.	pure Pd	99.8% Al_2O_3 in gr.	0.238	1.3808	2.1861	0.3497	(2030) (1.)	<0.75	$4.23X10^{-4}$	<0.515	-----
17b.	blank	99.8% Al_2O_3 in gr.	0.238	1.4162	------	0.1972	2030	<0.75	-------	-----	-----
17c.	pure Pd	99.99% graph.	0.238	0.8698	1.9488	0.0940	(2030) (1.)	<0.75	$4.23X10^{-4}$	<0.515	>0.18
18a.	pure Pd	99.99% graph.	0.238	0.8754	2.1621	0.3541	1776 (1.)	18.7	$2.14X10^{-5}$	0.694	0.51
18b.	blank	99.99% graph.	0.238	0.8890	-----	0.0004	1770	18.7	-------	-----	-----
19.	pure Pd	99.99% graph.	0.238	0.8883	2.2067	0.1288	1683 (s.)	19.0	$5.42X10^{-6}$	0.184	0.70

TABLE 8 (cont'd)

	Material	Cell	Diam.	Tare	Gross	Loss	T(K)	Time	P^o	S.S. Loss	Activity
20a.	pure Pd	99.9% W in gr.	0.238	3.9586	4.8921	0.1169	1960 (1.)	1.67	$2.02X10^{-4}$	0.558	0.21
20b.	blank	99.9% W in gr.	0.238	3.8514	-----	0.0011	1960	1.67	-------	-----	-----
21.	pure Pd	from run 20b	0.238	3.8499	4.8144	0.1189	1935 (1.)	2.0	$1.53X10^{-4}$	0.511	0.23
22.	pure Pd	from run 21	0.238	3.8499	5.0538	0.2148	2041 (1.)	1.0	$4.73X10^{-4}$	0.766	0.28
23a.	74.7±0.4 at.%Pd-Ta	99.99% graph.	0.237	0.8674	2.5390	0.0422	1973 (s.)	2.0	$2.33X10^{-4}$	0.763	0.055
23b.	74.8±0.1 at.%Pd-Hf	99.99% graph.	0.237	0.8988	2.4465	0.0062	1973 (s.)	2.0	$2.33X10^{-4}$	0.763	0.0081
24a.	blank	10μ Ti on 99.99% gr.	0.257	0.8637	-----	0.0015	(2108)	0.5	-------	-----	-----
24b.	blank	10μ Ti on 99.99% gr.	0.257	0.8727	-----	0.0012	(2108)	0.5	-------	-----	-----
24c.	blank	10μ Ti on 99.99% gr.	0.257	0.8746	-----	0.0013	(2108)	0.5	-------	-----	-----
24d.	blank	10μ Ti on 99.99% gr.	0.257	0.8973	-----	0.0014	2108	0.5	-------	-----	-----

TABLE 8 (cont'd)

	Material	Cell	Diam.	Tare	Gross	Loss	T(K)	Time	P^o	S.S. Loss	Activity
25a.	~75at.% Ti-Ir	from run 24a	0.257	0.8623	2.0164	Creep/ Diffusion	2071 (1.)	2.5	-------	-----	-----
25b.	pure Ti	from run 24d	0.257	0.8957	2.0400	Creep/ Diffusion	2064 (1.)	2.5	-------	-----	-----
26.	pure Ti	97% ZrO_2 (CaO stab.)	~1.3 (no lid)	-----	-----	Rxn.	(2173) (1.)	mins.	-------	-----	-----
27.	blank	99.5% ThO_2	1.08 (no lid)	16.2511	-----	0.0131	2198	0.5	-------	-----	-----
28.	74.8±0.2 at.%Ti-Ir	from run 27	1.08 (no lid)	16.2381	20.3697	0.0336	2008 (1.)	1.0	$1.40X10^{-5}$	0.316	0.11
29.	blank	99.8% Al_2O_3	0.508	10.0444	-----	<0.0098> Gain	2173	1.0	-------	-----	-----
30.	pure Pd	from run 29	0.508	10.0541	25.2481	3.963	1936 (1.)	3.0	$1.55X10^{-4}$	3.530	1.12
31.	blank	99.8% Al_2O_3	0.508	11.2398	------	0.0039	(1930)	1.3	-------	-------	-----
32.	pure Pd	99.8% Al_2O_3	0.508	11.1508	15.5303	1.516	1703 by T.C. (s.)	18.3	$7.37X10^{-6}$	1.091	1.39

diameters are accurate to ±0.005 cm. and the masses to ±0.1 mg. although all weighings were to 0.05 mg. The mass losses from empty ("blank") graphite Knudsen cells ranged from 0.4 mg. to 1.8 mg. with the average for the nine blank runs being 1.3 mg. with a standard deviation of 0.4 mg.; since blank runs were often carried out at particularly high temperatures and some weight loss experiments utilized cells already run as blanks (for which subsequent cell weight losses should have been smaller) a blank loss of 1±0.8 mg. was used and 1 mg. was subtracted from all of the actual mass losses to obtain the values given in column 6 of Table 8 for the graphite cell runs. Because of this blank loss correction, runs involving a mass loss of <~6 mg. (i.e., run 5a) include an additional source of significant uncertainty which is not contained in the ±2X assignment. Although the ThO_2 crucible used in run 28 had shown a blank loss of 13.1 mg. at ~2200 K it was assumed that any correction at ~2000 K would be relatively minor. The Al_2O_3 cell of run 29 showed a weight gain of 9.8 mg. when fired empty, this presumably due to additional oxidation despite the operation of the furnace at $<10^{-4}$ torr; this cell was subsequently used for run 30 and no blank correction was applied. Similarly, no blank correction was applied to run 32 but any such correction would certainly have been small relative to the 1.5 g. total mass loss.

In certain cases it was not possible to sight directly into a particular Knudsen cell with the optical pyrometer and its temperature was therefore inferred from that of a neighboring cell(s) as signified

by the placing of parentheses around the temperature given in column 7 of Table 8. A somewhat larger (perhaps $\pm 40^{o}$) uncertainty may be associated with these indirectly established temperatures. Below each weight loss temperature is indicated whether the alloy or pure metal had melted in the course of the experiment. The alloy of run 3a was found to have only partially melted so that the 1877±30 K weight loss temperature is taken to be in the two phase region for this composition range of 71.6±3.0 at.% Pd-Nb; this is in agreement with the phase diagram of Giessen, et al.[95] which shows the liquidus to occur at ~1890 K for Pd-Nb alloys in this composition region. That the pure Pd in graphite sample of run 18a was liquid at 1776±30 K despite that the melting point of Pd occurs at 1827 K is in accord with the work of Darling[27] who found that carbon depresses the melting point of Pd to 1777±16 K. The standard state pressures, P_i^o, for the volatile Pd, Au, or Ti component are from Hutgren, et al.[75] and the corresponding standard state losses given in column 9 of Table 8 result from inserting the appropriate P_T^o along with the other parameters for each particular run into the Kinetic Theory expression for mass flux which was given above; the activity is then given by: a = Actual Loss ÷ Std. State Loss.

The liquid alloys always spread out and wetted the Knudsen cell, to the extent of creeping up the cell wall and sometimes out of the orifice in the case of graphite cells. Severe creep of $NbPd_3$ (run 6b), $TaPd_3$ (run 15a), Ti_3Ir (run 25a), and pure Ti (run 25b) out of the graphite cell rendered certain runs useless as noted in the

"Loss" column of Table 8. Since the liquid Pd did not generally even wet the graphite cells and remained as a ball on the bottom of the cell it seems clear that the creep reflects the high affinity of the acid metal components of the alloys for graphite (they all form stable carbides) which effectively reduces the liquid alloy surface tension. Since the mass loss from a Pd alloy cell was frequently greater than that from a neighboring pure Pd cell (runs 1, 2, 3, 12, 14, 16) tests were performed to insure that non-apparent creep or diffusion through the cell wall was not causing extra large weight losses from the alloy cells. Since the vapor pressure of Nb is relatively negligible at the experimental temperatures (e.g., $1X10^{-11}$ atm. at 2200 K[75]) any significant liquid Nb-Pd alloy creep onto the graphite lid outer surface would have been expected to result in vaporization of the volatile Pd component leaving the refractory Nb component on the lid, possibly as a carbide. The surface layer (~10-100μ) of the top of the lid from run 2a was scraped off, dissolved in HCl + tartaric acid, and tested for Nb with a 2% benzenearsonic acid solution. That no Nb was detected to a sensitivity of 2 ppm confirms that undetected creep was not in fact a problem. The possibility of diffusion through the cell wall was checked for by cutting several cells (runs, 2a, 3a, 8a) longitudinally, polishing, and obtaining an EPMA compositional profile of the alloy and cell wall. In Figure 13 is shown the optical micrograph of the cell wall - alloy interface from run 2a. At the right in the photograph is the remaining shiny liquid (solid in the room temp.

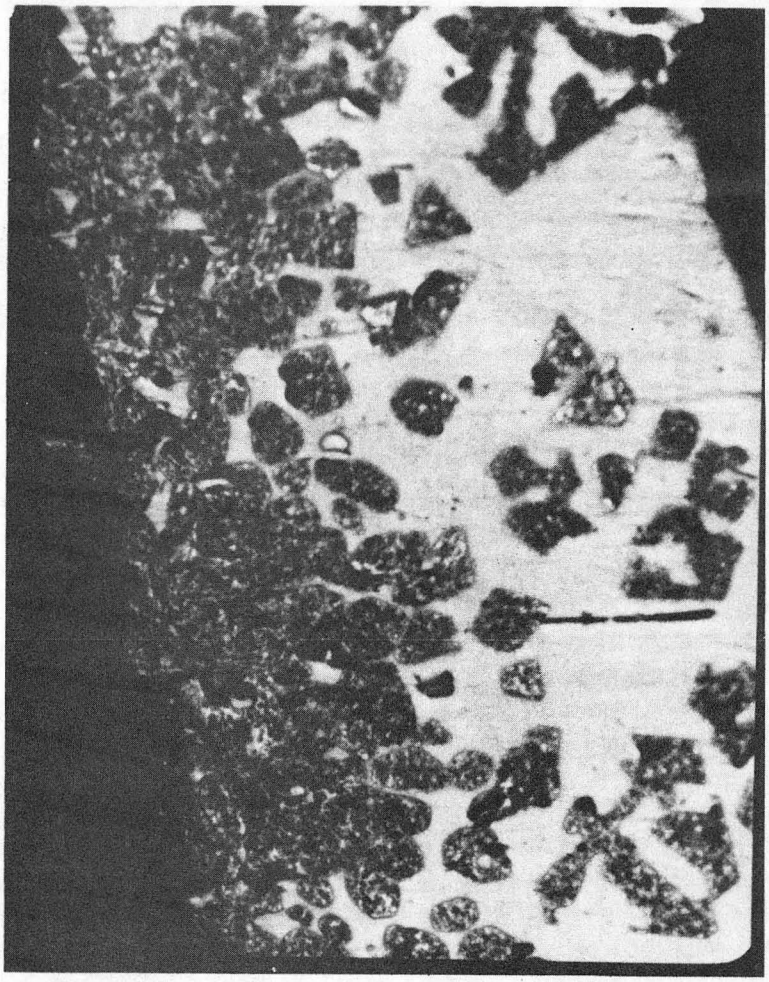

XBB 836-5392

100 μ

Thermogravimetric
Run # 2a

Figure 13

photo) Nb-Pd alloy which had crept up and wet the cell wall; the second phase in the alloy and clustered towards the graphite wall on the left was found by EPMA to contain Nb but no Pd (EPMA cannot analyze for C) and is undoubtedly NbC and/or Nb_2C; the dark phase at the left is the graphite wall and was found to contain no significant amounts of Nb or Pd. Similar results were obtained for the cells from runs 3a and 8a except that no detectable Au-less (ZrC) layer was found between the $ZrAu_3$ and uncontaminated graphite phases of run 8a. These results eliminate the diffusion possibility and are in accord with what was subsequently found in carbide equilibration runs 18-20: that $a_{Nb(NbPd_3)} > a_{Nb(NbC)}$ and 15±2 at.% Nb-Pd is in equilibrium with NbC. The absence of a ZrC layer between graphite and liquid $ZrAu_3$ would be surprising in light of the results Brewer and Wengert[22] who found that a 9.5±3.5 at.% Zr-Au alloy was in equilibrium with graphite and ZrC; it is therefore assumed that a very thin (unresolvable by EPMA) ZrC layer was established between the graphite and $ZrAu_3$ phases of run 8a but that diffusion through this layer was very slow. Since it appears from the morphology evident in Figure 13 for run 2a that the carbide phase in the Nb-Pd case may have largely been precipitated from the liquid alloy phase, the differing behaviour in these two systems may be related to the appreciable solubility of C in liquid Pd[28].

Since the formation of a carbide layer in runs 2a, 3a, and possibly others involving liquid Nb-Pd alloys in graphite consumed some

of the Nb, the relatively acid-metal rich compositional ranges calculated considering only the vaporization of the volatile Pd component and given in Table 8 may not always be entirely appropriate. In fact, the final alloy compositions based upon weight loss were calculated as 68 and 68.6 at.% Pd-Nb for runs 2a and 3a, respectively, but were found to actually be 75±3 and 80±3 at.% Pd-Nb, respectively, by EPMA. Since run 3a involved a two-phase alloy system and only the liquid phase was compositionally analyzed the actual Nb depletion in that case may not have been as extreme as implied but the effect is clearly not negligible. Without analyzing all of the post-run alloys it is difficult to quantify the extent of depletion, but in those cases where a liquid Nb-Pd alloy was successfully run in a graphite cell (runs 1a, 2a, 3a, 14a) the actual composition should be considered as somewhat more Pd-rich than indicated in Table 8.

To confirm that solid-state diffusion of the relatively volatile alloy component to the surface was not limiting in those cases where the alloy did not melt, the remaining solid Pd-Zr alloy from run 7a was ground down into the bulk on SiC paper, polished, and an EPMA profile of its composition obtained. Although the bulk alloy showed slight inhomogeneities there was no evidence of surface depletion to the ~1μ resolution of the microprobe. That diffusion through a solid 18 at.% Nb-Pd alloy was not limiting was confirmed with the mass spectrometric experiments by observing continuity in $P_{Pd(alloy)}$ through the alloy melting point which was detected by a halt in the I^{+}_{Pd} vs. time curve during heating or cooling.

A disturbing aspect of the first few thermogravimetric experiments was that the weight losses from pure liquid Pd at supposedly unit activity in graphite Knudsen cells (runs 1b, 2b, 2c, 3b, 3c) suggested a value for a_{Pd} in the range of 0.03 to 0.4, well outside the range of the assigned uncertainty. Subsequent runs with solid Pd in graphite (runs 4b, 4c, 5c, 5d) and liquid or solid Pd in Al_2O_3 cells (runs 30, 32) gave results for a_{Pd} of unity within the assigned uncertainty while further experiments with liquid Pd in graphite (runs 6c, 6d, 7b, 7c, 10b, 11c, 12b, 14b, 16c) continued to result in Pd activities as low as 0.08. The solid Pd runs and the liquid Pd in Al_2O_3 run confirmed the validity of this experimental method so that the vaporization of Pd(g) from liquid Pd in graphite must have been inhibited. One explanation for a low vaporization coefficient involves the fact that solid Pd dissolves 4.3 at.% C at 1400°C and liquid Pd dissolves appreciably more[28] (thus the melting point depression). The small temperature fluctuations and gradients inherent in these experiments result in a varying carbon solubility in the liquid Pd and any excess carbon precipitated out may be as thin sheets with a graphitic structure which coat the metal surface and inhibit vaporization from it. This explanation is consistent with the observation that reduced vaporization tended to be greatest at high temperatures where carbon solubility and temperature gradients are largest (hydrodynamical behaviour, incidentally, would have the opposite effect), and with the fact that the Pd of run 2b, which had

previously been run in graphite at ~2300 K, showed much more of an effect than the fresh Pd sample of run 2c run simultaneously. This problem, coupled with the inherent uncertainty involved in these experiments being greater than that assigned to the P^o_{Pd} values available, motivated abandoning the original intention of using internal standards and/or accurately determining P^o_{Pd}. It is assumed that the affinity of the acid components for carbon eliminated this vaporization reduction for the alloys since the excess carbon would be precipitated as a carbide.

Several different Knudsen cell geometries and materials were tried in attempts to reduce or eliminate interaction of the material being studied with the cell material. As mentioned above, the weight loss from pure liquid Pd in an Al_2O_3 cell (run 30) gave rather good agreement with the Hultgren value for P^o_{Pd}. The cells used in runs 12-14 were all "double cells" which consisted of a small graphite cup inside of a graphite cell, the idea being that a liquid alloy would have to creep up the inside and down the outside of the inner cup and then up the inside of the cell before reaching the orifice; run 12a involved a degree of internal creep which would likely have rendered the run useless (as was 6b at an even lower temperature) had a regular cell been used. The 1μ layer of Nb which had been vacuum deposited onto the inside of a graphite cell and then fired to form NbC did not seem to have an appreciable effect on run 14a, which is not surprising since a carbide layer ~100μ thick was observed after run 2a (Fig. 13). The 10μ Ti layer fired onto the graphite cells of

runs 25a and 25b did not prevent the liquid Ti-Ir alloy and pure Ti samples from creeping all over and actually diffusing through the relatively porous ECV graphite cell walls. The CaO stabilized ZrO_2 crucible of run 26 reacted with the liquid Ti to leave only a dark blob within a matter of minutes at ~2200 K. Only the ThO_2 crucible of run 28 effectively contained liquid Ti_3Ir; since no lid was available the crucible inside diameter of 1.08 cm. was used as the "orifice diameter" but given the P_{Ti} of only $\sim 10^{-6}$ atm. at 2008 K, flow should nonetheless have been primarily molecular.

In run 17a an Al_2O_3 cup inside of a graphite cell was used to contain pure liquid Pd but 0.2 g. was lost from the adjacent blank cell (run 17b) before the furnace shut off (presumably the chamber pressure had risen above the vacuum interlock setting) and reaction of the Al_2O_3 with the graphite cell was obvious upon inspection. One possible reaction which occurred is:

$$Al_2O_3(s) + 3C(gr) = 2Al(g) + 3CO(g)$$

for which $K_{2000\ K} = 1.1X10^{-9}$ atm.^{5} $= P^2_{Al(g)} \times P^3_{CO(g)}$.[40] The only other type of cell used was a graphite cell with a 99.9% W cup inside (run 20) which it was hoped would contain liquid Pd without appreciable reaction. Run 20a resulted in another low a_{Pd} over pure Pd and a dull white oxide-like layer was found coating the clean metal. A subsequent run was performed (without weighing) using the already fired empty cell of run 20b in hopes that any volatile contaminants had been eliminated, but the oxide-like coating again appeared.

After mechanical removal of this layer to reveal the clean, shiny metal this cell with the remaining sample was fired once more, and the dull white layer formed yet again. Although the cause of this effect is not readily apparent, it may be related to the fact that liquid Pd dissovles ~10 at.% W in the temperature range of these experiments[59] which fact would likely render W an inappropriate container material anyway.

In Table 8A is presented a more concise summary of the most relevant results of these weight loss experiments. For the Nb-Pd system, only runs whose calculated average composition (based upon weight loss) lay between 70 and 75 at.% Pd-Nb are presented; due to the carbide formation effect, many of these compositions are taken as 75±5 at.% Pd-Nb (as implied by the "$NbPd_{\sim 3}$" heading) but this system is relatively weakly bound and a_{Pd} is not expected to vary particularly rapidly in this composition range. Although most (but not all) of the activity vs. temperature trends are in the expected direction of incresasing a with increasing T and all are at least reasonable when the net activity uncertainties are considered, it is readily clear that no quantitative estimate of $\Delta\bar{H}_{Pd,\ Au,\ or\ Ti}$ can be made from a Second Law treatment of these data. These results are most useful for comparing the stabilities of the various alloys and are most effective for this when systems run simultaneously are considered, as, for example, the following: $a_{Pd(ZrPd_3)} < a_{Pd(NbPd_3)}$ from run 5,

TABLE 8A

$NbPd_{\sim 3}$

Run	T(K)	a_{Pd}
5b	1659	0.12
4a	1693	0.04
16b	1761	0.10
3a	1877	0.4
2a	1954	0.4
1a	1974	0.3

$ZrPd_3$

Run	T(K)	a_{Pd}
5a	1640	~0.01
6a	1865	0.03
11a	1955	0.03
7a	1981	0.03
15c	2053	>0.02

$TaPd_3$

Run	T(K)	a_{Pd}
16a	1808	0.04
23a	1973	0.06

$HfPd_3$

Run	T(K)	a_{Pd}
11b	1955	0.03
23b	1973	0.008
10a	2010	0.014
15b	2053	>0.02

$ZrAu_3$

Run	T(K)	a_{Au}
9a	1487	0.2
8a	1668	0.7

Ti_3Ir

Run	T(K)	a_{Ti}
28	2008	0.11

$a_{Pd(TaPd_3)} < a_{Pd(NbPd_3)}$ from run 16, $a_{Pd(HfPd_3)} \sim a_{Pd(ZrPd_3)}$ from runs 11 and 15, and $a_{Pd(HfPd_3)} < a_{Pd(TaPd_3)}$ from run 23.

The results of runs 8a and 9a confirm what Brewer and Wengert[22] had established previously by monitoring a_{Zr}: that there is some acid-base stabilization in the Zr-Au system but it is one of the weaker interactions. It may not be particularly appropriate to compare the Ti_3Ir result with the others since there the acid metal activity was measured.

These results will be returned to later in the context of how they fit in with other experiments and how they may be interpreted in terms of the Engel-Brewer theory.

IV. MASS SPECTROMETRIC

All of these experiments were carried out in collaboration with Professor K.A. Gingerich using a Nuclide 12-90HT mass spectrometer in the Chemistry Department of Texas A&M University.

Three Nb-Pd alloys of compositions 18 at.% Nb-Pd, 50 at.% Nb-Pd, and 80 at.% Nb-Pd were investigated with mass spectrometric vapor pressure measurements. After cell alignment, Ag vapor pressure and Ag/Ag_2 pressure constant calibrations were performed at the start of each run and the results are presented in Table 9. The vapor pressure calibrations were performed below the Ag melting point of 1234 K to avoid reaction with the cell material or Nb-Pd alloy and thus ensure unit Ag activity; the Ag/Ag_2 method is independent of Ag activity

TABLE 9

Run I — 18 at.% Nb - Pd:

V.P. Calibration:		Ag/Ag_2 Calibration:	
1111K	k_{Ag} = 0.506atm/A·K	1377	k_{Ag} = 0.710atm/A·K
1140	0.435	1422	0.742
1173	0.427		
1212	0.404		

Use k_{Ag} = 0.49atm/A·K and γ_{Pd}/γ_{Ag} = 1.10±0.05 (from subsequent runs) to obtain k_{Pd} = 0.37atm/A·K.

Run II — 50 at.% Nb - Pd:

V.P. Calibration:		Ag/Ag_2 Calibration:	
1077K	$k_{Ag} = 6.38\times10^{-3}$atm/A·K	1162K	$k_{Kg} = 4.65\times10^{-3}$atm/A·K
1058	5.33×10^{-3}	1188	8.48×10^{-3}
1050	7.35×10^{-3}	1217	8.33×10^{-3}
1076	7.03×10^{-3}	1255	7.13×10^{-3}
1104	5.93×10^{-3}	1287	4.55×10^{-3}
1129	6.28×10^{-3}	1324	9.55×10^{-3}
1162	6.00×10^{-3}		

Use $k_{Ag} = 6.5\times10^{-3}$atm/A·K and γ_{Pd}/γ_{Ag} = 1.13 (measured) to obtain $k_{Pd} = 4.9\times10^{-3}$atm/A·K.

Table 9 (continued)

Run III — 80 at.% Nb - Pd:

V.P. Calibration:		Ag/Ag_2 Calibration:	
1054K -- K_{ag} =	$9.10X10^{-3}$ atm/A·K	1227K -- k_{Ag} =	$5.95X10^{-3}$ atm/A·K
1078K	$7.57X10^{-3}$		

Use $k_{Ag} = 7.6X10^{-3}$ atm/A·K and $\gamma_{Pd}/\gamma_{Ag} = 1.07$ (measured) to obtain $k_{Pd} = 6.0X10^{-3}$ atm/A·K.

Use $k_{Ag} = 7.6X10^{-3}$ atm/A·K and $\gamma_{Nb}/\gamma_{Ag} = 1.31$ (measured) to obtain $k_{Nb} = 3.8X10^{-3}$ atm/A·K.

and was generally carried out at higher temperatures in order to obtain an adequate Ag_2^+ intensity. The reasonable agreeement between the two types of calibrations suggests that the calibration constants are indeed accurate to within better than a factor of two. The values of k_{Ag} subsequently used to interpret the alloy data are indicated below the calibration results for each run and were chosen with an emphasis on the generally more reliable and less scattered vapor pressure results; for runs I and II the k_{Ag}'s used correspond to the average of the following two quantities: 1) the average of all of the k_{Ag}'s obtained, and 2) the average of the vapor pressure k_{Ag}'s, while simply an average of all three k_{Ag}'s obtained was used for run III because of the relatively few data and large difference between the two vapor pressure k_{Ag}'s. The three k_{Pd}'s and the k_{Nb} for run III were then arrived at using the indicated multiplier gain (γ) ratios and the ionization cross section ratios from Mann[79] ($\sigma_{Ag}/\sigma_{Pd} = 0.83$ and $\sigma_{Ag}/\sigma_{Nb} = 0.66$). The large difference between the k_{Ag} used for run I and those used for runs II and III was likely related to the larger Knudsen cell orifices used for the latter two runs, altered instrument sensitivity for the latter runs which were performed several months after the first run, and possibly poor alignment of the cell with the slit into the source region for run I.

Using these calibration constants to convert the measured I_i^+ into P_i through $P_i = k_i I_i^+ T$ all of the data obtained on these three alloys are shown chronologically in Tables 10A-10C. Also shown are

TABLE 10A -- 18at.% Nb - Pd

T(K)	DAY 1 $P_{Pd(alloy)}$ (atm.)	$P^{o\ 75}_{Pd}$ (atm.)	a_{Pd}	T(K)	DAY 2 $P_{Pd\ (alloy)}$ (atm.)	$P^{o\ 75}_{Pd}$ (atm.)	a_{Pd}
1569	3.36×10^{-7}	8.06×10^{-7}	0.417	1503	1.31×10^{-7}	2.34×10^{-7}	0.560
1609	7.19×10^{-7}	1.62×10^{-6}	0.444	1558	3.75×10^{-7}	6.61×10^{-7}	0.567
1657	1.78×10^{-6}	3.59×10^{-6}	0.496	1620	1.07×10^{-6}	1.95×10^{-6}	.0549
1696	3.38×10^{-6}	6.62×10^{-6}	0.511	1680	2.43×10^{-6}	5.17×10^{-6}	0.470
1646	1.27×10^{-6}	3.01×10^{-6}	0.422	1680	2.57×10^{-6}	5.17×10^{-6}	0.497
1591	4.03×10^{-7}	1.19×10^{-6}	0.339	1690	3.82×10^{-6}	6.04×10^{-6}	0.632
1550	1.92×10^{-7}	5.71×10^{-7}	0.336	1741	8.18×10^{-6}	1.30×10^{-5}	0.629
1482	4.41×10^{-8}	1.83×10^{-7}	0.241	1769	1.40×10^{-5}	1.94×10^{-5}	0.722
1427	1.32×10^{-8}	4.88×10^{-8}	0.270	1805	2.12×10^{-5}	3.18×10^{-5}	0.667
1423	1.13×10^{-8}	4.47×10^{-8}	0.253	1810	2.70×10^{-5}	3.40×10^{-5}	0.794
1410	6.87×10^{-9}	3.36×10^{-8}	0.204	1827	Melting Observed		
1448	1.41×10^{-8}	7.65×10^{-8}	0.184	1841	3.12×10^{-5}	5.07×10^{-5}	0.615
1485	4.83×10^{-8}	1.64×10^{-7}	0.295	1820	Melting Observed		
1520	1.07×10^{-7}	3.25×10^{-7}	0.329	1832	Melting Obersved		
1535	1.84×10^{-7}	4.32×10^{-7}	0.426	1844	3.15×10^{-5}	5.26×10^{-5}	0.599
1562	2.64×10^{-7}	7.11×10^{-7}	0.371	1837	3.28×10^{-5}	4.82×10^{-5}	0.680
1577	3.89×10^{-7}	9.30×10^{-7}	0.418	1875	5.72×10^{-5}	7.66×10^{-5}	0.747
1632	1.02×10^{-6}	2.39×10^{-6}	0.427	1894	8.03×10^{-5}	9.59×10^{-5}	0.837
1668	1.85×10^{-6}	4.28×10^{-6}	0.432	1895	1.12×10^{-4}	9.70×10^{-5}	1.155
1702	3.73×10^{-6}	7.26×10^{-6}	0.514	1893	9.96×10^{-5}	9.48×10^{-5}	1.051
1734	6.36×10^{-6}	1.17×10^{-5}	0.544	1859	5.55×10^{-5}	6.32×10^{-5}	0.878

TABLE 10A (continued) -- 18at.% Nb - Pd

T(K)	DAY 1 $P_{Pd(alloy)}$ (atm.)	P^{o}_{Pd} 75 (atm.)	a_{Pd}	T(K)	DAY 2 $P_{Pd(alloy)}$ (atm.)	P^{o}_{Pd} 75 (atm.)	a_{Pd}
1767	$1.37X10^{-5}$	$1.88X10^{-5}$	0.729	1859	$5.59X10^{-5}$	$6.32X10^{-5}$	0.884
1728	$5.90X10^{-6}$	$1.07X10^{-5}$	0.551	1811	$2.89X10^{-5}$	$3.45X10^{-5}$	0.838
1809	$2.37X10^{-5}$	$3.36X10^{-5}$	0.705	1776	$1.92X10^{-5}$	$2.13X10^{-5}$	0.901
1785	$1.41X10^{-5}$	$2.42X10^{-5}$	0.583	1740	$1.02X10^{-5}$	$1.28X10^{-5}$	0.797
1814	Melting Observed			1711	$5.91X10^{-6}$	$8.32X10^{-6}$	0.710
1838	$2.59X10^{-5}$	$4.88X10^{-5}$	0.531	1659	$2.45X10^{-6}$	$3.71X10^{-6}$	0.660
1854	$4.39X10^{-5}$	$5.95X10^{-5}$	0.738	1646	$1.80X10^{-6}$	$3.01X10^{-6}$	0.598
1885	$6.66X10^{-5}$	$8.63X10^{-5}$	0.772	1572	$4.49X10^{-7}$	$8.51X10^{-7}$	0.528
1813	Melting Oberved			1513	$1.37X10^{-7}$	$2.84X10^{-7}$	0.482
1801	$1.81X10^{-5}$	$3.01X10^{-5}$	0.601	1480	$6.81X10^{-8}$	$1.48X10^{-7}$	0.460
1556	$2.02X10^{-7}$	$6.37X10^{-7}$	0.317				

TABLE 10B — 50 at.% Nb - Pd

T(K)	$P_{Pd(alloy)}$ (atm.)	$P^{o\ 75}_{Pd}$ (atm.)	a_{Pd}
1499	$2.78X10^{-9}$	$2.16X10^{-7}$	$1.28X10^{-2}$
1522	$4.67X10^{-9}$	$3.38X10^{-7}$	$1.38X10^{-2}$
1539	$6.70X10^{-9}$	$4.66X10^{-7}$	$1.43X10^{-2}$
1578	$1.59X10^{-8}$	$9.47X10^{-7}$	$1.68X10^{-2}$
1616	$2.89X10^{-8}$	$1.83X10^{-6}$	$1.59X10^{-2}$
1650	$7.14X10^{-8}$	$3.21X10^{-6}$	$2.22X10^{-2}$
1695	$1.40X10^{-7}$	$6.52X10^{-6}$	$2.14X10^{-2}$
1732	$2.93X10^{-7}$	$1.14X10^{-5}$	$2.58X10^{-2}$
1778	$5.66X10^{-7}$	$2.20X10^{-5}$	$2.58X10^{-2}$
1733	$2.37X10^{-7}$	$1.15X10^{-5}$	$2.07X10^{-2}$
1644	$7.72X10^{-8}$	$2.91X10^{-6}$	$2.65X10^{-2}$
1597	$2.73X10^{-8}$	$1.32X10^{-6}$	$2.07X10^{-2}$
1533	$7.88X10^{-9}$	$4.16X10^{-7}$	$1.89X10^{-2}$
1484	$2.59X10^{-9}$	$1.85X10^{-7}$	$1.40X10^{-2}$
1425	$5.13X10^{-10}$	$4.68X10^{-8}$	$1.10X10^{-2}$

TABLE 10C -- 80 at.% Nb - Pd

T(K)	DAY 1 $P_{Pd(alloy)}$ (atm.)	DAY 1 $P^{o\ 75}_{Pd}$ (atm.)	DAY 1 a_{Pd}	T(K)	DAY 2 $P_{Pd(alloy)}$ (atm.)	DAY 2 $P^{o\ 75}_{Pd(alloy)}$ (atm.)	DAY 2 a_{Pd}
1663	$1.17X10^{-8}$	$3.96X10^{-6}$	$2.95X10^{-3}$	1552	$8.45X10^{-10}$	$5.93X10^{-7}$	$1.42X10^{-3}$
1708	$3.00X10^{-8}$	$7.95X10^{-6}$	$3.77X10^{-3}$	1586	$1.68X10^{-9}$	$1.09X10^{-6}$	$1.54X10^{-3}$
1767	$1.55X10^{-7}$	$1.88X10^{-5}$	$8.24X10^{-3}$	1610	$2.79X10^{-9}$	$1.71X10^{-6}$	$1.63X10^{-3}$
1801	$2.66X10^{-7}$	$3.01X10^{-5}$	$8.84X10^{-3}$	1614	$4.41X10^{-9}$	$1.77X10^{-6}$	$2.49X10^{-3}$
1873	$6.33X10^{-7}$	$7.49X10^{-5}$	$8.45X10^{-3}$	1632	$7.16X10^{-9}$	$2.39X10^{-6}$	$3.00X10^{-3}$
1917	$8.18X10^{-7}$	$1.25X10^{-4}$	$6.54X10^{-3}$	1677	$1.06X10^{-8}$	$4.94X10^{-6}$	$2.15X10^{-3}$
1978	$1.04X10^{-6}$	$2.46X10^{-4}$	$4.23X10^{-3}$	1711	$1.74X10^{-8}$	$8.32X10^{-6}$	$2.09X10^{-3}$
2007	$1.25X10^{-6}$	$3.33X10^{-4}$	$3.75X10^{-3}$	1769	$3.03X10^{-8}$	$1.94X10^{-5}$	$1.56X10^{-3}$
1986	$6.73X10^{-7}$	$2.67X10^{-4}$	$2.52X10^{-3}$	1800	$4.84X10^{-8}$	$2.97X10^{-5}$	$1.63X10^{-3}$
1949	$4.20X10^{-7}$	$1.79X10^{-4}$	$2.35X10^{-3}$	1837	$7.50X10^{-8}$	$4.82X10^{-5}$	$1.56X10^{-3}$
1926	$2.97X10^{-7}$	$1.39X10^{-4}$	$2.14X10^{-3}$	1856	$1.19X10^{-7}$	$6.10X10^{-5}$	$1.95X10^{-3}$
1897	$2.08X10^{-7}$	$9.93X10^{-5}$	$2.09X10^{-3}$	1886	$1.87X10^{-7}$	$8.73X10^{-5}$	$2.14X10^{-3}$
1878	$1.46X10^{-7}$	$7.95X10^{-5}$	$1.84X10^{-3}$	1918	$2.94X10^{-7}$	$1.27X10^{-4}$	$2.31X10^{-3}$
1845	$9.28X10^{-8}$	$5.33X10^{-5}$	$1.74X10^{-3}$	1949	$4.07X10^{-7}$	$1.79X10^{-4}$	$2.27X10^{-3}$
1825	$5.93X10^{-8}$	$4.15X10^{-5}$	$1.43X10^{-3}$	1981	$5.55X10^{-7}$	$2.54X10^{-4}$	$2.19X10^{-3}$
1797	$3.99X10^{-8}$	$2.85X10^{-5}$	$1.40X10^{-3}$	1999	$7.84X10^{-7}$	$3.07X10^{-4}$	$2.55X10^{-3}$
1753	$2.43X10^{-8}$	$1.54X10^{-5}$	$1.58X10^{-3}$	2033*	$1.10X10^{-6}$	$4.36X10^{-4}$	$2.52X10^{-3}$
1731	$1.87X10^{-8}$	$1.12X10^{-5}$	$1.67X10^{-3}$	2052*	$1.74X10^{-6}$	$5.27X10^{-4}$	$3.30X10^{-3}$

TABLE 10C (continued) -- 80 at.% Nb - Pd

T(K)	DAY 1 $P_{Pd(alloy)}$ (atm.)	DAY 1 P^{o}_{Pd} (atm.)	DAY 1 a_{Pd}	T(K)	DAY 2 $P_{Pd(alloy)}$ (atm.)	DAY 2 $P^{o\ 75}_{Pd}$ (atm.)	DAY 2 a_{Pd}
1677	1.15×10^{-8}	4.93×10^{-6}	2.33×10^{-3}	2096*	2.00×10^{-6}	8.09×10^{-4}	2.47×10^{-3}
1667	9.15×10^{-9}	4.22×10^{-6}	2.17×10^{-3}	2128*	2.16×10^{-6}	1.09×10^{-4}	1.98×10^{-3}
1608	4.76×10^{-9}	1.60×10^{-6}	2.98×10^{-3}	2160*	3.06×10^{-6}	1.47×10^{-3}	2.08×10^{-3}
1580	2.46×10^{-9}	9.81×10^{-7}	2.51×10^{-3}	2212*	1.39×10^{-6}	2.31×10^{-3}	6.02×10^{-4}
1550	1.32×10^{-9}	5.71×10^{-7}	2.31×10^{-3}				
1508	4.68×10^{-10}	2.58×10^{-7}	1.81×10^{-3}				

*Fluctuating ion intensity at const. T.

TABLE 10C (cont'd.) — 80 at.% Nb - Pd

DAY 3

T(K)	$P_{Pd \text{ or } Nb(*)}$ (atm.)	$P^{o\ 75}_{Pd \text{ or } Nb(*)}$ (atm.)	$a_{Pd \text{ or } Nb(*)}$
1624	$9.45X10^{-9}$	$2.09X10^{-6}$	$4.52X10^{-3}$
1664	$1.81X10^{-8}$	$5.55X10^{-6}$	$3.26X10^{-3}$
1696	$3.04X10^{-8}$	$6.62X10^{-6}$	$4.59X10^{-3}$
1735	$4.35X10^{-8}$	$1.19X10^{-5}$	$3.66X10^{-3}$
1771	$5.75X10^{-8}$	$1.99X10^{-5}$	$2.89X10^{-3}$
1788	$7.83X10^{-8}$	$2.52X10^{-5}$	$3.11X10^{-3}$
1830	$1.11X10^{-7}$	$4.42X10^{-5}$	$2.51X10^{-3}$
1879	$2.38X10^{-7}$	$8.04X10^{-5}$	$2.96X10^{-3}$
1923	$8.65X10^{-7}$	$1.34X10^{-4}$	$6.46X10^{-3}$
1986	$1.11X10^{-6}$	$2.67X10^{-4}$	$4.16X10^{-3}$
2007	$1.97X10^{-6}$	$3.33X10^{-4}$	$5.92X10^{-3}$
2081	$3.10X10^{-6}$	$7.01X10^{-4}$	$4.42X10^{-3}$
2128	$1.66X10^{-6}$	$1.09X10^{-3}$	$1.52X10^{-3}$
2144	$1.99X10^{-9*}$	$2.05X10^{-10*}$	9.71^{*}
2123	$2.08X10^{-6}$	$1.04X10^{-3}$	$2.00X10^{-3}$
2144	$4.14X10^{-6}$	$1.55X10^{-3}$	$2.67X10^{-3}$
2212	$1.73X10^{-9*}$	$7.06X10^{-10*}$	2.45^{*}
2181	$3.01X10^{-9*}$	$4.06X10^{-10*}$	7.41^{*}
2249	$1.06X10^{-8*}$	$1.34X10^{-9*}$	7.91^{*}
2243	$1.42X10^{-6}$	$3.01X10^{-3}$	$4.72X10^{-4}$

TABLE 10C (cont'd.) -- 80 at.% Nb - Pd

DAY 3

T(K)	$P_{Pd \text{ or } Nb(*)}$ (atm.)	$P^{o\ 75}_{Pd \text{ or } Nb(*)}$ (atm.)	$a_{Pd \text{ or } Nb(*)}$
2243	$9.42X10^{-9*}$	$1.21X10^{-9*}$	7.79^{*}
2281	$1.33X10^{-8*}$	$2.28X10^{-9*}$	5.83^{*}
2286	$2.69X10^{-7}$	$4.28X10^{-3}$	$6.29X10^{-5}$
2350	$3.49X10^{-8*}$	$6.90X10^{-9*}$	5.06^{*}
2355	$1.70x10^{-7}$	$7.34X10^{-3}$	$2.32X10^{-5}$
2392	$4.01X10^{-8*}$	$1.31X10^{-8*}$	3.06^{*}
2456	$5.86X10^{-8*}$	$3.34X10^{-8*}$	1.75^{*}
2467	$1.66X10^{-7}$	$1.66X10^{-2}$	$1.00X10^{-5}$
2472	$5.45X10^{-8*}$	$4.19X10^{-8*}$	1.30^{*}
2472	$1.04X10^{-7}$	$1.71X10^{-2}$	$6.08X10^{-6}$
2504	$7.66X10^{-8*}$	$6.53X10^{-8*}$	1.17^{*}
2504	$7.88X10^{-8}$	$2.13X10^{-2}$	$3.70X10^{-6}$
2626	$1.87X10^{-7*}$	$3.21X10^{-7*}$	0.58^{*}

the corresponding values of P_i^o from Hultgren, et al.[75] and the resulting $a_i = P_i/P_i^o$. All of the data are for Pd except for those on Nb given in Table 10C for Day 3 of run III. The 18 at.% Nb-Pd alloy was run in a CS grade 99.7% graphite Knudsen cell with a 0.102 cm. diameter orifice with a knife edge (~0.005 cm. thick). To increase sensitivity (particularly to the refractory Nb component) the subsequent two runs were carried out with 0.254 cm. diameter orifices, and with orifice edges ~0.05 cm. thick to avoid the slight orifice enlargement evident after run I. The 50 at.% Nb-Pd alloy was also run in a CS graphite cell but the 80 at.% Nb-Pd alloy was run in a cell machined from hot-pressed 99.8% NbC due to its larger a_{Nb}. It is probably fortunate that the 50 at.% Nb-Pd alloy did not melt since the carbide equilibria showed 15±2 at.% Nb-Pd to be in equilibrium with graphite and NbC, and the reaction of a liquid NbPd alloy with a graphite cell would likely have been more extreme than the reaction of liquid $NbPd_3$ with graphite observed in several of the thermogravimetric runs.

In Table 10A is noted the melting point of the 18 at.% Nb-Pd as detected by a small halt in the I_{Pd}^+ vs. time curve during heating or cooling. The observed melting point of 1821±11 K is lower than the ~1870 K reported by Giessen, et al.[95] but the liquidus temperatures of these Pd-rich alloys may be somewhat depressed by the presence of graphite just as for pure Pd.[27] That the alloy melting point seemed to have shifted up by ~10° between the first and second days of run I is undoubtedly due to Pd-depletion of the alloy (which effect was

confirmed by post-run EPMA analysis, as discussed below) and is consistent with the Nb-Pd phase diagram.[95] The 50 at.% Nb-Pd alloy had not melted up to the maximum temperature of 1778 K, also consistent with the phase diagram, which assigns an ~1810 K liquidus to this composition. That the ~2250 K melting point of the 80 at.% Nb-Pd alloy was not detected by a sharp halt in the I^+_{Pd} vs. time curve may be due to a wide two-phase liquid/solid region at this composition. Because of the high liquidus temperature of the 80 at. Nb-Pd alloy, all of the data taken for this system on Days 1 and 2 and much of that taken on Day 3 should have involved only a solid sample.

The smallest measured pressures were $5X10^{-10}$ atm. Pd(g) at. 1425 K over 50 at.% Nb-Pd and $2X10^{-9}$ atm. Nb(g) over 80 at.% Nb-Pd at 2212 K. The only other species which were established as effusing from a cell were C(g) which gave a clearly shutterable I^+_C signal at 2340 K and C_2(g) which gave a weaker but shutterable $I^+_{C_2}$ signal at 2472 K, both during run III; these data were not adequate to attempt to obtain a calibration constant through the gaseous carbon species equilibria analogously to the Ag/Ag_2 approach.

The highest-temperature results of Day 2, run III (for the 80 at.% Nb-Pd alloy, and given in Table 10C) exhibited fluctuating ion intensities which may have been caused by solid-state Pd diffusion becoming limiting just below the alloy melting point or, perhaps more likely, by instrument malfunction, but whatever the cause of this behaviour, the data taken under these circumstances are somewhat more uncertain. The results from Day 3 for the same 80 at.% Nb-Pd system (Table 10C)

exhibited features which suggest serious problems with at least portions of that particular run. At 2144 K I^{+}_{Nb} was first measured and an apparent a_{Nb} of 9.7 was established. Since it is impossible to have an equilibrium system with an activity (using the pure element standard state) greater than unity and the calibration constant was presumably not inaccurate by a factor of 10, the most likely explanation of this result (^{93}Nb was monitored and no interfering species seems likely) is vaporization of Nb contamination on or in the outer Ta cell or Mo/W heat shields, and/or vapor transport of Nb(g) as, for example, $NbCl_5(g)$ due to NaCl contamination from extensive handling of the components in the furnace region. These explanations are consistent with the thermodynamically unlikely subsequent behaviour of a falling a_{Nb} with increasing temperatures beyond 2144 K since such contamination effects would have been continually reduced through vaporization of the offending material at higher temperatures. Simultaneous with this effect the Pd activity was observed to be decreasing with increasing temperature and fell rapidly above 2144 K, from $3X10^{-3}$ at that temperature to $4X10^{-6}$ at 2504 K. The obvious explanation of this is that the already Pd-poor alloy was being rapidly depleted of its volatile Pd component and was moving towards the congruently vaporizing composition; in fact the measured Nb and Pd pressures at 2504 K were essentially the same and this composition may have been attained. All three of the post-run alloys were polished and compositionally analyzed alongside of the starting alloys by EPMA and the run III (80 at.% Nb-Pd) alloy was found to contain <1 at.%Pd

after the run, in accord with the observed behaviour. The unmelted run II (50 at.% Nb-Pd) alloy showed slight Pd depletion to a homogeneous composition of ~53 at.% Nb-Pd at the end of the experiment, and the 18 at.% Nb-Pd alloy of run I had a final composition of <1 at.% Pd but the most severe Pd-depletion in that case probably occurred subsequent to the experiments reported here since that particular sample was later maintained at high temperatures for prolonged periods to obtain additional data. Because of this depletion effect the low-temperature results are taken to be most reliable and the very high-temperature data taken for the "80 at.% Nb-Pd" system on Day 3 are considered essentially worthless.

In Figure 14 is presented an Arrhenius plot of all of the results except for those obtained above 2160 K on the 80 at.% Nb-Pd system; those data left off simply show a plummeting a_{Pd} and an a_{Nb} coming down to approximately unity and are consistent with a very dilute Pd-Nb alloy. The points which fall well above the others for the 20 at.% Pd-Nb system were taken during the initial temperature increase and the apparently high P_{Pd}'s likely included a contribution from vaporization of Pd which had condensed on the heat shields during the previous (50 at.% Pd-Nb) run. The pure Pd vapor pressure values from Hultgren, et al.[75] have been included for comparison and where the 82 at.% Pd-Nb data breaks through the P^{o}_{Pd} curve a Pd activity

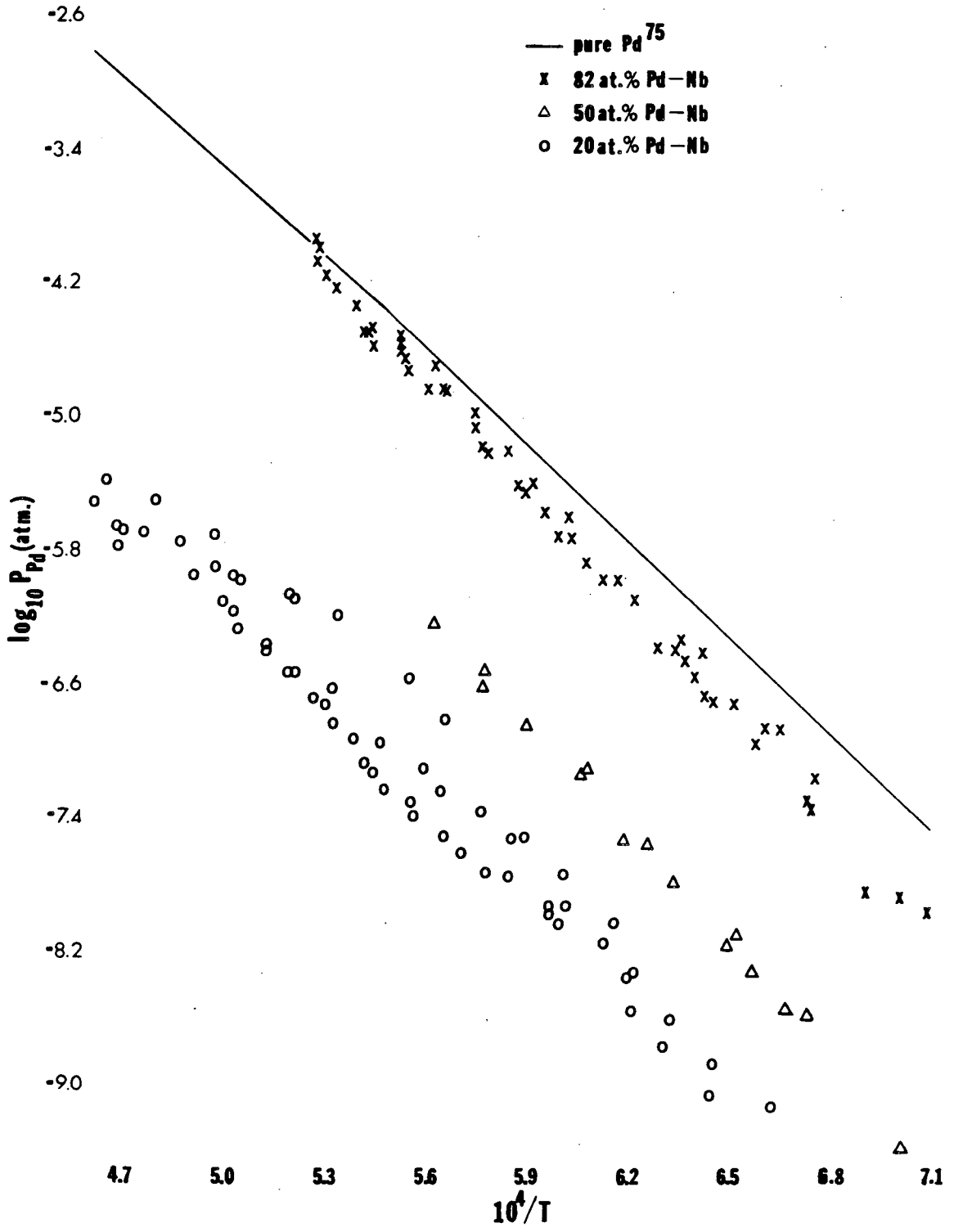
-2.6
-3.4
-4.2
-5.0
-5.8
-6.6
-7.4
-8.2
-9.0
$\log_{10} P_{Pd}$ (atm.)
4.7
5.0
5.3
5.6
5.9
6.2
6.5
6.8
7.1
$10^4/T$
pure Pd 75
82 at.% Pd—Nb
50 at.% Pd—Nb
20 at.% Pd—Nb
XBL 836-10318

Figure 14

(P_{Pd}/P^{o}_{Pd}) of slightly greater than unity is suggested; the apparent a_{Pd} got as high as 1.16 and this unreasonable result is taken to reflect a somewhat too large k_{Pd} and/or the possible 30% uncertainty assigned to the standard state vapor pressures.

The slope of the log(P) vs. 1/T plots should be reasonably constant and ideally give values for $\Delta\bar{H}_{Pd,vap.}$ for these alloys through the Gibbs-Helmholtz equation.[54] A measure of additional stabilization (bonding) upon transferring Pd from the pure condensed standard state to the alloy is what is of interest here and the quantity required is thus:

$$\Delta\bar{H}_{Pd,mix} = \Delta\bar{H}^{o}_{Pd,vap} - \Delta\bar{H}_{Pd,vap}(alloy)$$

but the differences between these large vaporization enthalpies (log[P] vs. 1/T slopes) are relatively small and these data don't appear to be of a sufficient quality to obtain Second Law alloying enthalpies though it does seem clear from the data that $\Delta\bar{H}_{v}(alloy) > \Delta\bar{H}^{o}_{v}$ for at least the 82 and 50 at.% Pd-Nb systems. Also encouraging is the obvious trend of decreasing P_{Pd} (a_{Pd}) with increasing Pd-dilution. To obtain a quantitative value for the relative stabilization of Pd in these three alloys the more reliable low-temperature (1400-1800 K) data was considered and, to eliminate the scatter, the best line was fit to these data and Pd activites obtained at 1515 K

($10^4/T = 6.6$) from the resulting curves. The corresponding $\Delta\bar{G}^{xs}_{Pd}$ at 1515 K are then obtained from: $\Delta\bar{G}^{xs}_{Pd} = \Delta\bar{G}_{Pd} + T\Delta\bar{S}^{id}_{Pd}$ where $\Delta\bar{G}_{Pd} = RT\ln(a_{Pd})$ and $\Delta\bar{S}^{id}_{Pd} = -R\ln(X_{Pd})$. The activities and excess free energies at 1515 K so obtained are:

	a_{Pd}	$\Delta\bar{G}^{xs}_{Pd}$ (kcal)
82 at.% Pd–Nb	0.40	-2.2
50 at.% Pd–Nb	0.013	-11.0
20 at.% Pd–Nb	0.0019	-14.0

Although $\Delta\bar{G}^{xs}$ itself represents a measure of the thermal (i.e., nonconfigurational) stabilization and may differ little from $\Delta\bar{H}$ here since $\Delta\bar{S}^{xs}$ is expected to be small for this solid-state transfer, ΔH contains the bonding information of interest and a reasonable lower limit for this quantity ($\Delta\bar{G}^{xs}$ is taken as a reasonable upper limit) may be established by assuming $\Delta\bar{S}^{xs} = k\Delta\bar{H}$ as Kubaschewski has shown to be a reasonable approximation in many cases[96] and taking a minimum $\Delta\bar{S}^{xs}$ of -2 e.u. for the 20 at.% Pd–Nb system since smaller values seem unlikely given, for example, that $\Delta S^{o}_{fus} = \sim 2.3$ e.u. for Pd. This treatment results in the following values, again at 1515 K:

	$\Delta\bar{S}^{xs}_{Pd}$(min., e.u.)	$\Delta\bar{H}_{Pd}$(min., kcal)
82 at.% Pd–Nb	–0.3	–2.7
50 at.% Pd–Nb	–1.6	–13.4
20 at.% Pd–Nb	–2(ass.)	–17.0

Taking these $\Delta\bar{H}$ as lower limits and the $\Delta\bar{G}^{xs}$ as upper limits, the $\Delta\bar{H}_{Pd,alloy}$ values obtained are, in kcal: -2.5 ± 0.3, -12.2 ± 1.2, and -15.5 ± 1.5 for the 82, 50, and 20 at.% Pd–Nb systems, respectively. Although the net activity uncertainty of ±2X introduces an additional $\Delta\bar{H}$ uncertainty of approximately ±2 kcal., the point is clear that the increase in stabilization (bonding) of Pd upon going from 82 to 50 at.% Pd–Nb is large relative to the additional stabilization obtained upon going from 50 to 20 at.% Pd–Nb and indeed this fact is readily evident from the pressure vs. composition (at constant temperature) relations in Figure 14.

To interpret this result, consider the integral ground state valence electronic configurations of solid Nb and Pd as given by the Engel-Brewer theory: Nb = [Kr] $4d^4$ $5s^1$ and Pd = [Kr] $4d^7$ $5s^1$ $5p^2$. Thus Nb has one vacant valence d orbital available for acid–base bonding and Pd has two sets of internally paired non-bonding valence d electrons for donation. As Nb is added to pure Pd the most effective

of the basic Pd electrons are donated into the relatively few available vacant Nb d orbitals until the composition NbPd is approached, at which point all of the most effective of the two types of Pd non-bonding valence d electrons have been utilized and the further addition of Nb beyond NbPd must result in donation of the less effective Pd electrons if there is to be any additional acid-base stabilization. The results of these mass spectrometric experiments show a large stabilization of Pd in NbPd relative to pure Pd or even 80 at.% Pd-Nb but indicate very little additional stabilization (beyond the ideal configurational effect) upon further dilution to 20 at.% Pd-Nb; this suggests that the second available pair of non-bonding valence d electrons in Pd is not nearly as effective in acid-base bonding with neighboring Nb atoms as the first, this presumably due to a non-spherically-symmetrical crystal field whereby certain valence d orbitals become extended while others contract due to the presence of neighboring atoms. This interpretation assumes that no significant net charge transfer from the basic element (Pd) to the acidic element (Nb) occurs as a result of the donor-acceptor interaction since a net positively charged Pd atom would clearly be resistant to further donation regardless of how appropriate the orbital containing the second available electron pair. That Pd is more electronegative than Nb on both the Pauling scale (ref. 10, p. 93 - Nb:1.6, Pd:2.2) and as measured by work functions[98] (Nb:4.3 eV, Pd:5.1 eV) would suggest that any large net flow of charge from Pd to Nb is improbable and it is assumed that polarization of the bonds towards Pd and "back-bonding"

from Nb to Pd using other orbitals (as in $Cr(CO)_6$ -- see, for example, Ref. 97, pp. 82-83) negates the formal charge transfer involved in the acid-base reaction. The properties of the pure transition elements clearly reflect the crystal field effect on bonding efficiency since the bonding enthalpy per unpaired d electron reaches a distinct minimum at five unpaired where all orbitals must be used for bonding;[6] it is not surprising that similar behaviour is evident in these alloys.

Although somewhat analogous interpretations of some of the other experimental results will be offered below, no other compositional dependence studies were performed for direct comparison with these Nb-Pd results. These mass spectrometric results will later be related to the $NbPd_3$ thermogravimetric experiments and the carbide equilibrations of this system.

DISCUSSION

Interconsistencies:

One motivation for repeating here the carbide and nitride equilibration experiments on the Zr–Pt system which had previously been carried out by Brewer and Wengert[22] and Goodman[53] was that Goodman had found a 45 at.% Zr–Pt alloy to be in equilibrium with ZrN and 1.0 atm. N_2 at 2258 K (a_{Zr} = 2.4X20^{-4}) and suggested that the conflicting result of the earlier carbide work reflected non-equilibration. By starting with both Pt and ZrPt in separate runs and obtaining the $ZrPt_3$ intermetallic in both cases, the experiments here have conclusively confirmed the finding of Brewer and Wengert that this is the phase in equilibrium with ZrC and graphite. The experiments reported here also confirmed equilibration in the ZrN–Pt experiments and indicated that ~29 at.% Zr–Pt, and not 45 at.% Zr–Pt, is the equilibrium alloy under the experimental conditions. The carbide and nitride results obtained here are, in fact, entirely consistent with each other since the former provides a_{Zr} = 5.4X10^{-5} in $ZrPt_3$ and the latter gives a_{Zr} = 1.4Z10^{-4} in a slightly Zr-richer alloy, both at 2200 K. Since the earlier nitride equilibrations were carried out under essentially identical conditions to those reported here, the most likely explanation for the discrepancy lies in the the chemical separation and wet analytical procedures used previously.

Amoung the experiments which have been performed by others on $ZrPt_3$ are the galvanic cell measurements of Meschter and Worrell[15] and high-temperature mass spectrometry by Carbonara and Blue.[16] The

EMF study extended only to ~1300 K at which temperature it was found that $a_{Zr} = 6.5X10^{-16}$ and $a_{Pt} = 0.84$ for a Pt-rich $ZrPt_3$ alloy. If If the same three phase ZrC-graphite-$ZrPt_3$ equilibrium established up to 2300 K in this work and down to 1850 K by Brewer and Wengert[22] is assumed to exist at 1300 K then $a_{Zr(ZrPt_3),1300\ K} = 4.0X10^{-8}$ is predicted using the JANAF[40] thermochemical data for ZrC. Although the EMF results must be considered at least somewhat suspect given their unusually large entropy values (e.g., $\Delta\bar{S}^{xs}_{Zr(ZrPt_3),1300\ K}$ = -22.3 e.u. compared with $\Delta S^{o\ 75}_{vap,Zr,1300\ K}$ = 32 e.u.), an eight order of magnitude activity differnece within an ordered, narrow, and strongly bonded phase is not necessarily unreasonable as evidenced, for example, by the system $Na_1Cl_{1\pm x}$; the EMF measurements were on an alloy at the Pt-rich edge of the $ZrPt_3$ phase (actually on a two phase system) as reflected by $a_{Pt} = 0.84$, and comparison of the carbide and nitride results suggests that the $ZrPt_3$ phase in equilibrium with ZrC and graphite was near the Zr-rich boundary of that intermetallic. The mass spectrometric studies[16] seem also to have been on Pt-rich $ZrPt_3$ since they gave $a_{Zr} = 8.4X10^{-9}$ and a_{Pt} = 0.94 at 2200 K to be compared with $a_{Zr(ZrPt_3)} = 5.4X10^{-5}$ at the same temperature from the carbide equilibrium. Again, these results are taken to reflect the rapid variation of a_{Zr} with composition across the narrow $ZrPt_3$ intermetallic phase.

Comparisons for interconsistency may also be made for the Nb-Pd system which was studied here by all four of the experimental methods available. The carbide equilibrations resulted in a ~15 at.% Nb-Pd alloy with $a_{Pd} = 1.5X10^{-3}$ when the short extrapolation of the 2300 K results to 2400 K is made, and the nitride experiments provided $a_{Nb} = 3X10^{-2}$ at 2400 K for a ~27 at.% Nb-Pd system so that the outcomes of these two experiments are in at least qualitative accord. From the thermogravimetric studies, $a_{Pd} = 0.12$ at 1659 K in 75 at.% Pd-Nb was obtained, compared with $a_{Pd} = 0.5$ in 82 at.% Pd-Nb and $a_{Pd} = 0.020$ in 50 at.% Pd-Nb at the same temperature from the mass spectrometric experiments so that these results are also qualitatively interconsistent.

Carbide Results:

Several of the carbide equilibrations performed previously by Brewer and Wengert[22] were repeated here; as discussed above, the $ZrPt_3$ phase was confirmed as the equilibrium phase and both that intermetallic and $ZrIr_3$ were found to coexist with ZrC and graphite up to 2300 K (and down to 1850 K from the earlier work) thus establishing the relative temperature insensitivity of these equilibria. One result of the earlier work was that Ru dissolved 0.75 at.% Zr ($\gamma_{Zr(Ru)} = 4.7X10^{-4}$) in the presence of ZrC and graphite whereas Os dissolved <0.06 at.% Zr (below EPMA detection limit; $\gamma_{Zr(Os)} > 7.9X10^{-3}$), both at 1770 K. Since the Engel-Brewer theory predicts a stronger acid-base interaction of the 5d element Os with Zr these results were

surprising and these experiments were repeated at a higher temperature with an outcome in better accord with expectations. At 2216 K, Os in equilibrium with ZrC and grahite was found to have dissolved a concentration of Zr also below the EPMA detection limit but this limit was here estimated at 0.1±0.05 at.% Zr-Os with the result $\gamma_{Zr(Os),2216K} > 6.0X10^{-2}$. The corresponding ZrC-graphite-Ru equilibraion at 2061 K resulted in 0.1±0.05 at.% Zr-Ru as measured by EPMA and $\gamma_{Zr(Ru)} = 2.0X10^{-2}$. If both of these results are extrapolated to 2150 K assuming $\Delta S^{xs}_{Zr} = 0$ the activity coefficients so obtained are: $\gamma_{Zr(Os)} > 5.7X10^{-2}$ and $\gamma_{Zr(ru)} = 2.4X10^{-2}$ with an uncertainty of approximately $\pm 3\gamma$ associated with each. Because of the relatively large uncertainties involved, these results are not definitive but clearly do not suggest the significantly greater binding of Zr by Ru indicated by the earlier work.

Since the carbide runs which resulted in MPl_3 intermetallics involved a_M differences of less than two orders of magnitude and the $ZrPt_3$ discussion above suggests rapid activity variations within these phases, it may not be reasonable to attempt to establish stability trends with these results. It is clear that all of these MPl_3 phases are extraordinarily stable as is also reflected in their high degree of long-range order, mechanical properties (e.g., extreme brittleness), and very high congruent melting points. Although it is difficult to make any definitive comparisons between the TaC-Os and NbC-Os results, it does seem clear that the Hf-Os interaction is

stronger than those of Zr-Os, Ta-Os, or Nb-Os which may be taken to reflect both the greater bonding effectiveness of the Hf 5d orbitals compared with the 4d's of Zr and the greater number of vacant valence d orbitals available on Hf relative to Ta and Nb (with such an excess of basic electrons around, it is impossible to say whether this reflects a crystal field effect or simply the involvement of more orbitals in acid-base bonding or some combination of both effects). The carbide equilibrations of Pd with NbC and TaC clearly show greater bonding in $TaPd_3$ than in 15 at.% Nb-Pd in accord with expectations based upon degree of valence d orbital bonding overlap. Finally, the WC runs gave activity coefficients for W in 9.5 at.% W-Ir and 0.4 at.% W-Os alloys of 0.32 and 7.3, respectively, at ~2225 K suggesting some small stabilization in the W-Ir case and a repulsive interaction (likely due to internal pressure and size differences) in the W-Os system, this in accord with the fact that bcc W has the configuraton [Xe] $5d^5$ $6s^1$ and no vacant or fully occupied valence d orbitals: any acid-base interaction must involve the valence s and p orbitals of W and is expected to be relatively weak since these orbitals are very delocalized and will not interact strongly with the relatively localized valence d orbtials of a neighboring Pt-group element.

Nitride Results:

Although the resolution of these experiments was disappointingly poor due to inaccurate compositional analyses and uncertain nitride thermodynamic values, and no meaningful information could be obtained

from pressure or temperature dependences, a few comparisons are available from these results. Although the equilibrium Ti-Pt, Zr-Pt, and Hf-Pt alloys were all of composition ~30 at.% M-Pt and the equilibrium Nb-Pt alloy was ~50 at.% Nb-Pt, it does seem clear that the interaction in the latter system is somewhat less than in the others; this again is taken to reflect the relative dirth of available vacant valence d orbitals on Nb and may or may not involve a significant crystal field effect since all of these systems involve an excess of basic electrons. The comparison may only be marginally meaningful here, but these results seem to suggest somewhat reduced stability for the Ti-Pt system relative to the Zr-Pt and Hf-Pt systems in accord with both the predictions of the Engel-Brewer theory and the EMF results on these three systems of Meschter and Worrell.[14,15] That the activity coefficients for Nb in 50 at.% Nb-Pt (Pt: [Xe] $5d^7$ $6s^1$ $6p^2$) and 27 at.% Nb-Pd (Pd: [Kr] $4d^7$ $5s^1$ $5p^2$) alloys were found to be approximately comparable implies a greater bonding effectiveness of Pt relative to Pd so that all of the comparisons which can be made within the resolution of these experiments are entirely in accord with the predictions of the Engel-Brewer theory.

Vapor Pressure Results:

An interpretation of the mass spectrometric data was offered above with the results and their interconsistency with the thermogravimetric $NbPd_3$ experiments was also established above. The relatively small interaction in Zr-Au system as established with the thermogravimetric

experiments on $ZrAu_3$ is taken to be due to the relatively large effective nuclear charge on Au preventing it from readily releasing its non-bonding valence d electrons for acid-base bonding. Pelino, et al.[19] investigated a two phase Ti_3Ir-80 at.% Ti-Ir alloy mass spectrometrically and found $a_{Ti(Ti\text{-rich } Ti_3Ir)} = 0.026$ at 1623 K which extrapolates to $a_{Ti(Ti\text{-rich } Ti_3Ir)} = 0.050$ at 2008 K (assuming $\Delta\bar{S}^{xs}_{Ti} = 0$), in at least reasonable agreement with the $a_{Ti(Ti_3Ir),\ 2008K} = 0.11 \pm 2.6X$ result obtained here.

The relationships established by the MPd_3 weight loss experiments are, again: $a_{Pd(ZrPd_3)} < a_{Pd(NbPd_3)}$, $a_{Pd(HfPd_3)} < a_{Pd(TaPd_3)}$, $a_{Pd(TaPd_3)} < a_{Pd(NbPd_3)}$, and $a_{Pd(HfPd_3)} \sim a_{Pd(ZrPd_3)}$. The first two of these comparisons reconfirm the additional bonding effectiveness provided by the two available vacant valence d orbitals of the group IVB elements compared with the single available orbital of the corresponding VB elements. To estabish conclusively that this to some extent reflects a crystal field effect and not simply increased accommodation of the large excess of internally paired non-bonding valence d electrons in these Pd-rich alloys, these experiments should be repeated using, for example, Hf_3Pd and Ta_3Pd where the extra vacant Hf valence d orbital is of no particular value since all of the strongly basic Pd electrons can be accommodated in the single most effective acidic orbital. The $TaPd_3$ - $NbPd_3$ comparison is in accord with predictions based upon 5d vs. 4d orbital overlap considerations but the comparable bonding of Pd in $HfPd_3$ and $ZrPd_3$ seems to suggest that this effect is not important there. It is possible that the

less effective d orbitals of Ta and Nb which must be used for acid-base bonding are more sensitive to the relatively small d orbital contraction upon moving from the third to second transition series than are the more bonding-effective orbitals available to Hf and Zr.

Both Ti and Pd are relatively volatile so that Ti-Pd alloys cannot be investigated by total weight loss experiments, but Choudary, et al.[20] have used high-temperature mass spectrometry to study several of these systems. They obtained $a_{Pd(TiPd_3),\ 1873K} = 0.19$ as compared with $a_{Pd} = 0.03$ for both $ZrPd_3$ and $HfPd_3$ at essentially that same temperature by the weight loss experiments reported here; the valence d orbital contraction is most extreme upon going from the second to first transition series and the reduced bonding effectiveness shows up clearly. Kleykamp[21] performed solid-state galvanic cell measurements on Rh-rich $NbRh_3$ which may be compared with the $NbPd_3$ results obtained here. He found $a_{Rh(78\ at.\%\ Rh-Nb)} = 0.85$ at 1200 K which extrapolates (assuming $\Delta\bar{S}^{xs}_{Rh} = 0$) to $a_{Rh(78\ at.\%\ Rh-Nb)} = 0.83$ at 1650 K ($\gamma_{Rh} = 1.07$) as compared with $a_{Pd(NbPd_3)} = 0.12$ at 1659 K which was obtained here; it seems clear that the Nb-Rh interaction is weaker than that of Nb-Pd and this is taken to reflect the availability of two non-bonding valence d electron pairs in Pd compared with only one in Rh. Since only the most effective of the two available Pd basic electron pairs can be accommodated by the relatively few strongly acidic Nb orbitals in this Pd-rich Nb-Pd alloy, it is clear that the greater bonding effectiveness of Pd is due to a

crystal field effect and not to the availability of a greater number of non-bonding valence d electrons relative to Rh. This agrees with the mass spectrometric finding that the second available non-bonding pair of Pd is relatively ineffective in acid-base bonding.

Conclusion:

The results of these experiments clearly support the Engel-Brewer theory of acid-base bonding in this class of transition metal alloys since every comparison which can reasonably be made is entirely consistent with the predictions of that theory. The comparisons presented above stress the significantly greater acid effectiveness of the group IVB elements with their two vacant valence d orbitals relative to the VB elements with their single such orbital. The d orbital contraction effect has been seen upon moving from Ta to Nb and from Zr to Ti but was found to be much less of a factor in comparing the effectiveness of Zr and Hf. Although Au, with its three non-bonding valence d electron pairs, it is not a particularly effective donor, the two such pairs available in Pd seem to make it a much more effective base than neighboring Rh. Despite that the compositional dependence study carried out mass spectrometrically is not as compelete or accurate as would be desirable, it does rather clearly suggest that the first basic electron pair donated by Pd to Nb may be much more effective than the second available pair.

Most the of the acid–base effectiveness trends across and down the periodic table have been at least qualitatively established by the many other investigations of these systems along with the work reported here. Future studies should focus on obtaining more complete and accurate acid–base titration curves (a_i vs. X_i) which can be interpreted in terms of the progress of the acid–base interaction and thus quantitatively clarify which factors determine the extent of this type of bonding.

REFERENCES

1. H.J. Schaller, Berichte der Bunsen-Gesellschaft 80 (1976) 999-1002.
2. L. Brewer, Acta Met. 15 (1967) 553-556.
3. N. Engel, Ingenioeren M101 (1939).
4. N. Engel, Powder Met. Bull. 7 (1954) 8-18.
5. N. Engel, Acta Met. 15 (1967) 557-563.
6. L. Brewer, Science 161 (1968) 115-122.
7. L. Brewer, J. Nuclear Materials 51 (1974) 2-11.
8. L. Brewer, in V.F. Zackay (ed.), "High-strength Materials," John Wiley and Sons, Inc., New York, 1965, 12-103.
9. L. Brewer, in P. Rudman, J. Stringer, and R.I. Jaffee (eds.), "Phase Stability in Metals and Alloys," McGraw-Hill, Inc., New York, 1967, 39-61.
10. L. Pauling, "The Nature of the Chemical Bond," 3rd ed., Cornell University Press, 1960, 433.
11. V. Srikrishnan, and P.J. Ficalora, Met. Trans. 5 (1974) 1471-1475.
12. O. Kubaschewski, Trans. Faraday Soc. 54 (1958) 814-820.
13. W. A. Harrison, "Electronic Structure and the Properties of Solids," W.H. Freeman and Co., San Francisco, 1980, 516.
14. P.J. Meschter, and W.L. Worrell, Met Trans. 7A (1976) 299-305.
15. P.J. Meschter, and W.L. Worrell, Met. Trans. 8A (1977) 503-509.
16. R.S. Carbonara, and G.D. Blue, High Temp. Sci. 3 (1971) 225-230.
17. K.D. Carlson, P.W. Gilles, and R.J. Thorn, J. Chem. Phys. 38 (1963) 2725-2735.

18. U.V. Choudary, K.A. Gingerich, and L.R. Cornwell, J. Less-Common Metals 50 (1976) 201-211.

19. M. Pelino, S.K. Gupta, L.R. Cornwell, and K.A. Gingerich, J. Less-Common Metals, 68 (1979) P31-P38.

20. U.V. Choudary, K.A. Gingerich, and L.R. Cornwell, Met. Trans. 8A (1977) 1487-1491.

21. H. Kleykamp, J. Less-Common Metals 83 (1982) 105-113.

22. L. Brewer and P.R. Wengert, Met. Trans. 4 (1973) 83-104.

23. F.A. Shunk, "Constitution of Binary Alloys, 2nd Supplement," McGraw-Hill Book Co., New York, 1969.

24. B. Jeantet, and A.G. Knapton, Planseeberichte fur Pulvermetallurgie 12 (1964) 12-18.

25. E. Raub, and G. Falkenburg, Z. Metallkunde 55 (1964) 190-192.

26. E. Raub, and G. Falkenburg, Z. Metallkunde 55 (1964) 186-189.

27. A.S. Darling, Platinum Metals Review 8 (1964) 101.

28. G.L. Selman, P.J. Ellison, and A.S. Darling, Platinum Metals Review 14 (1970) 14-20.

29. W. Trzebiatowski, and J. Rudzinski, Z. Chem. 2 (1962) 158.

30. M. Battuelo, and T. Ricolfi, High Temp. - High Pres. 12 (1980) 247-252.

31. Y.S. Touloukian, and D. P. DeWitt, "Thermophysical Properties of Matter," v. 8, IFI/Plenum Data Corp., New York, 1972.

32. E. Raub, and G. Falkenburg, Metallwissenschaft und Technick 27 (1973) 669-679.

33. H.L. Schick (ed.), "Thermodynamics of Certain Refractory Compounds," v. 1 and 2, Academic Press, New York, 1966.

34. E.K. Storms, "The Refractory Carbides," Academic Press, N.Y., 1967.

35. L.E. Toth, "Transition Metal Carbides and Nitrides," Academic Press, New York, 1971.

36. V.I. Lavrentev, et al., "Niobium: Physico-Chemical Properties of its Compounds and Alloys," I.A.E.A., Vienna, 1968.

37. Ya. I. Gerassimov, et al., "Tantalum: Physico-Chemical Properties of its Compounds and Alloys," I.A.E.A., Vienna, 1972.

38. C.B. Alcock, et al., "Zirconium: Physico-Chemical Properties of Its Compounds and Alloys," I.A.E.A., Vienna, 1976.

39. P.J. Spencer, et al., "Hafnium: Physico-Chemical Properties of its Compounds and Alloys," I.A.E.A., Vienna, 1981.

40. JANAF Thermochemical Tables, U.S. Dept. of Commerce/N.B.S./Inst. for Applied Thechnology, Michigan, through 1979.

41. R. Hultgren, et al., "Selected Values of the Thermodynamic Properties of Binary Alloys," Amer. Soc. Met., Ohio, 1973.

42. C.E. Holcombe, USAEC Oak Ridge Y-12 Plant, Report Y1887, 1973 — reported in Ref. 47.

43. A. Amendola, Polytechnic Inst. of Brooklyn, N.Y., 1958 — reported in Ref. 47.

44. T.F. Chase and E.F. Juenke, General Electric, Cincinnati, 1968, — reported in Ref. 47.

45. P.G. Cotter and J.A. Kohn, J. Am. Cer. Soc. 37 (1954) 415-420.

46. J.M. Bind and G.J. McCarthy, Penn. State U., 1973 -- reported in Ref. 47.

47. JCPDS Powder Diffraction Files, International Centre for Diffraction Data, Swarthmore, Penn.

48. A.E. Dwight and P.A. Beck, Trans. AIME 215 (1959) 967-979.

49. J.W. Downey, Met. Div., Argonne Nat'l Lab., Ill., 1964 -- reported in Ref. 47.

50. A. Raman and K. Schubert, Z Metallk. 55 (1964) 704-710.

51. J.W. Colby, MAGIC - a computer program for quantitative electron microprobe analysis, Bell Telephone Labs, Penn.

52. L.S. Birks, "Electron Probe Microanalysis," 2nd ed., John Wiley and Sons, Inc., New York, 1971, Chapter 7.

53. D. Goodman, Ph.D. Thesis, Univ. of California, Berkeley, 1980.

54. K. Pitzer and L. Brewer, revision of G.N. Lewis and M. Randall, "Thermodynamics," 2nd Ed., McGraw-Hill Book Co., N.Y., 1961.

55. L.H. Bennet, A.J. McAlister, and R.E. Watson, Physics Today 30 (1977) 34-41.

56. E.I. Gal'braikh, O.P. Kulik, A.A. Kuznetsov, M.D. Lyutaya, and M.P. Morozova, Poroshk. Metall. 10 (1970) 62.

57. E. Fromm and E. Gebhardt, "Gase und Kohlenstoff in Metallen," Springer-Verlag, Berlin, 1976.

58. E. Rudy, "Compendium of Phase Diagram Data," U.S.A.F. Materials Laboratory report AFML-65-2, Wright-Patterson AFB, Ohio, 1969.

59. T. Lyman (ed.), "Metals Handbook," v. 8, 8th Ed., American Society for Metals, Ohio, 1973.

60. R.P. Elliott, "Constitution of Binary Alloys, 1st Supplement," McGraw-Hill Book Co., New York, 1965.

61. M. Hansen and K. Anderko, "Constitution of Binary Alloys," 2nd Ed., McGraw-Hill Book Co, New York, 1958.

62. A. Taylor and N.J. Doyle, J. Less-Common Metals 13 (1967) 413-430.

63. "Oxisorb" high-pressure oxygen and water eliminator supplied by Scientific Gas Products, South Plainfield, N.J.

64. L. Brewer, P.W. Gilles, and F.A. Jenkins, J. Chem. Phys. 16 (1948) 797-807.

65. U.V. Choudary, K.A. Gingerich, and L.R. Cornwell, J. Less-Common Metals 50 (1976) 201-211.

66. M.Pelino, S.K. Gupta, L.R. Cornwell, and K.A. Gingerrich, J. Less-Common Metals 68 (1979) P31-P38.

67. U.V. Choudary, K.A. Gingerich, and L.R. Cornwell, Met. Trans. 8A (1977) 1487-1491.

68. K.D. Carlson in J.L. Margrave (ed.), "The Characterization of High-Temperature Vapors," John Wiley and Sons, N.Y., 1967. 115-129.

69. M.Knudsen, Ann. Physik 28 (1909) 75-130.

70. K.D. Carlson, P.W. Gilles, and R.J. Thorn, J. Chem. Phys. 38 (1963) 2725-2735.

71. R.C. Evans, "An Introduction to Chrystal Chemistry," 2nd Ed., Cambridge Univ. Press, N.Y., 1978, 87.

72. P.W. Atkins, "Physical Chemistry," W.H. Freeman and Co., San Francisco, 1978, 800-803.

73. R.C. Paule and J.L. Margrave in J.L. Margrave (ed.), "The Characterization of High-Temperature Vapors," John Wiley and Sons, Inc., N.Y., 1967, 130-151.

74. L.H. Dreger and J.L. Margrave, J. Phys. Chem. 64 (1960) 1323-1324.

75. R. Hultgren, et al., "Selected Values of the Thernodynamic Properties of the Elements," American Soc. for Metals, Ohio, 1973.

76. J.W. Ward, R.N.R. Mulford, and M. Kahn, J. Chem. Phys. 47 (1967) 1710-1717.

77. K.A. Gingerich in E. Kaldis (ed.), "Current Topics in Materials Science," v. 6, North-Holland Publishing Co., N.Y., 1980, 345-462.

78. D.L. Cocke and K.A. Gingerich, J. Phys. Chem. 76 (1972) 2332-2336, Erratum, p. 4042.

79. J.B. Mann, J. Chem. Phys. 46 (1967) 1646-1651.

80. F.E. Stafford, High Temperatures-High Pressures 3 (1971) 213-222.

81. R.F. Pottie, D.L. Cocke, and K.A. Gingerich, Int'l. J. Mass Spec. and Ion Phys. 11 (1973) 41-48.

82. K. Hilpet and K.A. Gingerich, Ber. Bunsenges Phys. Chem. 84 (1980) 739-745.

83. R.W. Kaiser, "Introduction to Mass Spectrometry and its Applications," Prentice-Hall, Inc., N.J., 1965.

84. K.A. Gingerich, J. Chem. Phys. 49 (1968) 14-18.

85. J.S. Kane and J.H. Reynolds, J. Chem. Phys. 25 (1956) 342-349.

86. J.P. Hirth in J.L. Margrave (ed.), "The Characterization of High-Temperature Vapors," John Wiley and Sons, Inc., N.Y., 1967, 453-472.

87. O.C. Trulson and P.O. Schissel, J. Less-Common Metals 8 (1965) 262-265.

88. J.W. Ward, J. Chem. Phys. 47 (1967) 4030-4034.

89. J.W. Edwards, H.L. Johnston, and W.E. Ditmars, J. Am. Chem. Soc. 75 (1953) 2467-2470.

90. J.B. Darby, J.W. Downey, and L.J. Norton, Trans. Met. Soc. AIME 227 (1963) 1028-1029.

91. H.S. deBen, "Estimation of Detection Limits in Electron Probe Microanalysis," Electron Probe Analysis Society of American, Proceedings of the Third National Conference, 1968.

92. A.E. Dwight, Met. Div., Argonne Nat'l. Lab., Ill., 1966 -- reported in Ref. 47.

93. T. K. Biswas and K. Schubert, Z. Metallk. 58 (1967) 558-559.

94. J.I. Goldstein and J.W. Colby, in J.I. Goldstein and H. Yakowitz (eds.), "Practical Scanning Electron Microscopy," Plenum Press, N.Y., 1975, 435-489.

95. B.C. Giessen, N.J. Grant, D.P. Parker, R.C. Manuszewski, and R.M. Waterstrat, Net. Trans. 11A (1980) 709-715.

96. O.Kubaschewski, High Temperatures - High Pressures 13 (1981) 435-440.

97. F.A. Cotton and G. Wilkinson, "Advanced Inorganic Chemistry," 4th Ed., John Wiley and Son, N.Y., 1980, 644-652.

98. H.L. Anderson (ed.), "Physics Vade Mecum," American Institute of Physics, N.Y., 1981, 309.

TECHNICAL INFORMATION DEPARTMENT
LAWRENCE BERKELEY LABORATORY
UNIVERSITY OF CALIFORNIA
BERKELEY, CALIFORNIA 94720